INFORMATION TO USERS

This manuscript has been reproduced from the microfilm master. UMI films the text directly from the original or copy submitted. Thus, some thesis and dissertation copies are in typewriter face, while others may be from any type of computer printer.

The quality of this reproduction is dependent upon the quality of the copy submitted. Broken or indistinct print, colored or poor quality illustrations and photographs, print bleedthrough, substandard margins, and improper alignment can adversely affect reproduction.

In the unlikely event that the author did not send UMI a complete manuscript and there are missing pages, these will be noted. Also, if unauthorized copyright material had to be removed, a note will indicate the deletion.

Oversize materials (e.g., maps, drawings, charts) are reproduced by sectioning the original, beginning at the upper left-hand corner and continuing from left to right in equal sections with small overlaps.

Photographs included in the original manuscript have been reproduced xerographically in this copy. Higher quality 6" x 9" black and white photographic prints are available for any photographs or illustrations appearing in this copy for an additional charge. Contact UMI directly to order.

Bell & Howell Information and Learning
300 North Zeeb Road, Ann Arbor, MI 48106-1346 USA
800-521-0600

UMI®

A NEW VIEW OF STARLING'S HYPOTHESIS AT THE MICROSTRUCTURAL LEVEL

by

Xiaping Hu

A dissertation submitted to the Graduate Faculty in Engineering in partial fulfillment of the requirements for the degree of Doctor of Philosophy, The City University of New York

2000

This manuscript has been read and accepted for the Graduate Faculty in Engineering in satisfaction of the dissertation requirement for the degree of Doctor of Philosophy.

1/26/00
Date

Professor Sheldon Weinbaum
Chair of Examining Committee

January 26, 2000
Date

Professor Mumtaz K. Kassir
Executive Officer

Professor Fitz-Roy E. Curry

Professor Kung-Ming Jan

Professor Daniel Lemons

Professor Alan Weinstein
Supervisory Committee

The City University of New York

Abstract

A NEW VIEW OF STARLING'S HYPOTHESIS AT THE MICROSTRUCTURAL LEVEL

by

Xiaping Hu

Mentor: Professor Sheldon Weinbaum, Co-mentor: Professor Fitz-Roy Curry

Starling's hypothesis is the basic principle in physiology, which describes the fluid movement across microvessels. In contrast to the widely accepted view that the fluid is filtered out of the arterial side of the capillary and reabsorbed at the venous end leaving a small net filtration which is removed by the lymphatics, we have developed a new mathematical model at the cellular microstructural level which theoretically predicts that there is no sustained venous absorption even at very low capillary pressures. We have also proposed that the forces for filtration and oncotic reabsorption across the capillary wall are determined by the local difference in the hydrostatic and colloid osmotic pressure across the endothelial surface glycocalyx, the primary molecular sieve for plasma proteins, rather than the global difference in hydrostatic and oncotic pressure across the entire vessel wall between the plasma and tissue, as has been universally assumed until now. This subtle, but important modification, leads to a major revision of the Starling equation. Here, new theoretical and experimental results on individually perfused microvessels are presented to demonstrate that the effective oncotic pressure across the

capillary endothelium is not the global difference in oncotic pressure between blood and tissue.

We also investigate the effect of a parallel non-convective transcellular pathway on the transcapillary fluid filtration due to vesicular transport. The model predicts that the local protein concentration behind the surface glycocalyx can differ greatly from the interstitial protein concentration, since the presence of the junction strand prevents back diffusion of the proteins into the shielded cleft region between the backside of the surface matrix and the lumen side of the junction strand. Even though the presence of a non-convective pathway may greatly increase the interstitial protein concentration, there is only a modest effect on the local concentration at the backside of surface glycocalyx and, thus, only small changes in the fluid filtration across the capillary. The net result is that the filtration in the capillaries is far less than, heretofore, realized and there may be no need for venous reabsorption.

Acknowledgements

I would like to express my deepest gratitude to my mentor, Prof. Sheldon Weinbaum, who has influenced me greatly. In the past four years, he guided and encouraged me. Before I arrived at the City College, I did not have any background in Biomedical Engineering. When I look at the three papers that came out of this thesis, I am so excited. Without him, it would have never happened. As he told me, Ph. D study is not just finishing several projects and having papers published. He taught me how to become a research worker and inspired me to have enthusiasm for doing research in this field. His enthusiasm for the research and his work style will influence me forever.

I am also unconditionally grateful to my husband, Feng Zhang, and my parents for their support and encouragement throughout the course of this work. I have to mention Lidan You, Liyun Wang, Xiang Long and all my other fellow graduate students who helped me enormously and provided me an excellent environment which allowed me to do research efficiently.

Thanks to Profs. Roger H. Adamson, Steven Cowin, Fitz-Roy E. Curry, Susannah Fritton and Bingmei Fu, who gave helpful suggestions and advice in this work.

This research is supported by NIH grant HL 44485 and a Whitaker Foundation sponsored Center for Biomedical Engineering Fellowship.

Contents

List of Tables

List of Figures

(including Fig. 3.3). The filled circles are measured experimental data. The dotted line is the steady state without tissue loading, $C_i=J_s/J_v$, and $\sigma_f=0.94$ and the dash-three-dot curve is for $\sigma_f=0.8$. The solid line is the steady state curve in the presence of tissue loading, $C_i=C_c$, and $\sigma_f=0.94$ and the long-dashed curve is for $\sigma_f=0.8$. This range of reflection coefficients corresponds to a net effective oncotic force in the high filtration limit of 17-23 cmH_2O (calculated as $\sigma_f^2\pi_c$) in Tables 3.1 and 3.2 in the absence of tissue albumin. The dash-dot line is based on classical theory, where P_i and π_i are evaluated in the tissue space. It indicates that the classical theory overestimates the fluid filtration and the present model can predict the experimental fluid filtration results very well except Fig. 3.4c. Fig. 3.4a, $L_p=0.67\times10^{-7}$ $cm/(cmH_2O\cdot s)$ and 2D=10160 nm. Fig. 3.4b, $L_p=1.2\times10^{-7}$ $cm/(cmH_2O\cdot s)$ and 2D=5666 nm. Fig. 3.4c, $L_p=3.0\times10^{-7}$ $cm/(cmH_2O\cdot s)$ and 2D=2266 nm. Fig. 3.4d (Data from Fig. 3.3), $L_p=2.44\times10^{-7}$ $cm/(cmH_2O\cdot s)$ and 2D=2786 nm. In all figures 2d=150 nm, $L_C=95$ μm, $L_l=25$ nm. 100

3.5 Predictions of the theoretical model without tissue loading for dimensionless concentration profiles in the cleft and tissue space at different y locations for the high filtration steady state, $P_c=35$ cm H_2O. Protein concentration at x=0, just behind the surface glycocalyx, approaches the convection limit, $(1-\sigma_f)C_c$. Curves y=0 and y=75 nm nearly overlap. The inset shows that the concentration in region C decreases nearly linearly with distance to x=100 μm where tissue concentration is assumed to be the same as in the

Chapter 1 Introduction

1996 marked the 100th anniversary of Starling's (1896) pioneering paper outlining his hypothesis for the filtration and reabsorption of water in capillaries and the formation of lymph. With the notable exception of the chapter by Levick (1995) in *Introduction to Physiology*, nearly every contemporary physiology text has explained Starling's hypothesis in terms of a classic Landis-Starling diagram in which there is net filtration in the capillaries on the arterial side and a nearly equal reabsorption on the venous side due to osmotic forces leaving a small net positive filtration that accounts for the lymph flow. The latter, which has been estimated to be between 2 and 4 liters a day for the entire body, is less than 1 part in 2000 of the daily cardiac output. This widely accepted view was seriously challenged in the provocative review by Levick (1991). Levick shows that if one uses the latest measurements of the local average interstitial oncotic pressure in calculating the combined effective oncotic pressure difference opposing filtration, P_{co}, one finds that in nearly every tissue except the renal capillaries and the gut mucosa the hydraulic pressure in the postcapillary venules significantly exceeds the local value of P_{co} and there should be net filtration rather than reabsorption. This fundamental paradox was a central theme in the 1996 Starling Symposium commemorating Starling's original paper and the focus of a recent review by Michel (1997) summarizing our latest understanding of microvascular fluid exchange.

1.1 Starling's hypothesis

Starling's hypothesis is the basic principle of cardiovascular and renal physiology governing fluid movement in microvascular exchange. He recognized that the rate of the

fluid flow across the capillary is determined by the imbalance of two pressure gradients, the hydraulic and osmotic, which are present between the blood and tissue (Starling, 1896). Starling's hypothesis is universally described by an equation of the form

$$J_v/A = L_p[(P_c - P_i) - \sigma(\pi_c - \pi_i)] \quad (1.1)$$

where J_v/A is the fluid filtration rate across the capillary wall per unit area, L_p is hydraulic permeability of the capillary wall, σ the osmotic reflection coefficient and P_c, π_c and P_i, π_i are global values for the hydrostatic and colloidal osmotic pressures in the plasma and tissue, respectively.

The experimental verification of the Starling hypothesis rests in large measure on the classic experiments of Landis (1930a,b) and Pappenheimer and Soto-Rivera (1948). The former showed that the arterial and venous capillary pressures P_c in the human fingernail-folds at heart level, 32 and 12 mmHg, respectively, bracketed the mean oncotic pressure of plasma, 24 mmHg. It appeared to support the nearly universally held view that there is filtration on the arterial side of the capillaries and reabsorption on the venous side. Pappenheimer and Soto-Rivera introduced the concept of an "isogravimetric state" for whole limbs in which the weight of a whole limb would remain constant when there was no net fluid movement between capillary blood and tissue. The isogravimetric pressure at the local capillary level, P_{co}, is determined by the value of P_c when there is no net fluid flow, $J_v/A=0$, or $P_{co}=P_i+\sigma(\pi_c-\pi_i)$. Pappenheimer and Soto-Rivera (1948) showed that for whole limbs the isogravimetric pressure varied directly with the perfusate oncotic pressure and the gain or loss in weight was proportional to the difference between the mean capillary pressure and its value in the isogravimetric state. It was assumed that when $P_c < P_{co}$ there was net reabsorption in the venular capillaries.

1.2 Discrepancies in the classical application of Starling's hypothesis

The experimental evidence cited in (Landis, 1930a,b and Pappernheimer and Soto-Rivera, 1948) was taken for many years as definitive support for Starlings hypothesis for arterial filtration and venous reabsorption. In 1987, Michel and Phillips performed a provocative experiment on isolated perfused frog mesentery microvessels. Two fundamentally different behaviors were observed. In the transient case where the measurement was made immediately after occluding the vessel, the relation between the transcapillary fluid filtration and the capillary pressure was consistent with the classical Landis-Starling diagram and Pappenheimer and Soto-Rivera's experiments. In contrast, in the steady state experiments the net fluid flow followed the transient behavior when P_c exceeded the perfusate oncotic pressure, whereas there was no reabsorption but a small net positive filtration for all values of pressures below the plasma oncotic pressure. This non-linear relationship in the steady state is also consistent with Guyton and Lindsey's (1959) and Perl *et al.* (1975) experiments on the accumulation of fluid in dog lungs when the left atrial pressure is varied. The former observed that at left atrial pressures above 25 mmHg fluid leaves the capillaries and enters the lung tissue and lung weight varies linearly with the atrial pressure and that at pressures below 25 mmHg the lung weight remains almost constant. These experiments strongly support the view that there is no sustained venous absorption in the steady state and water is filtered out of the continuous capillaries in most tissues except the gut mucosa and renal peritubule.

Levick (1991) also showed that if one uses the most recent measurements of tissue oncotic pressure there should be no oncotic reaborption of water in the venous capillaries

in most tissues and the classic Landis-Starling diagram which predicts arterial filtration and venous reabsorption with a small net lymph flow is not possible.

A new conceptual mathematical model is developed in chapter 2 to explain at the cellular level why there is only oncotic reabsorption at low capillary pressures in the short lived transient experiments of Michel and Phillips (1987), but a positive filtration in their steady state experiments.

1.3 Effective Starling force opposing fluid filtration

If there is no venous reabsorption under steady state conditions, the fluid filtration across the capillary should be consistent with measurements of the low lymphatic flow. Levick (1991) pointed out that the required difference in hydraulic and osmotic pressure, which determined the fluid filtration across the capillary wall, should only amount to 1-2 mmHg. However, the value estimated from experimental measurements in many tissues (Levick, 1991) is much higher than this required value.

1.3.1 Application of Starling's equation

Michel (1997) and Weinbaum (1998) independently proposed a new cellular level model for the effective osmotic barrier that acts across capillary endothelium and the role of small pores in the interendothelial cleft in the determining the Starling forces. According to their hypothesis, the local Starling forces that determine the water flux across capillary endothelium are due to the local difference in hydrostatic and oncotic pressure across the surface matrix layer rather than the global difference in P and π between the plasma and tissue. These ideas will be quantitatively explored in chapters 2

and 3. In chapter 3, our theoretical model is used to explain the new experiments conducted by our collaborators at University of California at Davis (Dr. Fitz-Roy Curry and Roger Adamson) which unequivocally reveal that the effective Starling's force that opposes the fluid filtration across the capillary is not the global difference in driving forces between the plasma and the tissue. This is demonstrated by gently damaging the mesothelium of frog mesentery capillary and loading the tissue to have the same protein concentration as the plasma. One finds that there is only a small change in the fluid filtration compared with the results obtained when albumin was only present in the plasma. This result has been interpreted using a three-dimensional mathematical model in which equation (1.1) is applied locally across the endothelial surface glycocalyx rather than the globally across the entire endothelium. This change, we shall show, will have a profound effect on the predicted magnitude of the Starling forces and lead to a fundamentally new view of the classic Landis-Starling diagram.

The application of the Starling's equation is much more subtle than has been realized. Heretofore, the Starling equation has been applied across the entire transendothelial barrier and the Starling forces evaluated by global measurements of P and π in the plasma and the tissue space. In our new hypothesis and mathematical model, equation (1.1) will be applied locally across the endothelial surface glycocalyx, which we propose is the primary sieve for plasma proteins. The reason is that the oncotic driving force occurs primarily across the protein sieving layer at the endothelial surface, the surface glycocalyx, whereas the filtration driving force occurs across the entire endothelial cell layer. The transendothelial pressure difference is the sum of two pressure drops, one across the surface matrix layer and a second across the interendothelial cleft.

The latter pressure drop is largely due to the presence of the junction strands in the cleft. If there are no oncotic forces in the tissue or plasma, equation (1.1) can be applied across the entire endothelial cell layer, as done in Fu *et al.* (1995 and 1997), since the relationship between velocity and the transendothelial pressure drop is linear and the resistance of the surface matrix and the cleft is simply additive. In contrast, when oncotic forces are present in the plasma and tissue, the effective oncotic force across the surface matrix layer is determined by the local difference in protein concentration between the plasma and the fluid on the cellular side of the matrix layer, rather than, between the plasma and the interstitial fluid. Similarly, the pressure P_i that appears in equation (1.1) should be the local pressure on the cellular side of the glycocalyx, where the effective oncotic pressure is felt, and not the pressure in the tissue space at the cleft exit. The local value of π_i is determined by the protein distribution in the cleft and the latter is non-linearly coupled to the local water flux. This local concentration at the backside of the surface glycocalyx, we shall show, can differ greatly from that in the tissue due to the presence of the junction strand, which inhibits the back diffusion from the tissue to the protected region behind the surface glycocalyx on the lumen side of the junction strand.

1.3.2 Non-convective pathways

Michel (1997) proposed a hypothesis to resolve Levick's paradox (1991) concerning the unexpectedly high oncotic pressures measured in the interstitium of most tissues. The key insight he proposed is that there are two parallel pathways for water and protein transport across the capillary endothelium, one through the cleft, which is convective, and one which is vesicular, or non-convective. Water transport occurs primarily via the cleft pathway. It crosses the surface glycocalyx and then follows a

tortuous pathway through the junctional complex in the interendothelial clefts. In contrast, protein transport occurs through both pathways via large pores. These pores may be very occasional breaks in the glycocalyx or pathways through the endothelial cells, such as vesicles and transcytosis (Michel, 1996). The protein-poor filtrate emerging from the intercellular clefts mixes with the protein-rich solution released by vesicles at the abluminal side of the endothelium in the tissue to become a relatively higher protein concentration in the tissue than the fluid filtrate in the clefts. However, the effective osmotic force, which opposes the fluid filtration, is determined by the local concentration difference across the surface glycocalyx, if the surface glycocalyx is the sieving layer for proteins. Michel hypothesized that this local difference in oncotic pressure across the surface glycocalyx could differ greatly from the global difference between the plasma and the interstitium because the high protein-poor fluid flow through the cleft washes away the protein in the vicinity of the cleft exit and inhibits back diffusion from the tissue upstream into the cleft. Therefore, the fluid filtration across the capillary would be greatly reduced if we use the local value of hydraulic and oncotic pressure across the surface glycocalyx. This concept, which was first applied by Levick (1994) for fenestrated capillaries, is qualitatively correct, but too simple. The barrier that prevents upstream diffusion is not at the cleft exit but at the junction orifices on the luminal side of the cleft. In chapter 4, we will develop a three-dimensional model to predict the detailed protein concentration profiles in the surface glycocalyx, the cleft and the tissue surrounding the cleft exit when there is a parallel non-convective transcellular pathway, which contributes greatly to the total protein flux across the capillary endothelium. The model reveals a fundamental new phenomenon in which back diffusion is maximized when the capillary

pressure is equal to the effective oncotic pressure behind the surface glycocalyx, $\sigma^2\pi_c$, in the high filtration limit. The maximum of back diffusion results from two competing mechanisms. When $P_c>\sigma^2\pi_c$, the protein concentration gradient at the orifice opening decreases as P_c increases because the high water flow at the junction orifice washes away proteins in the vicinity of the junction orifice. When $P_c<\sigma^2\pi_c$, the average concentration behind the surface matrix increases as P_c decreases. Thus, the concentration gradient at the orifice opening decreases which leads to decrease in the back diffusion from the tissue. There is maximum back diffusion, which occurs when the capillary pressure equals the effective oncotic pressure at the high filtration limit, $\sigma^2\pi_c$.

1.4 Mammalian capillaries

Our present mathematical model is based on the microstructural measurements of frog mesenteric capillary using serial-section reconstruction techniques (Adamson and Michel, 1993) and measurements of glycocalyx thickness in Adamson and Clough (1992). There are no ultrastructural studies for mammalian capillaries equivalent to Adamson and Michel (1993) for frog mesentery. However, the structure of the interendothelial cleft and the organization of the junction strand observed in rat heart capillaries by Bundgarrd (1984) is qualitatively similar to frog mesenteric capillaries except that the length of the breaks is much shorter. In addition, the thickness of the surface glycocalyx, 0.4-0.5 μm, as estimated from fluorescent tracers in hamster cremaster muscle capillaries in vivo (Vink and Duling, 1996), is several times the thickness of frog capillaries in Adamson and Clough (1992). The present model for frog mesentery is thus modified to extend our theory to the mammalian capillary. Since L_p of

mammalian muscle capillaries is typically one fifth that of the frog mesentery, one needs to answer the critical question, is the fundamental new model equally valid for mammalian tissue?

1.5 Organization of the thesis

In the present research, a new three-dimensional microstructural model for frog mesenteric capillaries is proposed to explain osmotic behavior at the cellular and sub-cellular level. In particular, we wish to elucidate the structure-function relationship which couples water and solute flows at subcellular levels, namely the surface matrix, interendothelial cleft with its junctional complex and the mixing at the cleft exit. In chapter 2, the detailed distribution of pressure, velocity and concentration in the interendothelial cleft is described for representative arterial and venous pressures in both the steady and transient states. This new model will enable us to elucidate at the cellular level the large spatial heterogeneity in water and solute fluxes that result from the microstructure of the cleft and the mixing processes that occur at the cleft exit. It will lead to a detailed understanding of Michel and Phillips (1987) pioneering experiment, which showed for the first time that there is no venous reabsorption at low capillary pressure when a steady state is achieved, but rather, a small net filtration.

In chapter 3, we present new experimental results on individually perfused microvessels to demonstrate that the effective oncotic pressure across the capillary endothelium is not the global difference in oncotic pressure between blood and tissue. We purposely load the tissue to have the same concentration as the plasma. The results show that there are only small changes in the transcapillary fluid filtration compared with the results obtained when albumin is present only in the perfusate. This finding is interpreted

using a three-dimensional mathematical model of the endothelial cleft, surface glycocalyx and mixing in the tissue space surrounding the cleft exit.

In chapter 4, we will investigate the effect of parallel non-convective pathways on the fluid filtration across the capillary endothelium. The detailed concentration distributions in the surface glycocalyx, the interendothelial cleft and the tissue are described to illustrate the effect of mixing of the protein-rich flux exiting from the non-convective pathway and the protein-poor flux from the intercellular cleft. We also examine the factors that effect the back diffusion through the junction orifice due to elevated concentration in the tissue. The three-dimensional mathematical model is then modified for mammalian capillaries to provide the first predictions of the new microstructural model for mammalian muscle tissue.

Chapter 2 The new microstructural model for osmotic behavior

2.1 Introduction

In Michel (1997) and Weinbaum (1998) a new cellular level model is proposed for the effective osmotic barrier that acts across capillary endothelium and the role of small pores in the interendothelial cleft in determining the Starling forces and lymph flow in most tissues whose primary function is not reabsorption. In this spatially heterogeneous microstructural model the endothelial surface glycocalyx serves as the primary molecular filter for plasma proteins and, thus, the principal barrier that determines the effective oncotic force for water flow across capillary endothelium. According to this hypothesis the local Starling forces that determine the water flux across capillary endothelium are due to the local difference in pressure and solute concentration across the surface matrix layer rather than the global difference in P and π between plasma and tissue. These ideas were first quantitatively explored in the 1997 Whitaker Distinguished Lecture, Weinbaum (1998), where preliminary results for a detailed cellular level microstructural model are presented. In the present paper this mathematical model is more fully developed and detailed calculations are presented for Michel and Phillips' (1987) experiment on single perfused frog mesenteric capillaries and for the case where there is a parallel non-convective large pore transcellular pathway for albumin. This pathway increases the tissue concentration to values typical of those estimated by Levick (1991) for mammalian capillaries. For the latter case we explore the possibility that the presence of the junction

strand with its small pore openings might shield the region between the backside of the surface matrix and the junction strand from the concentration in the tissue space. Such shielding would uncouple the large and small pathways as suggested in Michel (1997).

According to the microstructural measurements of frog mesenteric capillaries by Adamson and Michel (1993), the typical dimensions of the small pores in the junction strand in the transendothelial cleft are 150×20 nm. Compared with the effective diameter of albumin, 7 nm, these pores are too large to be the molecular filter. We thus explore the possibility that the primary sieving layer for albumin, at least in frog mesentery, is the surface glycocalyx, as proposed in Michel (1997) and Weinbaum (1998).

In our new model, equation (1.1) will be applied locally across the surface matrix layer, and π_i will be replaced by the local protein concentration on the tissue side of the matrix layer. Similarly, the pressure P_i that appears in equation (1.1) will be replaced by the local pressure behind the surface glycocalyx, where the effective oncotic pressure is felt. This change will have a substantial effect on the predicted magnitude of the Starling forces and lead to major changes in the classical Landis-Starling diagram. The model has some similarity to that proposed by Taylor and Townsley (1987) in that P_i and π_i are spatially varying. The fundamental difference is that the spatial heterogeneity is not on the length scale of the capillary length, as proposed in Taylor and Townsley (1987), but on the length scale of the junction strand structure length.

Several investigators (Michel, 1984; Taylor and Townsley, 1987; Levick, 1991) have recognized that interstitial hydraulic pressure and interstitial oncotic pressure are dynamic variables, which depend on microvascular fluid flux as well as being a determinant of it. In 1987, Michel and Phillips performed a pioneering experiment on

isolated frog mesenteric microvessels. The variation of J_v/A with P_c was measured while maintaining a constant oncotic pressure in the perfusate. The essential results of this experiment are shown in Fig. 2.1. Two fundamentally different behaviors were observed. One was a short lived transient behavior when measurements were made within 15 to 30 seconds after the pressure was quickly reduced from its maximum value of 43 cmH_2O to some lower value and the tissue washed in protein free Ringer. The second was a steady state behavior that was obtained 2 to 5 minutes after the pressure P_c was changed and maintained constant until a new equilibrium was achieved. In the transient case the results were consistent with a classical Landis-Starling diagram in which there is arterial filtration at high capillary pressure and venous reabsorption at low capillary pressure. One observes a critical pressure for no flow, 24 cmH_2O, and J_v/A varies linearly with P_c about this value. In contrast, in the steady state experiments the net fluid flow followed the transient behavior when P_c exceeded the perfusate oncotic pressure, whereas there was no absorption but a small net positive filtration for all values of P_c below about 20 cmH_2O.

Michel in his 1987 paper developed a simple, but very insightful one-dimensional model, to explain these surprising observations. For the transient case he assumed the tissue oncotic pressure, π_i, was effectively zero, since if the hydraulic pressure is quickly dropped, there is insufficient time for the interstitial oncotic pressure to adjust and absorption will occur. Whereas, if the reduced hydrostatic pressure is maintained, the absorption across the vessel should gradually decrease as protein enters the tissue space until a new steady state equilibrium is achieved. Only if there is a high filtration flow into the interstitium, as in the kidney or intestine, can absorption be sustained (Michel, 1984).

For the steady-state case Michel calculated π_i by assuming that the convection through the capillary wall would eventually establish a condition in the tissue where the interstitial protein concentration C_i would eventually achieve an equilibrium value $C_i=J_s/J_v$, determined by the total water and solute fluxes into the tissue space. Here, J_s is the total protein flux across the capillary endothelium including both diffusion and convection, and J_v is the total fluid flux across the capillary. This relation for C_i would apply if the tissue outside the vessel behaved as a well stirred reservoir in which all the water and proteins passing through the capillary endothelium were thoroughly mixed and there was a uniform protein concentration in the tissue.

An important issue raised in Taylor and Townsley (1987) and Levick (1994) is the spatial heterogeneity of the fluid and protein fluxes in the tissue space at the cleft exit. Michel and Phillips in their one-dimensional model (1987) assumed that the water and solute fluxes are spatially uniform. However, it is clear from the junction ultrastructure of frog mesenteric capillary (Adamson and Michel, 1993) that there is spatial heterogeneity in the water flux along the length of the cleft. Levick (1994) had previously developed a model to examine the effect of local water fluxes through the discrete fenestra of synovial capillaries on near-pore oncotic and hydraulic gradients. He showed that the local flow across fenestrae will dilute the solute immediately outside the fenestrae and thus reduce the local Starling forces in the interstitium. The magnitude of this reduction is, however, small compared to that which can be achieved for continuous capillaries where there is a protective barrier with small pores that prevent back diffusion. A similar analysis to Levick (1994) is developed in Fu *et al.* (1997) for continuous capillaries. Concentration profiles for the non-uniformity in cleft exit concentration due to convection are predicted,

but these are uncoupled from the local oncotic forces that determine the water flow across the surface matrix. In this paper, we will provide a detailed picture as to how these water and solute fluxes relate to cellular level structure, namely the sieving matrix at the endothelial surface, the interendothelial cleft with its junction strand and the mixing region at the cleft exit. We shall also examine how the uniformity in protein concentration assumed in Michel's expression for C_i is achieved and what would happen if there were other parallel non-selective large pore transcellular pathways for protein flux due to, active vesicular transport, connected vesicle channels or transient gaps in the endothelium due to inflammatory agents.

2.2 Model Description

From an ultrastructural viewpoint the idealized model that has been proposed to explore the new hypothesis for the Starling forces is similar to earlier models developed in (Fu *et al.*, 1994; 1997; Weinbaum *et al.*, 1992) to predict the capillary filtration and diffusive permeability coefficients, L_p and P, in frog mesenteric capillary in terms of the structure of the interendothelial cleft and the endothelial surface glycocalyx. A schematic of this model is shown in Fig. 2.2. This ultrastructural model differs from our earlier studies only in that it neglects the narrow continuous 1.5 nm slit in the junction strand proposed in Fu *et al.* (1994). This narrow slit could also serve as an osmotic barrier. However, it would allow only a small additional water flux due to its large hydraulic resistance. Furthermore, Fu *et al.* (1998) have shown that a small tracer, Na fluorescein (0.8 nm), does not appear to cross this barrier indicating that if the slit is patent, its gap height is significantly less than 1.5 nm.

The model in Fig. 2.2 contains four regions. The first region is a surface glycocalyx of thickness L_f which covers the entire endothelial surface including the entrance region to the interendothelial cleft. Using cationized ferritin as a tracer to delineate the outer regions of this surface matrix, Adamson and Clough (1992) have estimated from electromicrographs that this surface layer is of roughly 0.1 μm thickness in frog mesenteric capillary. Furthermore, if this layer is to serve as the molecular sieve for proteins the size of albumin or larger, then the spacing of the fibers in this matrix is approximately 7 nm. An even thicker surface layer of 0.4 to 0.5 μm is observed *in vivo* in hamster cremaster capillaries, Vink and Duling (1996). However, the theoretical model in Fu *et al.* (1994) predicts that a sieving matrix layer of this thickness would offer too much

hydraulic resistance for the frog mesenteric capillary and that a more accurate estimate for this tissue is 0.1 μm. The second region is the cleft proper, region A. Serial section reconstructions of the junction strand in frog mesentery (Adamson and Michel, 1993) reveal a junction strand with discontinuous breaks or pores that are on average 150 nm long with a spacing that varies between 2 and 5 μm. The depth of the cleft is 0.4 μm and the gap height of the breaks, 20 nm, is the same as the nearly uniform wide part of the cleft.

In the model the pericapillary space is broken into two regions, a semicircular region B of 5 μm radius which surrounds the cleft exit, and a far field, region C. The radius of region B, L_B, is determined by the average spacing of the clefts, 10 μm, along the cross-sectional perimeter of the capillary. Region B describes the mixing of the wakes from the individual junction strand discontinuities in the tissue space immediately surrounding the cleft exit. In the event that there is an additional non-selective parallel pathway for plasma proteins, the concentration at the edge of region B can be elevated and its value specified. To explore what would happen if there were a large pore parallel pathway, we shall assume a typical value of the protein concentration at the edge of region B, C_a, which has been measured in many mammalian tissues, 0.4 C_c (Levick, 1991). In region C, the exit jets from the individual junction orifices and adjacent clefts merge with each other and form a uniform flux along the length of the cleft exit in the tissue space beyond region B. Therefore, region C can be approximated by a one-dimensional convection-diffusion model averaged across the height (thickness) of the tissue layer.

2.3 Mathematical formulation

2.3.1 Pressure and velocity field

(1) Fiber Matrix Layer

The fiber matrix layer lies in front of the cleft and covers the entire endothelial surface. This continuous fiber layer is assumed to have a uniform thickness L_f. For pure filtration, Darcy's law can be applied locally across the fiber layer along the length of the cleft in the y direction.

$$\overline{V}(y) = \frac{K_p}{\mu}\frac{P_c - P(0,y)}{L_f}. \tag{2.1}$$

Here K_p is the Darcy permeability, μ is the fluid viscosity and $\overline{V}(y)$ is the local average velocity at location y. P_c and P(0,y) are pressures in the lumen and at the entrance to the cleft behind the surface glycocalyx, respectively. This simple one-dimensional approximation can be applied across the surface matrix because pressure gradients, and hence velocities in the x direction are nearly two orders of magnitude greater than in the y direction.

If plasma proteins are present the local velocity across the fiber matrix layer is the resultant of two opposing forces, a hydraulic filtration pressure and an oncotic force. If the local oncotic force across the surface layer is considered, equation (2.1) can be written as:

$$\overline{V}(y) = \frac{K_p}{\mu L_f}\left[P_c - P(0,y) - \sigma_f(\pi_c - \pi(0,y))\right], \tag{2.2}$$

where σ_f is the reflection coefficient in the fiber matrix. $\pi(0,y)$ and π_c are osmotic pressures just behind the fiber matrix at x=0 and in the lumen, respectively. The colloid

osmotic pressure π (cmH_2O) is related to the concentration C (mg/ml) by the empirical relation (Landis and Pappenheimer, 1963):

$$\pi = 0.3808C + 2.448\times10^{-3}C^2 + 1.632\times10^{-5}C^3. \quad (2.3)$$

This equation is for 37 °C temperature, which needs to be corrected for frog mesentery at 20 °C.

Note both P(0,y) and π(0,y) vary along the length of the cleft entrance in equation (2.2). Equation (2.2) differs fundamentally, from equation (1.1) in that it is applied locally across just the surface sieving layer, rather than in a global sense across the entire endothelial layer.

(2) Region A; Cleft

Region A can be split into two subregions. Region 1 with depth L_1, $0\le x\le200$ nm, lies upstream of the junction strand behind the fiber matrix layer and region 2 with depth L_2 lies downstream of the junction strand, $200\le x\le400$ nm. The thickness of the junction strand, can be neglected compared to L_1 and L_2 and treated as a zero-thickness barrier, see Fig. 2.2.

Since the height of the cleft 2h is small compared to both the average distance between the pores 2D and the depths L_1 and L_2 of the cleft, the water flow in the wide part of the cleft can be approximated by a Hele-Shaw flow as first proposed in Tsay and Weinbaum (1989). Thus the velocity in the cleft can be expressed as:

$$\mathbf{V}(x,y,z) = \mathbf{V}_0(x,y)\left(1-\frac{z^2}{h^2}\right) \quad \text{and} \quad \mathbf{V}(x,y,z) = u(x,y,z)\mathbf{i} + v(x,y,z)\mathbf{j} + 0\mathbf{k}, \quad (2.4)$$

which satisfies the non-slip condition u=v=0 at $z=\pm h$ see Fig. 2.2b. $\mathbf{V}_0(x,y)$, the velocity in the center plane z=0, is given by:

$$\mathbf{V}_0(x,y) = -\frac{h^2}{2\mu}\nabla P \quad \text{and} \quad \mathbf{V}_0(x,y) = u_0(x,y)\mathbf{i} + v_0(x,y)\mathbf{j}. \tag{2.5}$$

For Hele-Shaw flow, the pressure in the cleft satisfies:

$$\frac{\partial^2 P}{\partial x^2} + \frac{\partial^2 P}{\partial y^2} = 0. \tag{2.6}$$

Note a two-dimensional pressure field is required to describe the flow in the cleft although L_1 and L_2 are not much greater than the thickness L_f of the matrix layer. This is required because pressure gradients in the x and y directions become comparable at the junction orifice due to the convergence of the fluid streamlines.

At x=0, the pressure and u component of velocity at rear of the surface matrix layer must equal the pressure and average value of u at the cleft entrance. The flow behind the matrix has a slip plane for the v component of the velocity. This is quite realistic since this slip occurs over a distance which is about half the channel height (Fu *et al.*, 1994). This thin fiber interaction layer is small compared to the half depth of the cleft. Integrating equation (2.5) over the height of the cleft, one finds the average velocity $\bar{\mathbf{V}}(x,y)$ is given by $\bar{\mathbf{V}}(x,y) = \frac{2}{3}\mathbf{V}_0(x,y)$.

Combining equations (2.3)-(2.5) one obtains the first matching condition at x=0:

$$P_c - P(0,y) - \sigma_f(\pi_c - \pi(0,y)) = -\frac{B^2 L_f}{3K_p}\left.\frac{\partial p^{(1)}}{\partial x}\right|_{x=0^+}. \tag{2.7a}$$

One notes that P(0,y), $\pi(0,y)$ and $\left.\frac{\partial P^{(1)}}{\partial x}\right|_{x=0^+}$ are all unknown and equation (2.7a) is a non-linear coupling condition. The other boundary and matching conditions for equation (2.6) are:

$$x = L_1 \qquad d < |y| \le D \qquad \frac{\partial P^{(i)}}{\partial x} = 0 \qquad i = 1,2 \tag{2.7b}$$

$$x = L_1 \qquad |y| \le d \qquad P^{(1)} = P^{(2)} \qquad \frac{\partial P^{(1)}}{\partial x} = \frac{\partial P^{(2)}}{\partial x} \tag{2.7c}$$

$$x = L \qquad |y| \le D \qquad P^{(2)} = P_i \tag{2.7d}$$

$$0 \le x \le L \qquad y = 0, D \qquad \frac{\partial P^{(i)}}{\partial y} = 0 \qquad i = 1,2. \tag{2.7e}$$

Boundary conditions equations (2.7b, c) require that the junctional strand be impermeable except at the junctional break and the pressure and velocity in the junctional breaks be continuous. Boundary condition equation (2.7d) requires that the pressure be continuous at the tissue front. Boundary conditions equation (2.7e) are the periodicity and symmetry conditions.

Interstitial hydraulic resistance is of minor importance in the present application because of the high permeability of interstitial matrix compared to the capillary wall. Therefore, the pressure drop in regions B and C will be neglected and a uniform pressure P_i is assumed which is -2 cmH_2O (Guyton, 1963).

2.3.2 Concentration field

(1) Fiber Matrix Layer

One-dimensional convection-diffusion is assumed locally across the surface matrix layer in front of the cleft entrance. The results of our model show that concentration gradients in the x direction in the matrix layer are more than two orders of magnitude

greater than in the y direction. The governing equation for solute conservation is, therefore,

$$D_f \frac{d^2C(x,y)}{dx^2} = \bar{u}_s(y)\frac{dC(x,y)}{dx}, \tag{2.8}$$

where $\bar{u}_s(y)$, the solute average velocity in the cleft, is related to $u_0(0,y)$, the water velocity in the center plane by $\bar{u}_s(y) = \frac{2}{3}\chi_f u_0(0,y)$. Here χ_f and D_f are the retardation and effective solute diffusion coefficients in the matrix layer, respectively.

The boundary and matching conditions for equation (2.8) are:

$$x = -L_f \qquad C = C_c, \tag{2.9a}$$

$$x = 0 \qquad C = C(0,y), \tag{2.9b}$$

$$-D_f\frac{\partial C}{\partial x}\Big|_{x=0^-} + \frac{2}{3}\chi_f u_0(0,y)C(0,y) = -D_c\frac{\partial C}{\partial x}\Big|_{x=0^+} + \frac{2}{3}\chi_c u_0(0,y)C(0,y). \tag{2.9c}$$

where χ_c and D_c are their values in the wide part of the cleft. Boundary conditions equations (2.9b,c) require that the protein concentration and solute flux be continuous at the cleft entrance, x=0.

Solving equation (2.8) subject to boundary conditions equations (2.9a,b), we find:

$$C = \frac{C_c - C(0,y)}{1 - e^{-Pe_f}}\left(1 - e^{Pe_f\frac{x}{L_f}}\right) + C(0,y), \tag{2.10}$$

where

$$Pe_f = \frac{2}{3}\frac{\chi_f u_0(0,y)L_f}{D_f} \tag{2.11}$$

is the local Peclet number in the surface matrix layer.

Substituting equation (2.10) into equation (2.9c), one obtains a second non-linear coupling condition between velocity and protein concentration at the rear of the surface glycocalyx:

$$D_f\left(\frac{C_c - C(0,y)}{1-e^{-Pe_f}}\right)\frac{Pe_f}{L_f} + \frac{2}{3}\chi_f u_0(0,y)C(0,y) = -D_c\frac{\partial C}{\partial x}\bigg|_{x=0^+} + \frac{2}{3}\chi_c u_0(0,y)C(0,y). \quad (2.12)$$

Note C(0,y), $u_0(0,y)$ and P(0,y) are all unknown and non-linearly coupled through equations (2.7a) and (2.12). They can not be solved for separately, but must be determined by the solution of the overall boundary value problem for u, P and C.

(2) Region A; Cleft

The governing equation for solute concentration in the cleft can be approximated by a steady two-dimensional convection-diffusion equation averaged across the cleft height.

$$D_c\left(\frac{\partial^2 C(x,y)}{\partial x^2} + \frac{\partial^2 C(x,y)}{\partial y^2}\right) = \frac{2}{3}\chi_c\left(u_0(x,y)\frac{\partial C(x,y)}{\partial x} + v_0(x,y)\frac{\partial C(x,y)}{\partial y}\right). \quad (2.13)$$

A two-dimensional concentration field must be used to describe the cleft since x and y gradients and velocity components are of comparable magnitude in the vicinity of the junction strand orifice.

In addition to equations (2.7a) and (2.12) the remaining boundary and matching conditions for solute transport for equation (2.13) are:

$$x = L_1 \qquad |y| \le d \qquad C^{(1)} = C^{(2)} \qquad \frac{\partial C^{(1)}}{\partial x} = \frac{\partial C^{(2)}}{\partial x}, \quad (2.14a)$$

$$x = L_1 \qquad d < |y| \le D \qquad -D_c\frac{\partial C^{(1)}}{\partial x} + \frac{2}{3}\chi_c u_0 C^{(1)} = 0 \quad (2.14b)$$

$$-D_c\frac{\partial C^{(2)}}{\partial x} + \frac{2}{3}\chi_c u_0 C^{(2)} = 0, \quad (2.14c)$$

$$x = L \qquad |y| \le D \qquad \left(-D_c \frac{\partial C^{(2)}}{\partial x} + \frac{2}{3}\chi_c u_0 C^{(2)}\right)\Big|_{x=L} * 2B = q(y), \quad (2.14d)$$

$$0 \le x \le L \qquad y = 0, D \qquad \frac{\partial C^{(i)}}{\partial y} = 0 \qquad i = 1,2. \quad (2.14e)$$

Boundary condition equations (2.14a-c) require that the junctional strand be impermeable except for the pore region $|y| \le d$. Matching condition equation (2.14d) is the equation for the local solute flux q(y) entering the tissue at the cleft exit. Boundary conditions equation (2.14e) are the periodicity and symmetry conditions.

(3) Region B; Cleft Exit Near Field

The average distance between neighboring clefts in the vessel wall is typically 10 μm. The gap height of the wide part of the cleft is merely 20 nm, which is much smaller than the radius of region B, 5 μm. Thus, the solute flux at the cleft exit can be treated as a line source of variable strength along the length of the cleft exit in the y direction. Since gradients in the y direction near the cleft exit are smaller than radial gradients, the governing equation for this region is

$$D_t\left(\frac{\partial^2 C(r,y)}{\partial r^2} + \frac{1}{r}\frac{\partial C(r,y)}{\partial r}\right) = \chi_t v_r \frac{\partial C(r,y)}{\partial r}. \quad (2.15)$$

Here D_t and χ_t are the solute diffusion and the protein retardation coefficients in the tissue and v_r is the radial velocity in region B. As the solute spreads from the cleft exit y gradients do become comparable to r gradients, but here the results show that both gradients are greatly reduced and equation (2.15) is still a reasonable if not accurate approximation.

The boundary and matching conditions for equation (2.15) are equation (2.14d) and

$$C^{(2)}\big|_{x=L} = C\big|_{r=B} \qquad \text{at} \quad r = B, \tag{2.16a}$$

$$\left(-D_t \frac{\partial C}{\partial r} + \chi_t v_B C\right)\Big|_{r=B} * \pi B = q(y) \qquad \text{at} \quad r = B, \tag{2.16b}$$

$$C(L_B) = C_a \qquad \text{at} \quad r = L_B, \tag{2.16c}$$

Here L_B, the radius of the intermediate region B, is the average half spacing between adjacent clefts, and q(y), the local solute flux at the cleft exit, is obtained from equation (2.14d). C_a is the solute concentration at the interface between regions B and C.

From simple continuity arguments, the radial velocity in the intermediate region B, v_r decays as 1/r, if the lateral spread of the cleft exit jet in the y direction is neglected. This is a reasonable approximation for a line source that is slowly varying along its length. Thus,

$$v_r(r,y) = \frac{B}{r} v_B(y), \tag{2.17a}$$

where

$$v_B(y) = \frac{4}{3\pi} u_0(x,y)\big|_{x=L}, \tag{2.17b}$$

is the locally varying average velocity at $r = B$, the cleft exit.

In the absence of convection, $v_r = v_B = 0$, the solution of equation (2.15) for the concentration in the tissue in region B is

$$C(r,y) = \frac{q(y)}{\pi D_t} \ln(L_B / r) + C_a. \tag{2.18}$$

If $v_r \neq 0$, the solution to equation (2.15) which satisfies equations (2.16b, c) and (2.17) is:

$$C(r,y) = C_a\left(\frac{r}{L_B}\right)^{Pe_t} + \frac{q(y)}{\pi B \chi_t v_B}\left[1-\left(\frac{r}{L_B}\right)^{Pe_t}\right], \tag{2.19a}$$

where

$$Pe_t = \frac{\chi_t v_B B}{D_t}. \tag{2.19b}$$

If there is a parallel non-selective pathway through the vessel wall, such as vesicular transport, the protein concentration in the tissue will be elevated. In this case the concentration at $r=L_B$ will be prescribed and we shall use the estimate $C(L_B)\cong 0.4C_c$ suggested by the data in Levick (1991). For the case where $C_i=J_s/J_v$, as proposed by Michel and Phillips (1987), C_a is unknown and provides a matching condition with region C, which is described next.

(4) Region C; Tissue Space Far Field

In region B the exit jets from the individual junction orifice and adjacent clefts merge with each other and form a uniform flux along the length of the cleft exit. Therefore, region C for frog mesentery can be approximated by a one-dimensional convection-diffusion equation averaged across the height of the tissue layer H,

$$D_t \frac{d^2C(x)}{dx^2} = \chi_t v_c \frac{dC(x)}{dx}. \tag{2.20}$$

The boundary conditions for equation (2.20) are

$$-D_t \frac{dC(x)}{dx} + \chi_t v_c C(x) = q_c \qquad \text{at } x=0, \tag{2.21a}$$

$$C=C_i \qquad \text{at } x=L_c, \tag{2.21b}$$

where q_c is average solute flux per unit tissue area normal to the flow direction. q_c is given by

$$q_c = \frac{N_c}{2H}\frac{J_s}{D}, \tag{2.22}$$

where N_c is the number of clefts on the half surface of the vessel and H is the height of tissue layer. J_s, the average flux per unit cleft length, is given by equation (A3) in the Appendix. v_c in equation (2.21) is the average velocity in region C which can be expressed as

$$v_c = \frac{N_c}{2H}\frac{J_v}{D}, \tag{2.23}$$

where J_v, the average water flux per unit cleft length, is given by equation (A4) in Appendix.

The solution to equation (2.20) subjected to the boundary conditions equations (2.21a, b) is

$$C = (C_i - \frac{q_c}{\chi_t v_c})e^{\frac{\chi_t v_c}{D_t}(x-L_c)} + \frac{q_c}{\chi_t v_c}. \tag{2.24}$$

Substituting x=0 into equation (2.24) and evaluating the solute concentration at the edge of region B, one obtains

$$C_a = (C_i - \frac{q_c}{\chi_t v_c})e^{-\frac{\chi_t v_c}{D_t}L_c} + \frac{q_c}{\chi_t v_c}. \tag{2.25}$$

For Michel and Phillips (1987), experiment equation (2.25) relates the concentration C_a to the concentration $C_i=J_s/J_v$, which is given by equation (A5) in the Appendix.

(5) Method of Solution

The original boundary value problem, which was formidable due to the non-linearity of the equations and matching conditions and the different length scales of the four different regions in Fig. 2.2, has been greatly simplified by the analytic solutions for the surface matrix layer and regions B and C in the tissue. The overall boundary value

problem has been reduced to that of obtaining a numerical solution, albeit for a system of non-linear equations and boundary conditions, for a single region, the cleft itself, region A. Regions B and C could have been treated numerically using a two-dimensional computer code but this would have greatly expanded computational costs with no new insight into the essential physics.

The simplified boundary value problem for region A just described has been solved using a time dependent relaxation technique. Instead of solving equations (2.6) and (2.13), we solve an initial value problem for their time dependent counterparts,

$$\frac{\partial P}{\partial t} = \frac{\partial^2 P}{\partial x^2} + \frac{\partial^2 P}{\partial y^2} \tag{2.26}$$

and

$$\frac{\partial C}{\partial t} = D_c\left(\frac{\partial^2 C}{\partial x^2} + \frac{\partial^2 C}{\partial y^2}\right) - \frac{2}{3}\chi_c\left(u_0\frac{\partial C}{\partial x} + v_0\frac{\partial C}{\partial y}\right). \tag{2.27}$$

When t approaches infinity, P and C relax to their steady state values, i.e., $\frac{\partial P}{\partial t} = 0$ and $\frac{\partial C}{\partial t} = 0$, which is the solution of the original problem. Finite-difference approximations are employed for the derivatives in equations (2.26), (2.27) and the corresponding boundary conditions, equations (2.7), (2.12) and (2.14). Arbitrary initial conditions can be used at each point. For convenience, we have assumed uniform pressure and concentration as initial conditions in the cleft. During each iteration, pressure and concentration at each mesh point are calculated from difference equations derived from equations (2.26) and (2.27), except for boundary mesh points which are required to satisfy the matching conditions and boundary conditions given by equations (2.7), (2.12) and (2.14). Because the pressure and concentration fields are coupled, these two fields are

calculated simultaneously. The numerical solution is advanced in time until every mesh point converges and satisfies a convergence condition that the relative error between the n^{th} and $(n+1)^{th}$ iteration values for P and C at each point, $\left|\frac{P^{(n+1)} - P^{(n)}}{P^{(n)}}\right|$ and $\left|\frac{C^{(n+1)} - C^{(n)}}{C^{(n)}}\right|$, differ by less than 10^{-6}.

2.4 Parameter values

2.4.1 Parameter values for anatomical structure

The thickness of fiber matrix layer L_f=150 nm and the average spacing of these breaks 2D=4320 nm has been chosen to satisfy the measured value of L_p=2.46*10^{-7} cm/s/cmH_2O (Michel and Phillips, 1987). The other values for describing the cleft geometry in Fig. 2.2 are the same as Fu *et al.* (1994), which are based on the measurements for frog mesenteric vessels. The cleft depth L=400 nm and height of wide part of the cleft 2h=20 nm. Junction breaks 2d*2h=150 nm*20 nm are centered at y=0. The radius of region B, L_B=5 μm. The length of Region C, 100 μm, is a typical half spacing for frog mesenteric capillaries.

2.4.2 Parameter values for transport

The osmotic reflection coefficient for albumin in the fiber matrix, σ_f=0.9 (Michel and Phillips, 1987). Since the molecular radius of Ficoll 70 is a little larger than that of albumin, σ_f=0.94 is assumed for Ficoll 70. A reasonable value for the reflection coefficient in the cleft for either molecule is σ=0.1. This estimate is based on calculations for the hydrodynamic interaction of a sphere with the plasmalemma boundaries. There are few measured values for the interstitial reflection coefficient. In this paper, we have used the simplifying assumption that σ_t=0 and χ_t=1 in the absence of better data.

An approximate theory for determining the diffusion coefficient D_f in a fiber matrix which takes account of both the hydraulic resistance and the steric hindrance of the fibers is given in Weinbaum *et al.* (1992). However, there is no adequate theory to predict the

diffusion coefficient, when proteins are of comparable or larger size than the fiber spacing or if the fibers are not rigid. In this paper, we have been able to circumvent this difficulty by requiring the model to provide an optimum fit of the steady state filtration profile obtained in Michel's experiment shown in Fig. 2.1. This comparison is shown in Fig. 2.10 of this paper and will be discussed later in greater detail. The model predicts a dense matrix whose value for D_f for albumin is 3 to 4 orders of magnitude smaller than its value in solution. This value of D_f refers only to the matrix at the entrance to the cleft pathway and should not be confused with the total measured permeability. The latter also includes active transport of albumin, vesicle channels and transient endothelial gaps. The diffusion coefficient D_c in the cleft is a restricted diffusivity given by Ganatos (1981) for a sphere diffusing in a channel without a matrix. The wide part of the cleft can be thought of as an adherens junction that contains cross bridging proteins. This should not greatly decrease D_c since these proteins appear in either localized regions or are widely dispersed. We have estimated the diffusion coefficient in the tissue D_t as $0.13D_\infty$ which is based on the measured value $D_t/D_\infty=0.14$ for Dextran fluorescein isothiocyanate 19,100 (Stokes radius=3.12 nm) (Fox and Wayland, 1979).

2.5 Results

To facilitate the discussion in the next section the results are presented under three headings: (1) Mathematical modeling of Michel and Phillips' experiments, (2) Analysis of parallel pathway and (3) Effect of D_f on filtration-pressure curve.

2.5.1 Mathematical modeling of Michel and Phillips' experiments

Key results corresponding to Michel and Phillips (1987) steady state and transient experiments in Fig. 2.1 are shown in Figs. 2.3, 2.4, 2.5 and 2.6 where detailed profiles are presented for the pressure, velocity and protein concentration profiles for three representative conditions: (A) high capillary pressure, (B) low capillary pressure steady state and (C) low capillary pressure transient state. The results in Fig. 2.3 are for a high filtration state corresponding to a high capillary pressure of P_c=43 cmH_2O. In this high filtration state, there is a little difference between the steady state and transient results in Fig. 2.1. The results in Figs. 2.4 and 2.5 show representative solutions for the steady state and transient profiles, respectively, corresponding to a low capillary pressure of P_c=15 cmH_2O, typical of venous capillaries, where one would normally anticipate venous reabsorption.

Pressure and concentration profiles are plotted at $x=-L_f$, in front of the surface matrix layer where we assume the pressure and concentration are constant; x=0, just behind the fiber matrix layer at the cleft entrance; $x=200^-$ nm and $x=200^+$ nm, just upstream and downstream of the junction strand and x=400 nm, the cleft exit where the tissue pressure is constant at -2 cmH_2O as mentioned earlier. The pressure and concentration profiles at $x=200^-$ and $x=200^+$ nm have been omitted in Figs. 2.3c, 2.4a,c

and 2.5c because these profiles are nearly identical to the profiles at x=0 and x=400 nm, respectively. The detailed concentration profiles in the cleft are shown on an enlarged scale in Fig. 2.6. The u component of the velocity profiles is shown only at x=0 and 400 nm in Figs. 2.3b, 2.4b and 2.5b since the u component of the velocity vanishes along the junction strand except at the break. However, more insightful for understanding the osmotic behavior is not the net u component profiles at x=0, but the separate u profiles for the hydraulic pressure and oncotically driven components of the local water flux, because the net u profile is the resultant of these two opposing flow components. Figs. 2.6a, b provide a blow up of the concentration distribution within the cleft, where profiles are shown for y=0, the orifice centerline; y=75 nm, the edge of the orifice and three other representative values of y along the length of the cleft, y=150, 1080 and 2160 nm, the last corresponding to y=D, the half spacing of the neighboring orifices.

(A) High Capillary Pressure

As shown in Fig. 2.3a, where P_c=43 cmH_2O, the pressure drop across the surface matrix layer along the cleft is approximately one half of the total transendothelial pressure drop except for the region in front of the orifice break in the junction strand. One notes in Fig. 2.3b that the u profiles at the entrance, x=0, and exit, x=400 nm, are not the same although the junction strand is located at the midpoint of the cleft depth. This differs from our previous model (Fu *et al.*, 1994; 1997) where the hydraulic resistance of the surface matrix was distributed evenly over the entire region, x<200 nm, in front of the junction strand and the profiles were identical. In contrast, if the fiber matrix is treated as a distinct fiber layer in the region, $-L_f$<x<0, in front of the cleft entrance, the fiber matrix will broaden the velocity profile on the luminal side of the junction strand and reduce the

peak velocity at y=0. The streamlines on the tissue side of the junction strand are much more constrained after they pass through the junction orifice and spread to a width at the cleft exit that is approximately three times the width of the orifice opening. The intriguing result for the velocity profiles is that the pressure driven component is nearly identically balanced by the osmotically driven component except for the region in the vicinity of the orifice opening, producing a net u profile that vanishes all along the cleft except in this region.

In Fig. 2.3c, the first surprising result is that the protein concentration at the cleft exit, x=400 nm, is uniform. Since the velocity profile at x=400 nm in Fig. 2.3b has a sharp peak below the orifice in the junction strand, one might expect that more protein will be washed away in this region and the exit concentration reduced. The value of $C_i=J_s/J_v$ proposed in (Michel and Phillips, 1987) has been applied at the edge of region C, in this case x=100 μm, yet the protein concentration at x=400 nm, the cleft exit, differs insignificantly on the scale shown from this value of C_i. This indicates that the protein concentration is uniform in the entire pericapillary region, when the only pathway for transendothelial protein transport is through the cleft. The second surprising result is that the protein concentration varies little within the cleft itself. The concentration profiles at x=0 and x=400 nm differ by less than three percent of the plasma concentration at any value of y. The detailed concentration profiles within the cleft for this case are shown in Fig. 2.6a.

(B) Low Capillary Pressure, Steady State

There are several fundamental differences between the profiles in Fig. 2.4, where P_c=15 cmH_2O, and those just described for the high filtration state. The pressure drop

across the fiber matrix layer, see Fig. 2.4a, far exceeds the pressure drop within the cleft itself. The striking result in Fig. 2.4b is that there is virtually no net water flow across the surface glycocalyx along the entire length of the cleft. The separate contributions of the hydrostatic pressure and the oncotic pressure to the net water flux almost cancel everywhere, including over the orifice opening. There is no net absorption at any y location, although the hydraulic pressure, 15 cmH_2O, is much lower than the plasma oncotic pressure, 26 cmH_2O. The concentration at the cleft exit has now risen to a value that is 32 percent of the plasma concentration, but the concentration gradient within the cleft is again remarkably small as shown in detail in Fig. 2.6b, where one observes that the concentration varies by less than one percent of the plasma concentration along the orifice centerline y=0. Nearly the entire concentration gradient is experienced across the surface glycocalyx, as in the high filtration state, but this time the oncotic force is sufficient to balance the filtration pressure everywhere. The pressure drop within in the cleft, Fig. 2.4a, is greatly diminished because the net filtration velocity u has nearly vanished everywhere.

(C) Low Capiliary Pressure, Transient State

In the case of the transient flow with P_c=15 cmH_2O, we assume the pressure is suddenly decreased from 43 cmH_2O to 15 cmH_2O and there is insufficient time for the tissue concentration to change from a pre-existing condition in which a high flow of protein-free perfusate washes over the tissue. Thus, we assume the concentration at the cleft exit is zero. The intriguing result in Fig. 2.5a is that the pressure inside the cleft is negative everywhere and lower than that at the cleft exit, -2 cmH_2O. The pressure at x=0 just behind the fiber matrix is nearly –7 cmH_2O and rises slightly above the orifice

opening. This negative pressure gradient is required to suck fluid from the tissue through the cleft before it can be absorbed across the surface glycocalyx into the capillary, as clearly shown in Fig. 2.5b. The oncotic pressure difference across the surface matrix layer, about 22 cmH_2O, exceeds the hydrostatic pressure drop across the surface layer, especially in the vicinity of the orifice opening, and there is negative velocity at x=0 and x=400 nm in the neighborhood of the breaks in the junction strand. The solute concentration within the cleft behind the surface matrix layer has adjusted such that the total oncotic pressure across this layer has nearly cancelled the net hydrostatic difference (15 cmH_2O minus –7 cmH_2O or 22 cmH_2O) except in the vicinity of the orifice opening. Note, once again that the net water flux vanishes everywhere except over the orifice.

2.5.2 Analysis of parallel large pore pathway

Figs. 2.3 and 2.4 describe conditions where the entire protein flux passes through the interendothelial cleft and an equilibrium state $C_i=J_s/J_v$ is established somewhere in the tissue space. In addition to the breaks in the cleft, a large non-selective pore may also contribute to protein transport. This pore can take the form of active vesicle transport, channels of fused vesicles or of transient gaps in an inflammatory response (Michel, 1997). Thus, in Fig. 2.7 we show the model predictions for the concentration profiles that would result if there is a parallel non-selective pathway for proteins, which would raise the concentration at the edge of region B to $0.4C_c$, a typical value for mammalian capillaries (Levick, 1991). All other conditions are the same as those shown in Fig. 2.3 where the capillary pressure, P_c=43 cmH_2O. This new value of C_a in the tissue space, which is more than six times the value of $C_i=0.063C_c$, shown in Figs. 2.3c and 2.6a, is due to the superposition of two fluxes, one through the cleft and a transcellular flux. The

remarkable result is that there is little change in the protein concentration profile at x=0, just behind the surface matrix layer in Fig. 2.7, and the corresponding profile in Fig. 2.3c, although there are now large concentration gradients within the cleft on the tissue side of the junction strand, at the cleft exit and in the pericapillary space as observed in Figs. 2.8a, b. The concentration in the protected region, $0<x<200$ nm, is very close to the predicted value for the convective limit, $C=(1-\sigma)C_c$. This striking new predication will be explained in the Discussion.

Fig. 2.8a shows both the cleft region A and the exit mixing region B, while Fig. 2.8b in a blow up of just region A to elucidate the important difference in behavior upstream and downstream of the junction strand. Because the concentration profiles at x=0 are almost unaltered, the pressure and velocity profiles are nearly the same as shown in Fig. 2.3a, b. Note that the protein concentration at the cleft exit is non-uniform and has a value close to that at the edge of region B, except the vicinity of the orifice opening, where the fluid flow washes the protein away and dilutes the solute concentration, a result similar to that observed for fenestrated capillaries (Levick, 1994). The solute profiles in the cleft at low capillary pressures, P_c=15 cmH_2O, are shown in Fig. 2.8c. In this case the net filtration is very low and the back diffusion into the cleft is more significant, even upstream of the junction strand. This back diffusion at low capillary pressures will be reduced if there are some matrix components in the cleft and the diffusion coefficient in the cleft, D_c, is decreased.

The upper set of curves in Fig. 2.9 for $C_a=0.4C_c$ clearly shows the dramatic difference in the net filtration predicted using the classical application of equation (1.1), where the Starling forces are based on the global transendothelial difference in

concentration and pressure between the plasma and tissue space, and the present spatially heterogeneous model where the oncotic and pressure forces are due to the local concentration and pressure differences across the surface matrix layer. Results are shown for two values of D_c, D_∞ and a value which is the same as in the tissue, $0.13D_\infty$. In the global model, the fluid flux per unit area through the capillary wall is calculated from equation (1.1) using the same hydraulic permeability L_p as in our spatially heterogeneous model. One observes that the new model predicts a marked reduction in filtration, which is especially significant for the lower value of D_c, when the capillary pressure is less than the plasma oncotic pressure. For this lower value of D_c the reduction in flux is more than a factor of five when $P_c<20$ cmH_2O. The large difference between the predictions of equation (1.1) and the new model is largely due to the fact that the protein concentration behind the surface matrix layer is far lower than in the tissue space as already noted in Figs. 2.7 and 2.8.

Fig. 2.9 also shows the predictions for Michel and Phillips experiment where all the solute transport is assumed to pass through the cleft. The difference between the dot-dash-dot curve, $C_a=0.4C_c$, and the dashed curve, $C_a=J_s/J_v$, for $D_c=D_\infty$ is due to back diffusion from the tissue space when $C_a=0.4C_c$. The dashed curve, thus, provides a lower limit for the fluid flux when the non-selective parallel pathway is removed.

2.5.3 Effect of D_f on filtration-pressure curve

Fig. 2.10 shows the effect of the diffusivity of the surface matrix layer, D_f, on the filtration pressure curve. Also shown is the transient response when the tissue is bathed in a protein–free perfusate and the protein concentration at the cleft exit is zero. As Michel and Phillips (1987) predicted, in the transient state there is absorption at low capillary

pressures and one obtains a classic Landis-Starling response. This transient response is nearly independent of D_f for $D_f<0.001D_\infty$ and changes only with the osmotic reflection coefficient, whose value has been fixed at $\sigma=0.94$ for all curves in Fig. 2.10. The other four curves correspond to different values of D_f in the surface matrix layer. The bend in the curves for J_v vs. P_c at steady state becomes more abrupt as D_f is decreased. As D_f decreases, the osmotic force across the surface matrix layer is increased since less solute can diffuse across the surface glycocalyx into the cleft. This leads to a decrease in fluid flux since the oncotic force for absorption is increased. As noted in the section on parameter values, there is no adequate theory for predicting D_f when the solute size approaches the fiber spacing. However, the results in Fig. 2.10 provide a means for estimating D_f. One observes that there is excellent agreement with Michel and Phillips (1987) experiment when D_f lies in the range 0.001 to $0.0001D_\infty$. This suggests a surface matrix that is a formidable barrier to albumin with a diffusion coefficient that is three orders of magnitude smaller than the free diffusion coefficient and a reflection coefficient that is close to one. Again, this value of D_f relates only to the cleft pathway. The total measured value of the permeability P also includes transcellular transport due to vesicles and transient gaps.

2.6 Discussion

The motivation for this study was the outgrowth of lengthy discussions between S. Weinbaum and J. R. Levick and C. C. Michel at the 1996 Starling Symposium. These discussions centered around five fundamental questions: (A) the spatial heterogeneity of the water and solute fluxes across the surface matrix layer; (B) the appropriate boundary conditions that should be applied in the tissue space; (C) how the protein concentration profiles behind the surface matrix layer were related to the tissue protein concentration if there were non-selective transcellular pathways for protein across the endothelium and (D) how the classic Starling equation should be applied, globally across the entire endothelial layer or locally across the protein sieving layer at the endothelial surface if the primary sieving layer is the surface glycocalyx. We will first address each of these basic questions.

2.6.1 Spatial heterogeneity of the filtration flux and oncotic force

In view of the large spatial variation in the local water flux crossing the surface glycocalyx, see Figs. 2.3b, 2.4b and 2.5b, one might anticipate that there are large spatial gradients in the albumin concentration behind the surface matrix layer and consequently large gradients in the local oncotic force. In fact, we initially expected, based on the one-dimensional model in Michel and Phillips (1987), that where the water flux was low in regions removed from the junction strand breaks, the albumin concentration would approach that in the plasma (the diffusion limit), whereas over the orifice opening, where the water flux was high, the concentration would approach the limiting value, $(1-\sigma)C_c$, predicted for the convective limit. However, the solutions presented in Figs. 2.3c, 2.4c

and 2.5c show, surprisingly, that the protein concentration profiles at x=0 have only a minor variation. This same behavior is observed whether there is filtration, Figs. 2.3c, 2.4c, or absorption, Fig. 2.5c.

In general, the detailed concentration profiles in Fig. 2.6 for Michel and Phillips experiment reveal that there are only small gradients in concentration throughout the cleft as intuitively argued in Michel (1997). In the case where the tissue concentration is elevated by the inclusion of a parallel large pore pathway, Fig. 2.8b, larger gradients appear on the tissue side of the junction strand, but the gradients in the protected region on the lumen side of the junction strand are comparable to those shown in Fig. 2.6a. These observations indicate there will be only small solute gradients behind the surface matrix layer provided the junction strand serves as an effective diffusive barrier and the diffusion coefficient in the cleft $D_c >> D_f$.

The fluid streamline pattern and y-direction velocity profiles exhibit a much greater spatial heterogeneity than the concentration profiles just described. This is because the cleft and the junction strand play a much more important role in determining the pressure distribution across the endothelial layer. In contrast to solute transport, a significant fraction of the total transendothelial pressure drop occurs across the cleft itself when there is a significant water flux. This is true for steady state filtration, Fig. 2.3a, or transient absorption, Fig. 2.5a. Due to this pressure distribution, the u profiles at x=0 and, therefore, the fluid streamlines are concentrated in the vicinity of the orifice opening in the junction strand as shown in Figs. 2.3b and 2.5b.

2.6.2 Boundary conditions in the tissue space

A central question in formulating the model and interpreting its results is the boundary condition in the tissue space. Starling in his original paper (1896) realized that the protein concentration in the tissue space depended on the flux of solute into the tissue. Michel and Phillips (1987) proposed that this equilibrium solute concentration is given in the steady state by the ratio of two fluxes, J_s to J_v. The condition, $C_i=J_s/J_v$, is appropriate only if the solute in the tissue is well mixed and uniform. The question as to how this uniformity is achieved is never addressed.

In the present model we have not assumed *a priori* that Michel's condition, $C_i=J_s/J_v$, applies at the cleft exit, since we wanted to leave open the possibility that the solute flux is non-uniform along the length of the cleft exit. Instead, we have required that the concentration at the edge of region B first achieve a uniform value C_a and then allow for further mixing in region C, before achieving the final well mixed condition, $C_i=J_s/J_v$. This condition was applied at different distances from 5 to 100 μm into the tissue. The results for Michel and Phillips experiment were insensitive to the size of region C. One finds that both regions B and C are, indeed, uniform when all the solute enters along with the water through the cleft. The entire tissue space does act like a well mixed reservoir, as proposed in Michel and Phillips (1987), provided, as we shall discuss next, there is not a parallel large pore pathway.

Suppose now that the tissue concentration at the edge of region B, C_a, is elevated by a flux through a large pore, transcellular non-convective pathway removed from the cleft, but region C is well mixed and uniform. This requires that $C_a > J_s/J_v$, where J_s and J_v are still the solute and water fluxes through the cleft. The ratio of the prescribed value of

C_a, in this case $0.4C_c$, to the value obtained from the expression, $C_i=J_s/J_v$, also represents the ratio of solute flux through all pathways to the solute flux through the cleft pathway in the steady state, if the local tissue region is at uniform concentration. Thus, in the convective limit, where $C_i=(1-\sigma)C_c$, one finds that the solute flux through the large pore pathway is nearly six times that through the cleft, if $\sigma=0.94$, and region B is highly non-uniform in contrast to the results for Michel and Phillips experiment. The intriguing result, which we shall now examine in more detail, is that the model predicts that one can substantially change the concentration in the tissue space without significantly changing the solute concentration on the lumen side of the junction strand. This has very important implications for the application of the Starling equation.

2.6.3 Large pore parallel pathway

The results in Figs. 2.7 and 2.8 show that when the protein concentration is elevated in the pericapillary space at the edge of region B due to a parallel large pore, non-convective pathway, large solute gradients are produced in the region downstream of the cleft exit. As observed in Fig. 2.8, the solute gradients feed upstream into the cleft. The important observation is that the large elevation in concentration that occurs in the tissue and in the cleft downstream of the junction strand is not communicated upstream through the orifice opening at the high capillary pressure, Figs. 2.8a, b. The region between the surface matrix layer and the junction strand is effectively insulated from the conditions in the tissue.

To examine the role of the orifice more carefully we have calculated the ratio of the convective to the diffusive flux of the solute at the orifice opening for the conditions shown in Fig. 2.8b. Convection was 47 times greater than diffusion and the local Peclet

number based on the cleft depth, 400 nm, and centerline velocity was 4.7. The orifice thus acts at high capillary pressures like a throat that prevents the back diffusion of solute into the shielded region in front of the junction strand. The oncotic pressure behind the surface glycocalyx is effectively uncoupled from the oncotic pressure in the tissue when the convective flux through the orifice opening dominates diffusion at this critical cleft location. Only for conditions of very low filtration will the tissue concentration significantly influence conditions behind the surface matrix layer. This is observed in Fig. 2.8c where the cleft solute profiles are shown for P_c=15 cmH_2O. The dimensionless concentration has risen to a value that is roughly 90 percent of that in the tissue space. The local Peclet number is now only 0.15 and the profiles on each side of the orifice opening are more symmetric indicating that solute diffusion now plays an important role.

In the present paper the edge of region B has been prescribed. It has been estimated on the basis of anatomical data to be 5 μm, half the average cleft spacing. One observes in Fig. 2.8a that the solute gradient is greatly diminished, but does not vanish at the edge of region B, L_B=5 μm. This implies that, according to the present model, the solute concentration is not uniform in region C, but only nearly so. A more sophisticated model is needed to more accurately describe the details of the mixing between the paracellular cleft and transcellular large pore or vesicular pathways.

2.6.4 Application of the Starling equation

The Starling equation has, heretofore, been universally applied to the global differences in protein concentration and pressure between the plasma and the tissue space. The present model is based on a new hypothesis, that the oncotic and hydrostatic pressures, π_i and P_i, must be applied locally to only that portion of the endothelial barrier

where we hypothesize the proteins are actually being sieved, namely, the surface matrix layer. This hypothesis leads to two fundamental changes in current thinking. First, the local Starling forces are spatially heterogeneous on the length scale of the spacing between junction orifices because of the large variation in local Peclet number as noted in subsection (A). Second, the local protein concentration and pressure behind the surface matrix layer can differ greatly from the tissue concentration and pressure.

Our model predicts that the cleft itself is able to support only minor concentration gradients when the exit condition, $C_i=J_s/J_v$, is satisfied. Michel's simple, one-dimensional model thus provides a reasonable estimate of the protein concentration in the tissue when the entire solute flux passes through the cleft, since the solute gradients across the cleft are small compared to those across the matrix layer and the concentration behind the matrix is well approximated by C_i. The pressure at the rear of the surface matrix layer, on the other hand, can differ greatly from the pressure in the tissue if the primary pressure drop occurs across the junctional strand, as observed in Fig. 2.3a.

The fact that the pressure and concentration behind the surface glycocalyx can differ greatly from their values in the tissue means that the Starling forces across the matrix layer will depart significantly from the global Starling forces across the entire endothelial layer. This can lead to drastically different results for the filtration flow as shown in Fig. 2.9. This difference will be particularly important in the case where there is a parallel, large pore solute pathway across the endothelium, since the oncotic pressure behind the surface matrix layer can be nearly independent of the tissue concentration, as is evident in Fig. 2.8b. However, even in the case where the entire water and solute flux is through the cleft, the Starling forces at the back of the matrix and in the tissue space will

not be the same. The oncotic forces will differ by only a few percent, because the solute gradients in the cleft are small, but the pressure forces can differ greatly as noted at the end of the previous paragraph.

2.6.5 The surface glycocalyx and other matrix structures

The basic hypothesis in our new conceptual mathematical model is that the surface glycocalyx is both the primary molecular sieve and diffusive barrier for plasma proteins and that this sieving matrix does not fill the entire interendothelial cleft as proposed in the original fiber matrix theory of Curry and Michel (1980). At present the evidence for this is only indirect since the matrix is not electron dense and, therefore, not easily observed. The most convincing evidence that the sieving structure is confined to a surface layer are the detailed calculations for L_p for frog mesentery in Fu *et al.* (1994), the measurements of the surface matrix layer thickness for this microvessel, Adamson and Clough (1992), and the recent theory and experiments for the labeling of the cleft using high molecular weight tracers (Fu *et al.*, 1997, 1998). A rigorous hydrodynamic theory has been developed for the hydraulic resistance of cleft spanning fibers in a channel in Tsay and Weinbaum (1991). This theory has been used in (Fu *et al.*, 1994) to estimate L_p in frog mesentery using the measured structure of the junction strands in (Adamson and Michel, 1993) that has been applied in the present model. These quantitative predictions show that the measured L_p of $2.0*10^{-7}$ cm/s/cmH_2O would be underpredicted by at least a factor of four if a sieving matrix for albumin with a fiber spacing of 7 nm, were to fill the wide part of the cleft. The predicted thickness of the matrix layer in (Fu *et al.*, 1994), 100 nm, was nearly the same as the measured thickness of the surface matrix layer in (Adamson and Clough, 1992). The latter was indicated by a dense band of cationized

ferritin (11 nm diameter) that was displaced from the endothelial surface. The serial section electronmicrographs in (Adamson and Michel, 1993) clearly reveal that the gap height of the breaks in the junction strand, 20 nm, is essentially the same as the wide part of the cleft. Thus, the junction strand itself is unlikely to provide the molecular sieve for plasma proteins. This combined evidence has led the authors in recent publications (Fu *et al.*, 1994; 1997), Weinbaum (1998) and Michel (1997) to hypothesize that the surface glycocalyx is the molecular filter, at least for frog mesenteric capillaries.

Additional evidence in support of the hypothesis that the surface matrix does not also fill the cleft comes from the theoretical predictions in Fu *et al.* (1997) and the recent unpublished experimental observations of R. Adamson for the labeling of the cleft using a high molecular weight tracer, horseradish peroxidase (HRP). In early experiments using HRP in pure Ringer, one would frequently see HRP penetrating the cleft up to the level of the junction strand and an occasional leakage of HRP which would extend throughout the depth of the cleft. However, the more recent studies of Adamson and Clough (1992) reveal that the surface matrix collapses in the absence of plasma proteins. When the HRP tracer experiment is performed *ex vivo* in frog mesentery, where the surface matrix is intact, there is no detectable filling of the cleft (R. Adamson, private communication). If the matrix were to fill the cleft, one would expect to see a linear decrease in peroxidase reaction product with distance into the cleft, which does not occur. The theoretical model in Fu *et al.* (1997) explains these observations by showing that even in the vicinity of a junction strand break, the concentration of HRP behind the surface matrix would be so reduced that its reaction product would not be visible. Thus, in contrast to the tracer labeling studies with the low molecular weight tracer, lanthanum, (Adamson and Michel,

1993) one would not expect to see HRP reaction product in the cleft, if there was a sieving matrix at the endothelial surface.

2.6.6 Is there a need for venous reabsorption

Fig. 2.9 shows that even if the tissue concentration is raised to $0.4C_c$ the filtration on the arterial side is far smaller than previously believed, and significantly less than the solid line in Fig. 2.9, where the Starling forces are based on global values of the pressure and concentration in the tissue. Based on the results in Fig. 2.9, there may be no need for venous reabsorption because the net filtration is much less than that predicted by a classical Landis-Starling diagram in which both P and π are based on their interstitial values. The magnitude of the reduction in the net filtration depends on how effective the junction strand is in preventing back diffusion from the tissue space. The critical parameter is the magnitude of the Peclet number evaluated at the junction strand orifices. When Pe>1 the concentration in the protected region behind the matrix layer is effectively uncoupled from that in the tissue space. The actual reduction in net filtration is not the difference in area under the curves in Fig. 2.9 although this provides a rough guide. One needs to examine the permeability-area distribution of the capillary and it is well recognized that capillaries on the venous side have a significantly larger area. This weights the venous end of the capillary where the model predicts that the filtration rate is very low.

An important issue that has not been addressed is what happens in more restrictive transport barriers in mammalian capillaries and other tissues where there are multiple junction strands and much lower hydraulic conductivities. The serial sections in rat heart capillaries by Bundgaard (1984) suggest that the junction strand breaks are both much

shorter, typically one section thickness, 400-500 nm, and more widely spaced. While these more complicated junction structures are beyond the scope of the present paper, it is anticipated that the same basic principle applies. For widely dispersed small pores L_p will be greatly decreased, but the small filtration flux will need to be funneled through a reduced population of small pores with the net result that the Peclet number at the junction orifices is not greatly different from the values predicted herein for frog mesentery. If this is the case the rear of the surface matrix would be shielded from back diffusion from the tissue and the effective oncotic pressure uncoupled from the tissue concentration as demonstrated for frog mesentery in the present study.

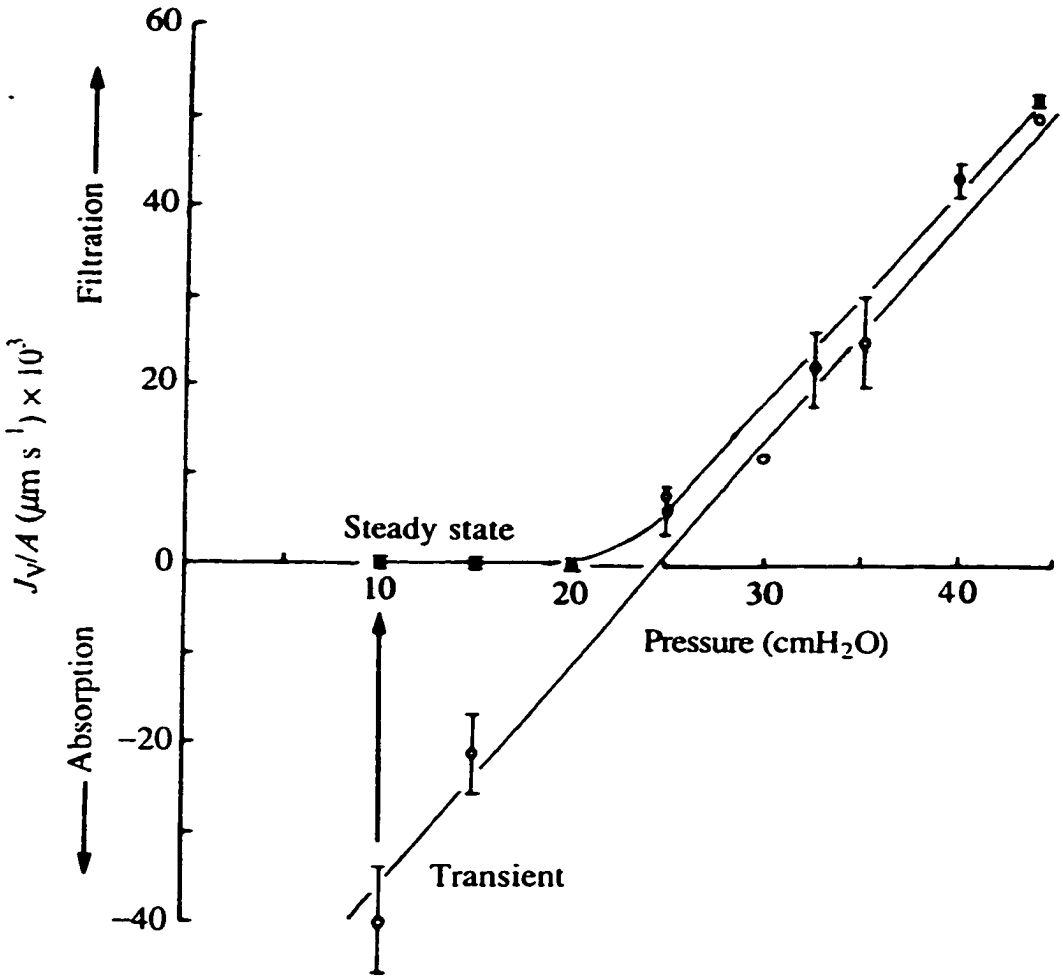

Figure 2.1 Water flux J_v/A in a single perfused frog mesentery capillary as a function of capillary pressure. For the transient state, measurements are performed in the first 15-30 seconds after the perfusion pressure is fixed, and for the steady state, measurements performed 2 to 5 minutes after the perfusion pressure is fixed. [From Michel and Phillips (1987), with permission].

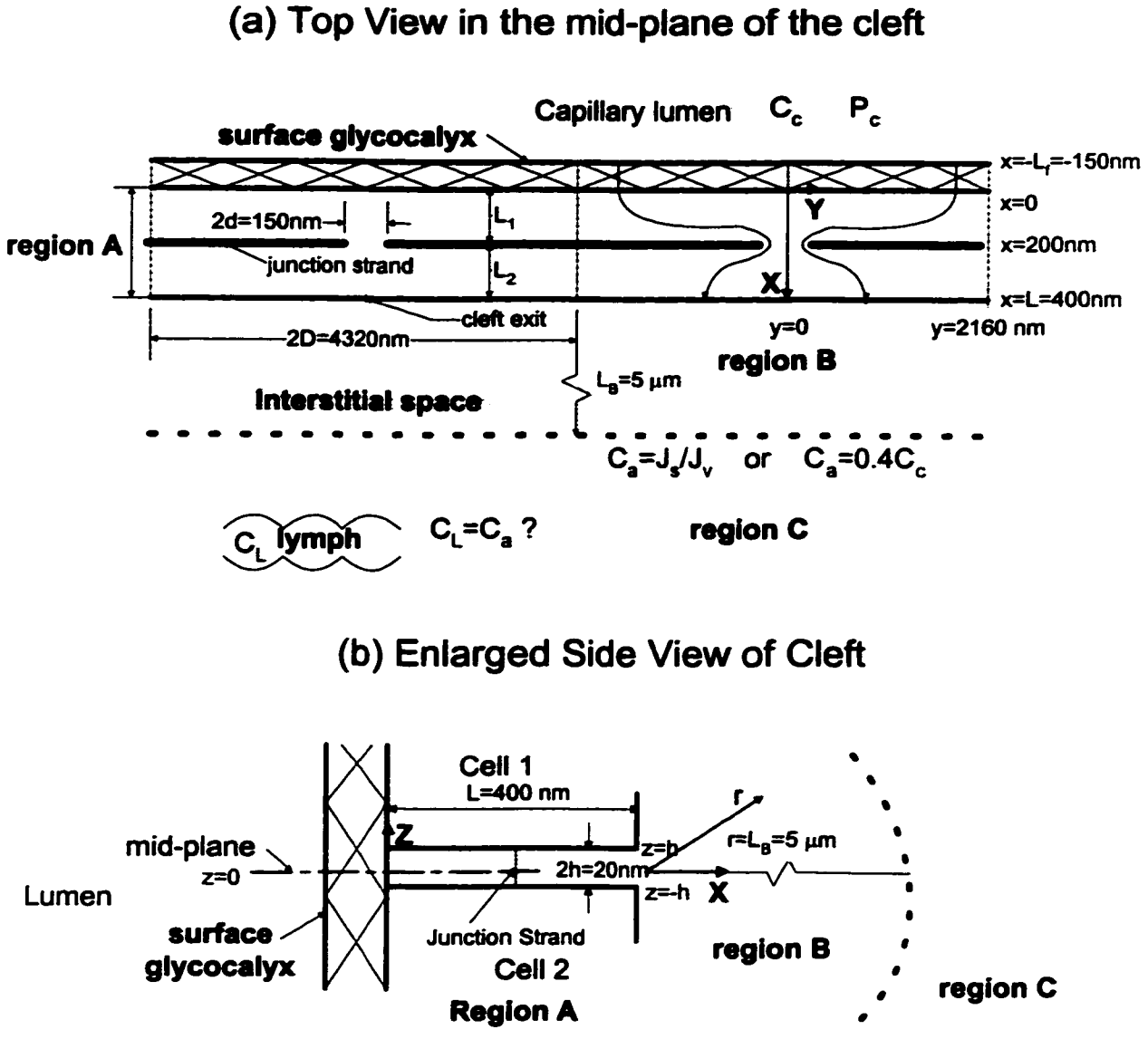

Figure 2.2 Schematic of idealized mathematical model showing surface matrix layer, cleft region A with junction strand and tissue regions B and C describing mixing at cleft exit. Dimensions shown are typical for frog mesentery capillary.

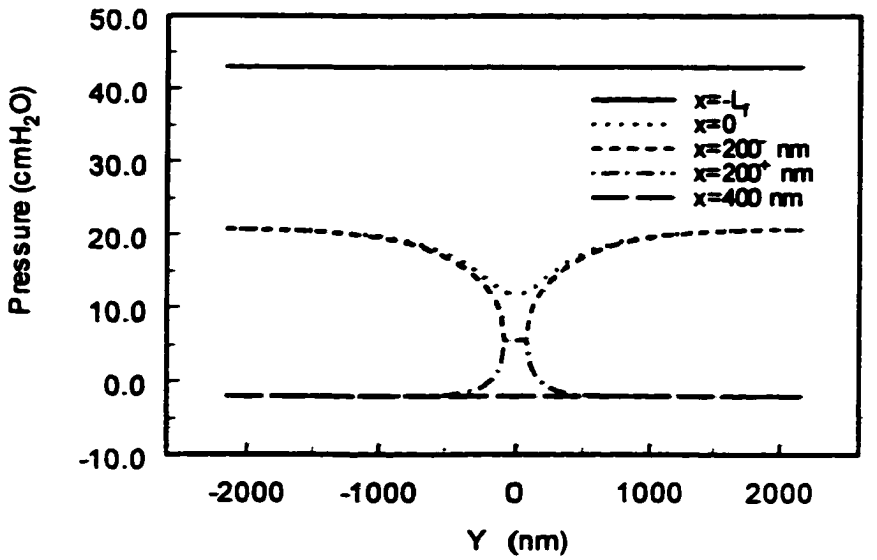

a

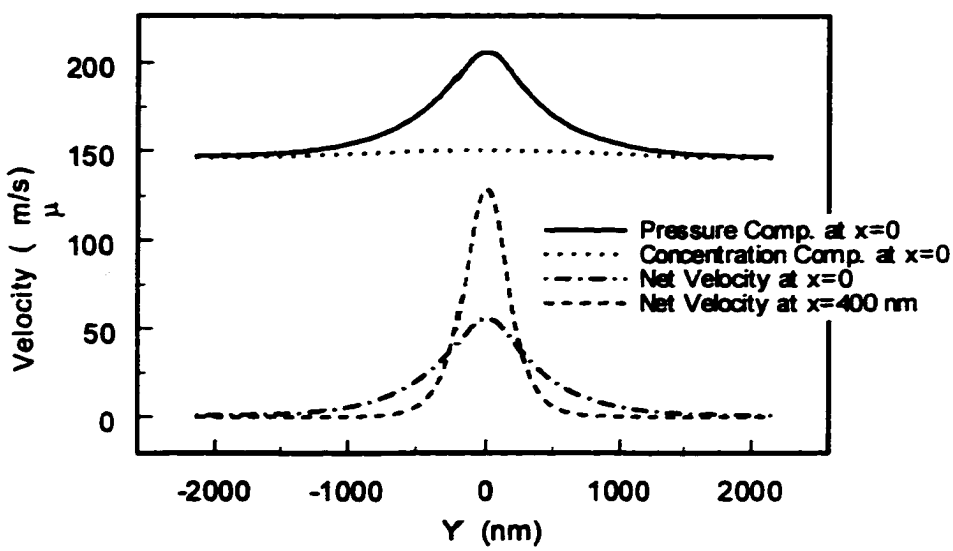

b

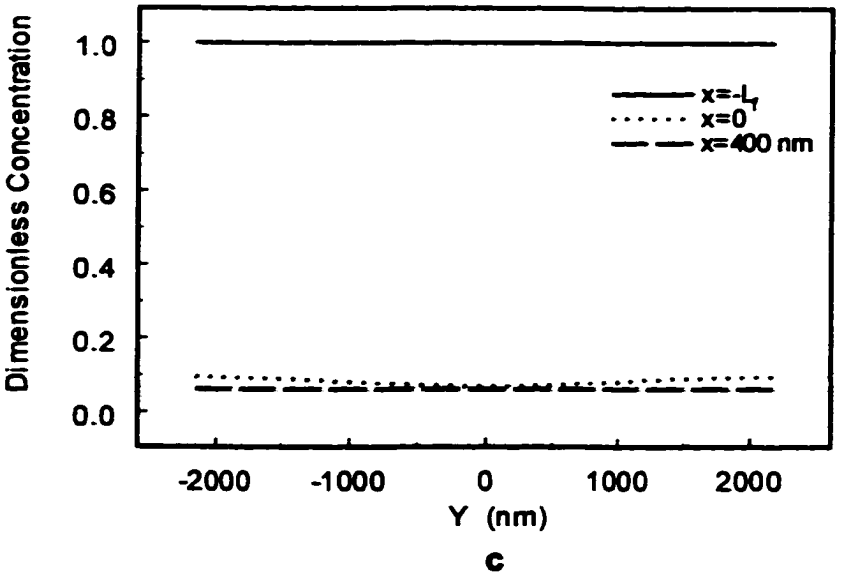

Figure 2.3 Predictions of theoretical model for P_c=43 cmH_2O for the steady state (a) pressure, (b) velocity and (c) protein concentration profiles at various locations in cleft identified in Fig. 2.2. Plasma oncotic pressure is 26 cmH_2O and σ=0.94. Note the individual contributions to the water flux crossing the surface glycocalyx from oncotic (protein concentration) and hydrostatic (pressure) components nearly cancel in Fig. 2.3b except for the region in front of the junction strand break, and the concentration gradients within the cleft are small in Fig. 2.3c. Fig. 2.3a shows that roughly half the pressure drop occurs across the matrix and half across the cleft.

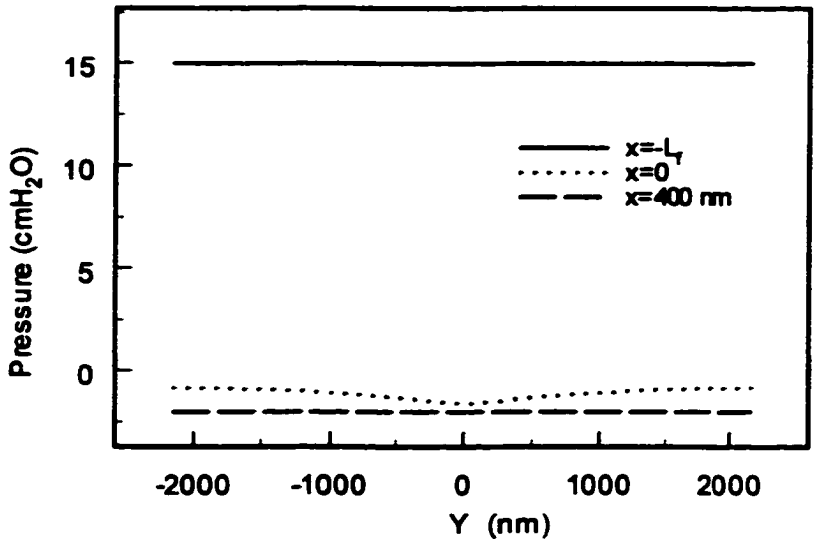

a

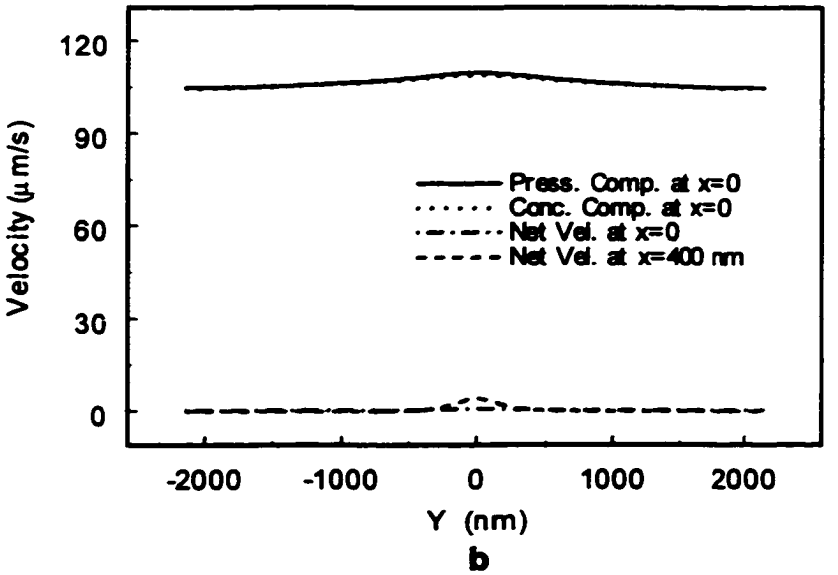

b

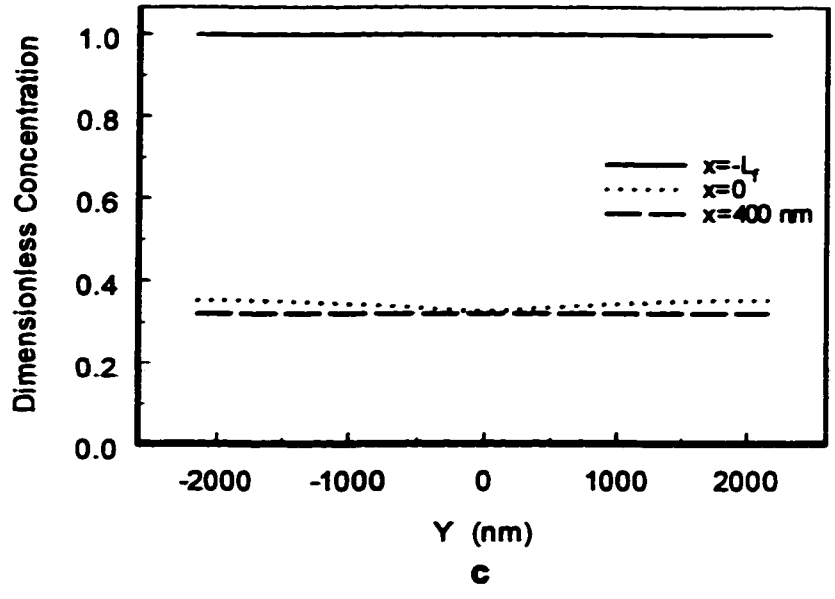

Figure 2.4 Predictions of theoretical model for P_c=15 cmH_2O for the steady state (a) pressure, (b) velocity and (c) protein concentration profiles at various locations in cleft identified in Fig. 2.2. Plasma oncotic pressure is 26 cmH_2O and σ=0.94. Note the individual contributions to the water flux crossing the surface glycocalyx from oncotic (protein concentration) and hydrostatic (pressure) components cancel everywhere in Fig. 2.4b leaving only a very small positive filtration in the steady state, and concentration gradients within the cleft are small, like in Fig. 2.3c. In contrast to Fig. 2.3a most of the pressure drop occurs across the surface matrix where the pressure and oncotic forces balance one another.

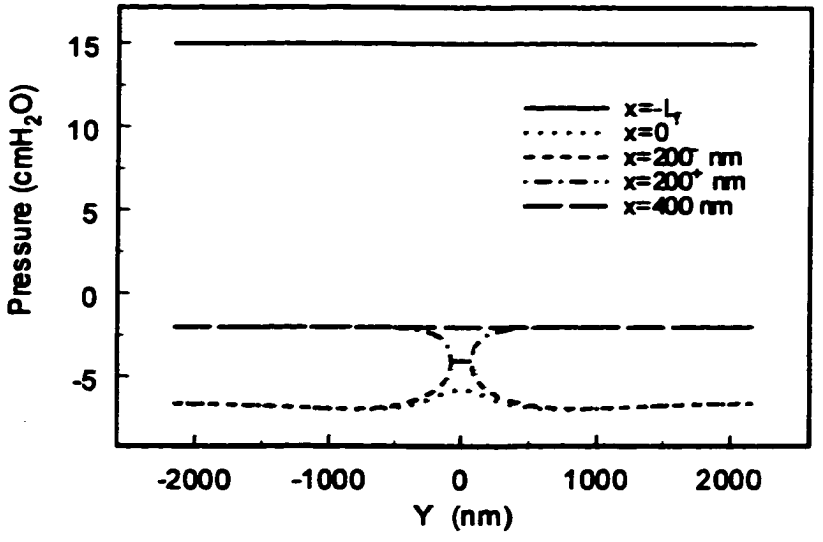

a

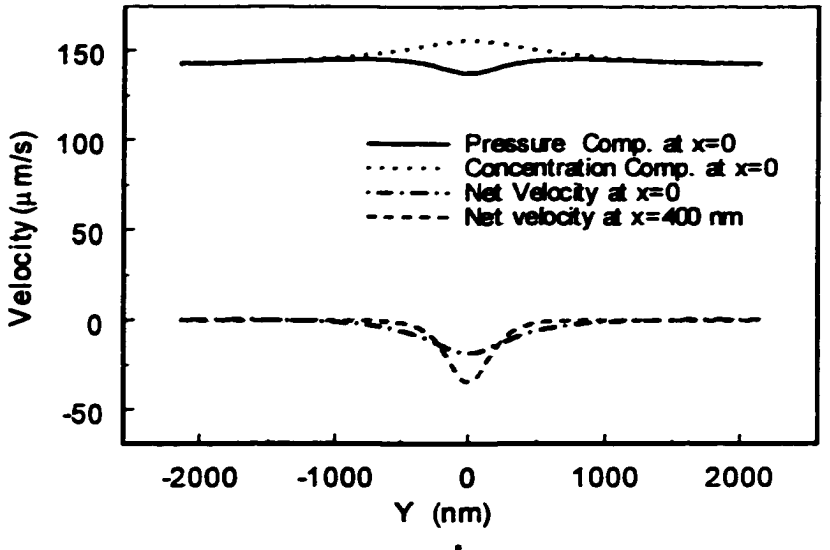

b

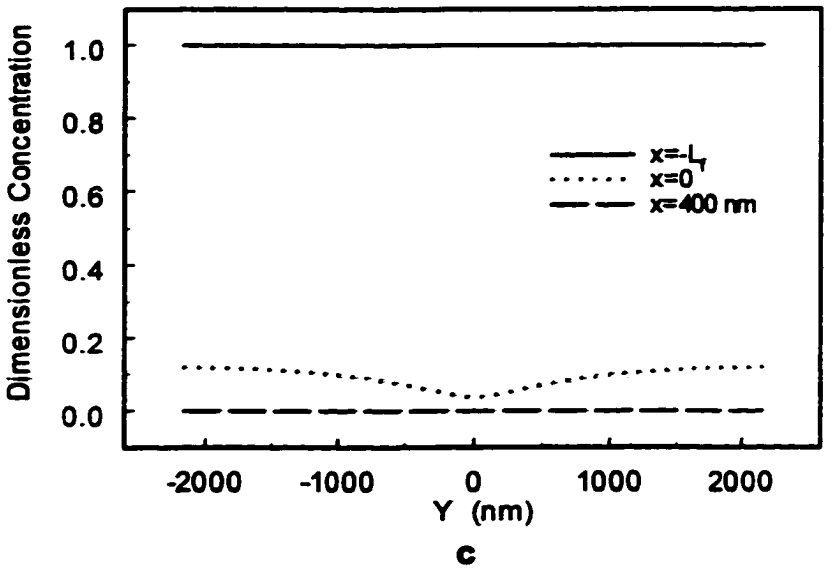

Figure 2.5 Predictions of theoretical model for P_c=15 cmH_2O for transient state (a) pressure, (b) velocity and (c) protein concentration profiles at various locations in cleft identified in Fig. 2.2. Plasma oncotic pressure is 26 cmH_2O and σ=0.94. Note the individual contribution to the water flux crossing the surface glycocalyx from the oncotic component (protein concentration) overrides the hydrostatic (pressure) component over the orifice opening in Fig. 2.4b, and there is a net negative velocity in the vicinity of the orifice opening. There is a negative pressure of approximately –7 cmH_2O behind the surface matrix, Fig. 2.5a, and a small standing gradient in concentration is produced across the cleft, Fig. 2.5c.

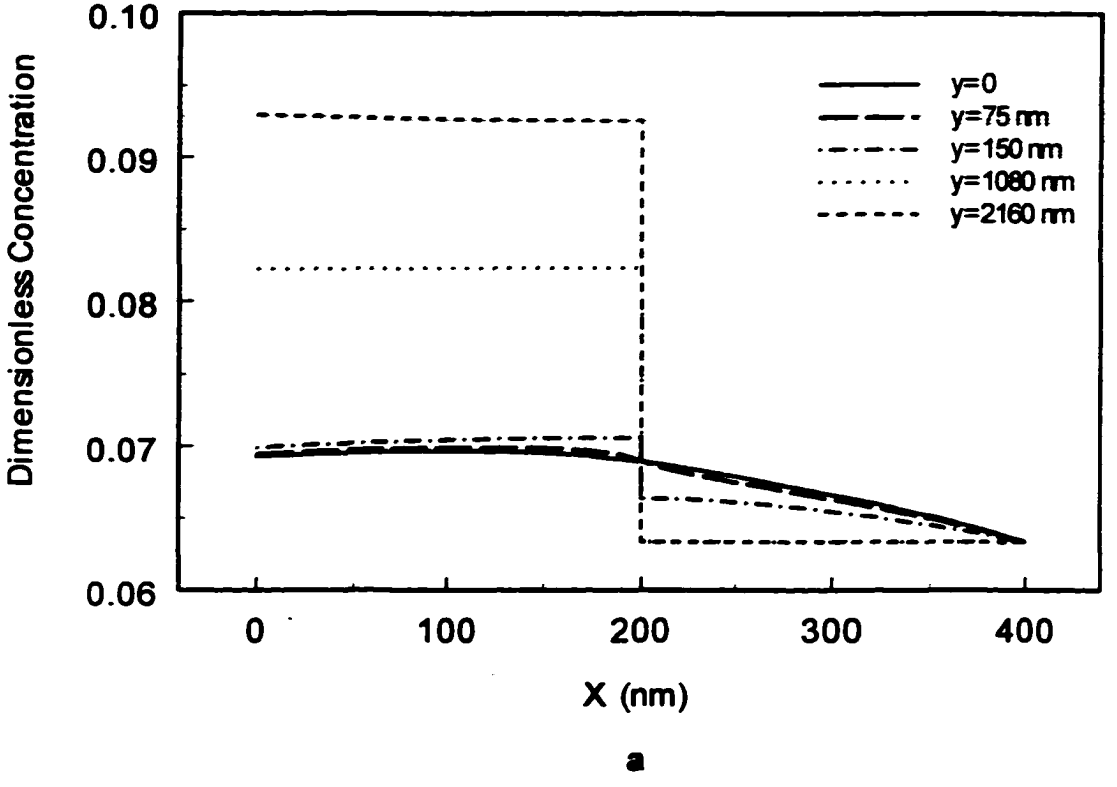

a

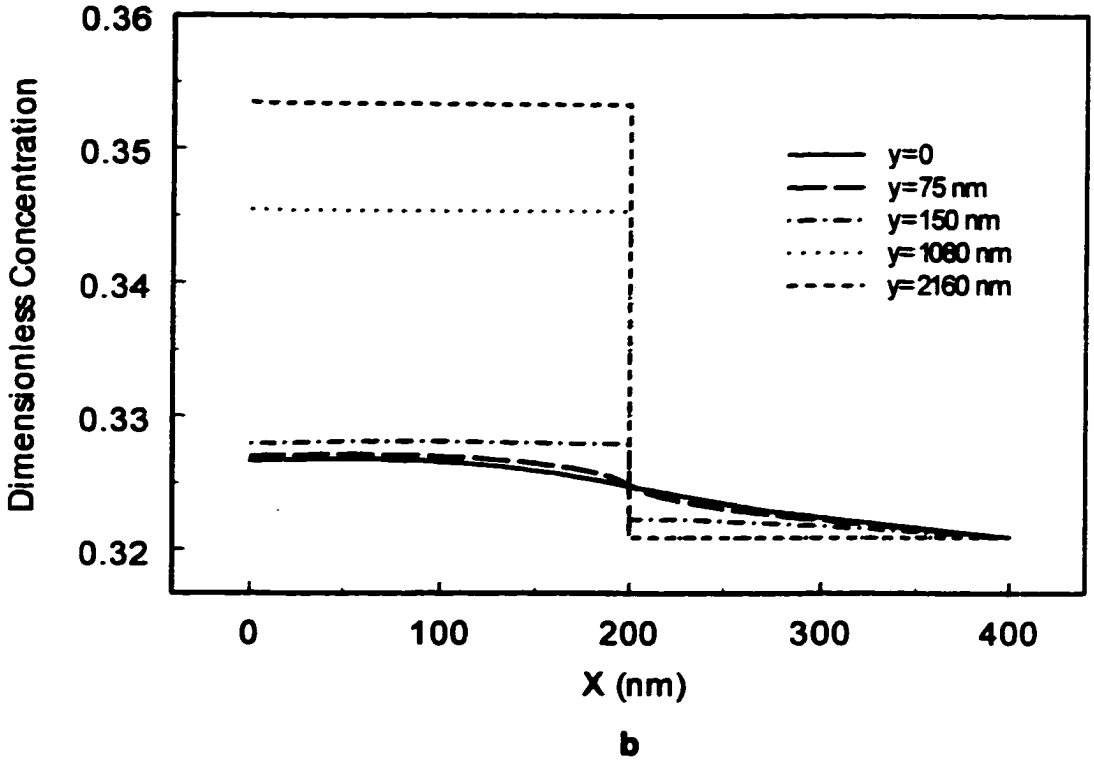

Figure 2.6 Predictions of the theoretical model for the dimensionless concentration profiles within the cleft at different y locations for (a) P_c=43 cmH_2O and (b) P_c=15 cmH_2O. $C_i=J_s/J_v$ is applied at the end of region C, x=100 μm. y=0, centerline; y=75 nm, edge of orifice; y=2160 nm, half spacing of junction strand breaks. Other conditions are the same as Figs. 2.3 and 2.4.

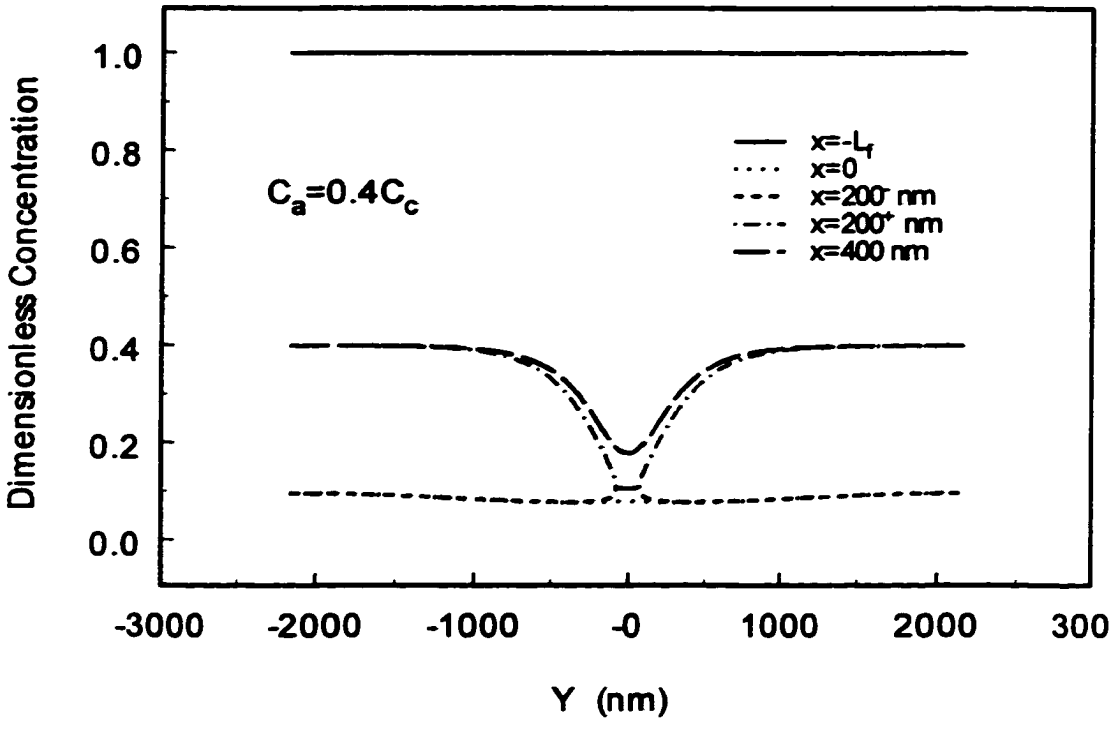

Figure 2.7 Concentration profiles in the cleft when P_c=43 cmH_2O and there is a parallel non-convective pathway for albumin which increases the tissue concentration at the edge of region B, C_a, to 0.4 C_c. Plasma oncotic pressure is 26 cmH_2O and σ=0.94. Note profile behind the surface matrix, at x=0, is nearly the same as concentration profile at x=0 in Fig. 2.3c.

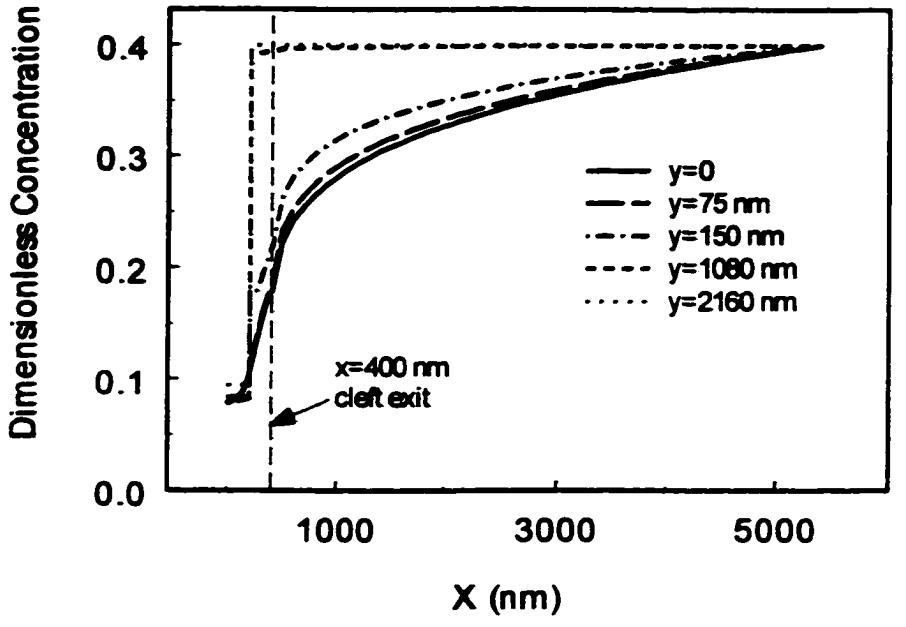

a

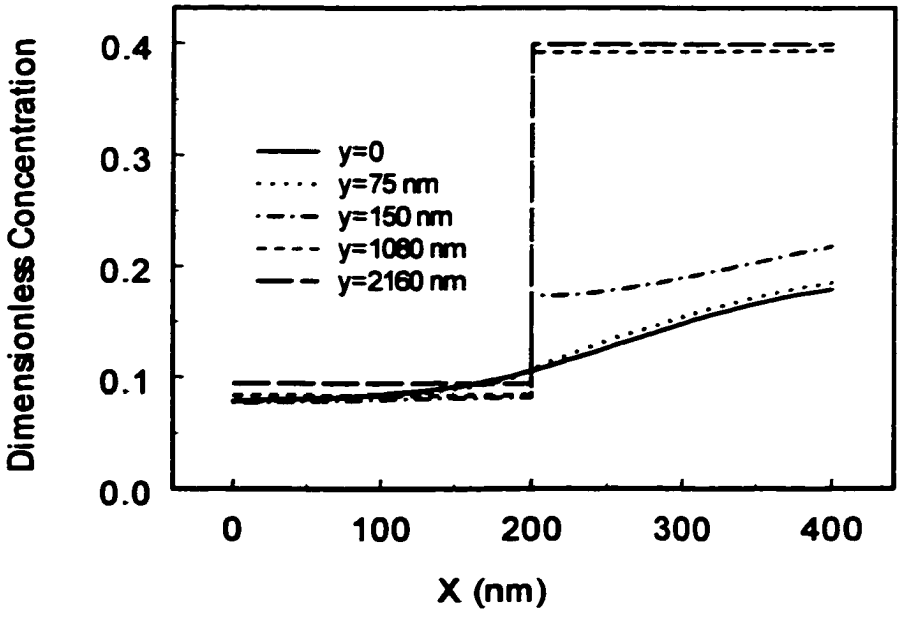

b

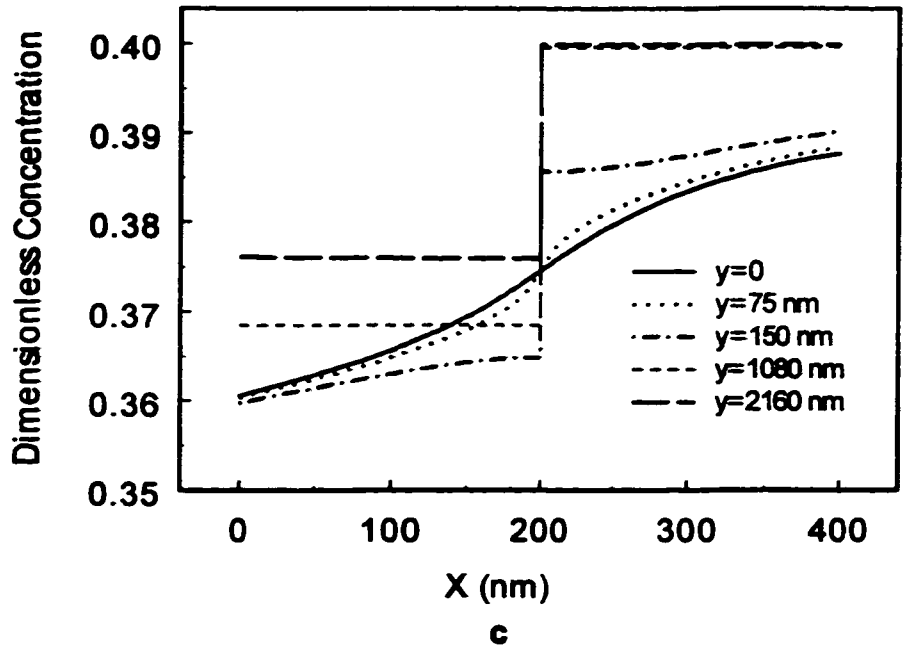

Figure 2.8 Concentration profiles at different y locations for (a, b) P_c=43 cmH_2O and (c) P_c=15 cmH_2O when there is a parallel non-convective pathway for albumin which increases the tissue concentration at the edge of region B, C_a, to $0.4C_c$. Fig. 2.8a shows the upstream spread of solute from the pericapillary region B into the cleft, whereas Figs. 2.8b, c show the detailed profiles within the cleft corresponding to Figs. 2.6a, b, where the entire flux is through the cleft.

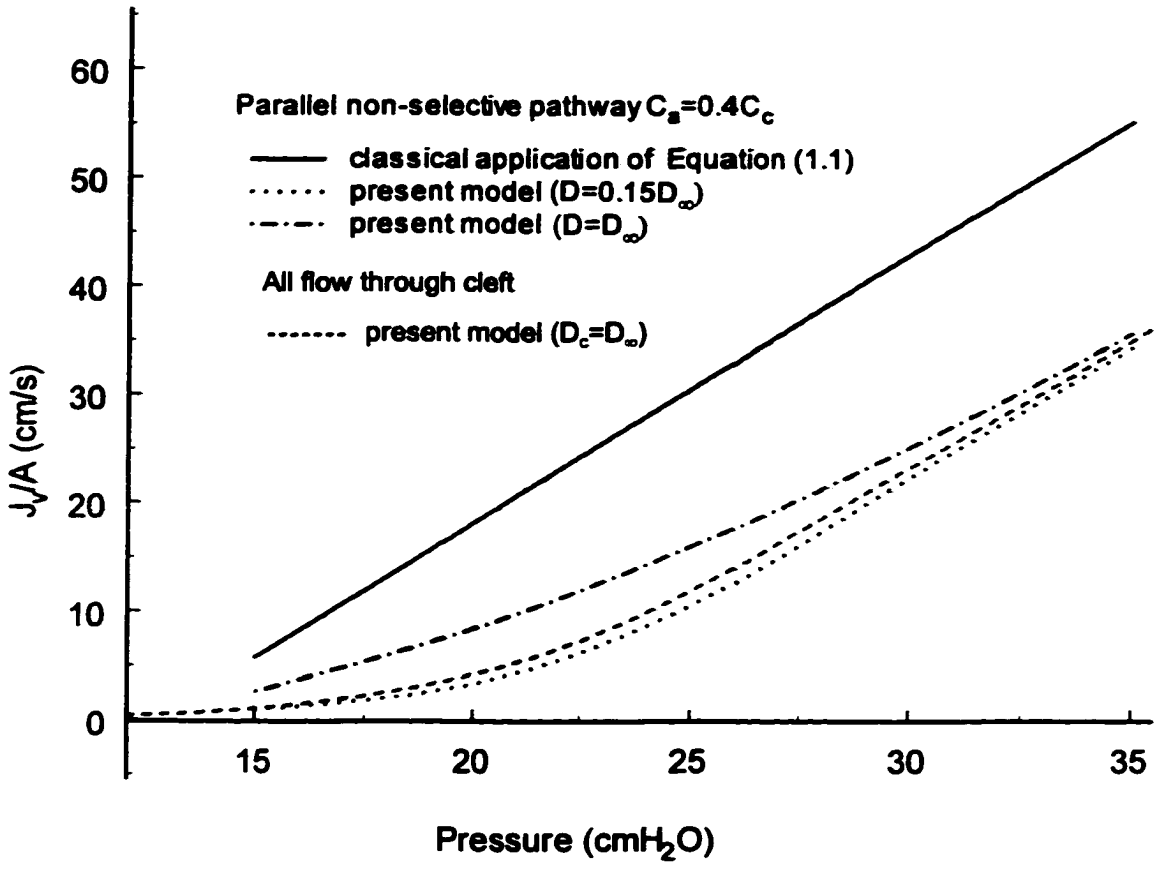

Figure 2.9 The comparison of the filtration flux, J_v/A, predicted by the present model and the classical application of Starling equation when C_a=0.4C_c and π_c=26 cmH_2O. According to classical theory, where P_i and π_i evaluated in tissue space, J_v/A varies linearly with capillary pressure P_c. In the present model, where P and π are evaluated locally across surface matrix layer, the filtration flow is highly non-linear and greatly reduced. The convective flux of solute through the junction strand orifice impedes the back diffusion of solute in the tissue from entering the protected region behind the surface matrix. This effect is significantly enhanced if the diffusion coefficient in the cleft is reduced to a value 0.13D_∞ representative of matrix components in the tissue space. Also shown for comparison are the results that would be obtained if the entire solute flux were through the cleft and C_a=J_s/J_v. D_f=0.001D_∞ in all cases.

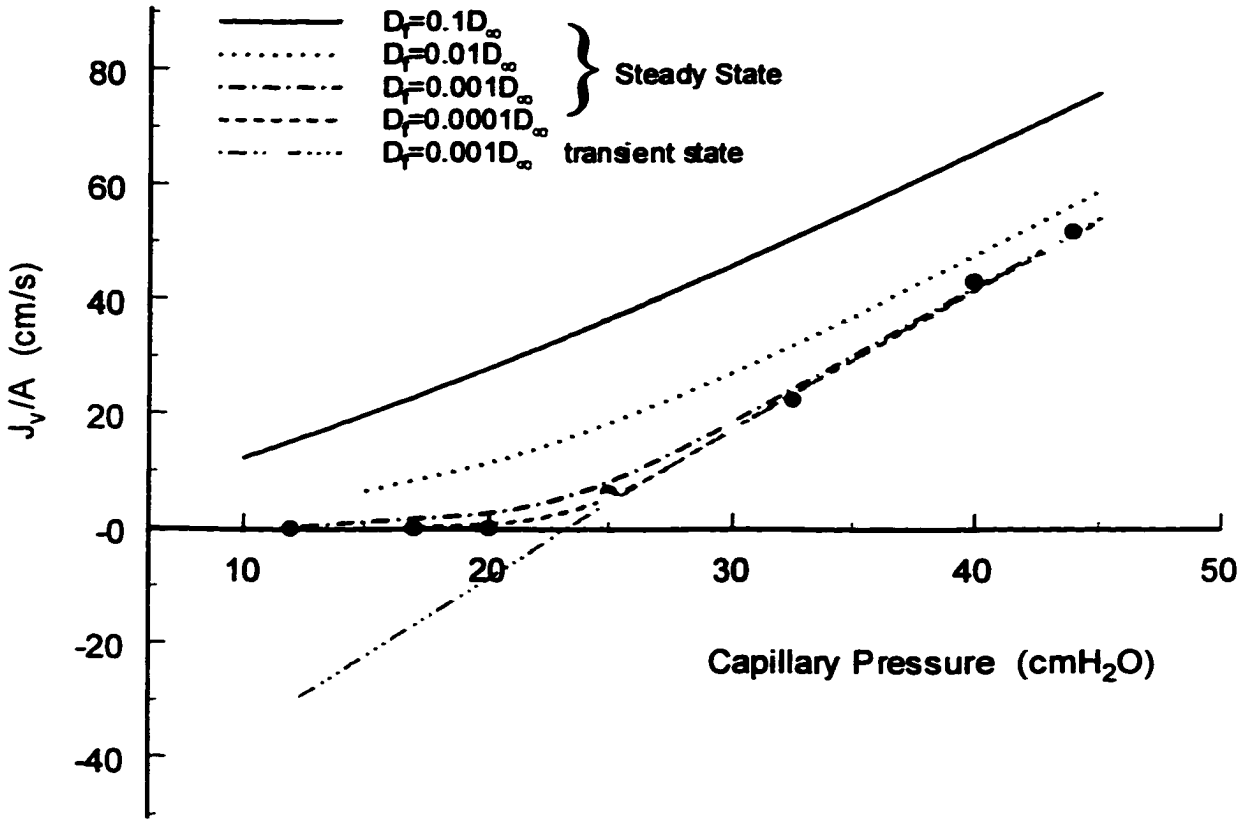

Figure 2.10 The relation between filtration flux, J_v/A, and capillary pressure, P_c, for different diffusion coefficients, D_f, of the surface matrix layer in both the steady and transient state. The filled circles (•) are the measured values from Michel and Phillips (1987). Note the close agreement between theory and experiment when D_f lies between 0.001 and $0.0001D_\infty$.

Chapter 3 The Starling forces that oppose filtration after tissue oncotic pressure is increased

3. 1 Introduction

1996 marked the 100th anniversary of Starling's (1896) pioneering paper outlining his hypothesis for the filtration and reabsorption of water in capillaries and the formation of lymph. He hypothesized that the difference in concentration of plasma proteins between the plasma and tissue was responsible for an osmotic pressure, which opposed the hydrostatic filtration. Thus, the driving force for fluid filtration rate across the vessel wall is determined by four pressures, the hydraulic and colloid osmotic pressures in the vessel and in the tissue space, respectively, shown as equation (1.1). The term $\sigma(\pi_c-\pi_i)$ in equation (1.1), which opposes the fluid filtration across the endothelial wall, is called the Starling oncotic force.

Starling's equation has been applied across the entire transendothelial barrier and the Starling forces evaluated by global measurements of P and π in the plasma and the tissue space. However, there is growing recognition that the application of the Starling equation is much subtler than has previously been realized. There exists a discrepancy between the measured Starling forces in the plasma and tissue and the forces which actually appear to determine filtration (Taylor and Townsley, 1987 and Levick, 1991). Further, Levick and coworkers have demonstrated that in the synovium the effect of extravascular albumin on fluid exchange is much less than the effect of intravascular albumin (Levick, 1994).

In Michel (1997) and Weinbaum (1998) a new hypothesis is proposed for the effective oncotic barrier that acts across capillary endothelium. Hu and Weinbaum (1999) present a detailed cellular level microstructural model to quantitatively examine this hypothesis. In this spatially heterogeneous microstructural model the endothelial surface glycocalyx, which covers the entire capillary endothelium, serves as the primary molecular filter for plasma proteins and, thus, the principal barrier that determines the effective oncotic force for water flow across the interendothelial cleft. Therefore, the effective oncotic force across the capillary is determined by the local difference in protein concentration across the surface matrix layer, rather than the global difference in concentration between the plasma and the interstitial fluid in the tissue. Consequently, the pressures P_i and π_i that appears in equation (1.1) will be the local hydrostatic and oncotic pressures behind the surface glycocalyx, where the effective oncotic pressure is felt, and not P_i and π_i in the tissue space at the cleft exit.

In the present studies the relation between the filtration rates across the capillary wall and the hydrostatic and oncotic pressure difference has been investigated using a combined experimental and theoretical approach in single perfused microvessels of frog mesentery. The idea for these experiments arose from the quantitative predictions by Hu and Weinbaum (1999) that the protein concentration in the tissue space may differ significantly from that just behind the glycocalyx if there are other parallel non-convective transcellular pathways for protein flux, in addition to the convective pathway through the interendothelial cleft of continuous capillaries. This model shows that the presence of a junction strand with small breaks and pores greatly inhibits back diffusion from the tissue into the shielded region on the lumen side of the junction strand. This

leads to a significant reduction in the fluid flux filtered by the capillaries in comparison with the magnitude predicted by the classical Starling equation.

We also present new experimental results on individually perfused microvessels to demonstrate that the effective oncotic pressure across the capillary endothelium is not the global difference in oncotic pressure between blood and tissue. The novel aspect of the present experiments is that tissue albumin concentration was maintained at levels equal to that in the perfusate by the continued presence of albumin in the superfusate ensuring the back diffusion of albumin from the superfusate into the tissue surrounding the microvessel. The effective filtration rates with albumin in the tissue were compared with the results on the same microvessel when albumin was present only in the perfusate. We show that loading the tissue with albumin from the tissue side produces only small changes in the effective oncotic pressure. These results have been interpreted using a detailed three-dimensional model of the endothelial cleft, surface glycocalyx and mixing in the tissue space surrounding the cleft exit. We also investigate the effect of the location of the junction strand and the spacing of junction breaks on the Starling forces.

3.2 Methods

3.2.1 Experimental methods

Methods to prepare frog mesenteric microvessels for microperfusion and measurement of transcapillary water flows and hydraulic conductivity during transient and steady state filtration have been described in detail (Curry *et al.*,1983 and Huxley, 1993). The mesentery was exposed through a lateral abdominal incision and the gut draped over a quartz pillar. The tissue was transilluminated and viewed through an inverted microscope equipped for simultaneous observation and recording. Glass micropipettes with tip diameters of 8-10 μm were held in position with micromanipulators and filled with Ringer's solution containing albumin.

A key requirement of the experimental design when albumin was added to the superfusate experiments was to set the albumin concentration in the tissue equal to the albumin concentration in the perfusate. To establish the time required for albumin in the superfusate to diffuse into the tissue surrounding the test microvessel, a scanning confocal microscope (BioRad MRC600) was used to record images such as in Fig. 3.1. The figure shows the distribution of tracer in the tissue space as a function of time after initiating superfusion with albumin. The frog mesentery preparation was as above. Figure 3.1A is a fluorescent confocal microscope image taken transverse to the longitudinal axis of a venular capillary in frog mesentery. The superfusate contains FITC-albumin (2 mg/ml) and fluorescence intensity was directly proportional to the local concentration of FITC-albumin. The lumen of the venular capillary in this image was perfused with the frog's own plasma and was not fluorescent. To reduce the resistance of the mesothelium

to albumin diffusion, the mesothelium approximately 100 μm from either side of the venular microvessel was gently stroked with a fine glass rod to irritate the mesothelial cells and facilitate solute diffusion between the tissue fluid space and superfusate. Figure 3.1B shows profiles of relative tissue concentration of albumin measured close to the centerline of the tissue over a period of 1-13 minutes. On this scale the superfusate concentration was 160 units. Therefore after 13 minutes, the albumin concentration had reached 75% of the superfusate concentration. We found that there was no difference between tissue and superfusate concentrations after 15-20 minutes. In our experiments we allowed up to 45 minutes for albumin to diffuse into the tissue.

Figure 3.1B shows that even though the tissue was stroked at a distance up to 100 μm from the vessel, there are no significant gradients in the tissue at distances greater than 10 μm from the vessel wall. Further the shape of the gradients close to the wall reflect the geometry of the vessel wall which is not a perfect cylinder and is surrounded by pericytes. The non-uniformities in the concentration gradient in the tissue indicate sites where isolated cells or clusters of collagen fibrils that exclude albumin are located.

Two different types of experiments were designed. In the first set, paired measurements were made of the effective oncotic pressure of albumin in the perfusate first when there was no albumin in the tissue (control), then when albumin was added to the superfusate at the same concentration as the perfusate. These are called transient experiments because the effective oncotic pressures were measured by rapidly reducing pressures in the vessel as explained below. In the second series of experiments we measured the steady state filtration rates at a series of pressures in each microvessel with the same albumin in both perfusate and the superfusate and compared these to the

filtration rates expected at each pressure if no oncotic forces oppose filtration. To calculate the latter we also measured the L_p for each vessel using the transient protocol. In each group of experiments only one microvessel in each animal was studied. The albumin concentration in all experiments was 50 mg/ml.

During control measurements in the first series of experiments, the upper surface of the tissue was continuously bathed with protein-free Ringer superfusate. The fluid flux per unit area, J_v/A, was estimated from the motion of marker erythrocytes using the modified Landis technique. Prior to each measurement the pressure in the vessel was held at 35 cm H_2O for 2 min by partial occlusion. This established a high filtration steady state in which the BSA concentration on the downstream side of the selectivity barrier was washed down to a minimal level, thus maximizing the effective oncotic pressure difference. This is another way of saying that the downstream BSA concentration approaches the convective limit, $(1-\sigma)C_c$, where C_c is the concentration in the capillary lumen (Michel, 1984 and Michel and Curry, 1999). The steady filtration rate was measured by occluding the vessel briefly (5-7 seconds) then releasing the occlusion. The measurements of J_v/A at a pressure of 10 cm H_2O were made after setting up steady filtration at 35 cm H_2O, then rapidly (0.5 s) switching the capillary pressure from 35 to 10 cm H_2O after occluding the microvessel. Reabsorption was marked by the movement of flow marker erythrocytes away from the site of cannulation as fluid moved into the capillary. 3-5 measurements of transcapillary water flow per unit area of vessel wall (J_v/A) were made at each pressure. Thus the control relationship between J_v/A and pressure is determined by the oncotic effects of the BSA gradients established at high filtration pressure and having no added protein in the superfusate. The slope of the

relation measures L_p, and the effective oncotic pressure exerted across the filtration barrier in the microvessel wall was measured from the intercept on the pressure axis (see Fig. 3.2).

To investigate the effect of adding albumin to the tissue on the effective oncotic pressure exerted across the capillary wall in this first series of experiments, measurements were repeated on each of the vessels, with the same protocol as that described above (perfusate albumin concentration 50 mg/ml) except that the superfusate also contained albumin at a concentration of 50 mg/ml applied for 45 minutes before beginning measurements of J_v/A (c.f. Fig. 3.1). Thus paired measurements of J_v/A at pressures of 35 and 10 cm H_2O with and without albumin in the superfusate were made on each microvessel. If a significant oncotic pressure was exerted across the glycocalyx even when the albumin concentration was equal in the tissue and the perfusate, we expected to measure net reabsorption of water across the vessel wall at the low pressure. The four experiments completed in this series are summarized in Table 3.1 of the Results.

The second series of experiments were designed to test whether oncotic gradients could be established across the surface matrix when albumin was added to the tissue at filtration rates that were lower than those set up 35 cm H_2O. We thus measured filtration rates after steady state filtration was set up not only at 35 cm H_2O, but also at 10 and 20 cm H_2O on the same capillary. The same protocol used to set up steady state filtration at 35 cm H_2O was also used at the lower pressures. The pressure in the microvessel was set by partially occluding the microvessel to increase resistance and raise the capillary pressure to that in the water manometer connected to the pipette. Two minutes were allowed for the new steady state to be achieved in the tissue at the cleft exit. This method

to set up steady state filtration at a series of pressures in the same microvessels is the same as that used by Michel and Phillips (1987) and Huxley *et al.* (1993). Figure 3.3 illustrates the experimental design on one of the vessels including a transient experiment to measure L_p and the effective oncotic pressure ($\Delta\pi$) after steady state filtration at 35 cm H_2O. These steady state results for four experiments on four different microvessels are shown in Figs. 3.4a-d. Table 3.2 summarizes the measurements of L_p and $\Delta\pi$ on the four vessels in Figs. 3.4a-d.

3.2.2 Theoretical methods

1. Model description

The idealized mathematical model that was used to interpret our experimental data is similar to the one introduced in the previous chapter shown as Fig. 2.2 except for the boundary conditions applied in the tissue space and the location of the junction strand. The essential physics of the model is contained in four regions. The first region is a surface glycocalyx of thickness L_f which covers the entire endothelial surface including the entrance region to the interendothelial cleft. The second region is the cleft itself showing the idealized junction strand with periodically distributed orifice breaks whose gap height is the same as the wide part of the cleft. In Hu and Weinbaum (1999), the junction strand was located at the midpoint of x=200 nm of the cleft depth for simplicity. However, experimental measurements (Adamson and Michel, 1993) show that the junction strand is frequently close to the cleft entrance with an effective average value for L_1 of only 25 nm. In the present chapter, we investigated the effect of the location of the junction strand on the Starling forces. We also explore two possible approaches in matching the measured value of the hydraulic permeability L_p. In one, we changed the

spacing of the junction strand breaks 2D and in the other we changed the width of the junction orifice 2d. The other dimensions shown in Fig. 2.2 are based on the measurements by Adamson and Michel (1993) of cleft ultrastructure in frog mesentery.

In the model the pericapillary space is broken into two regions, a semicircular region B which surrounds each cleft exit, and a far field, region C, where the exit flows merge, as shown in Fig. 2.2b. The radius of region B, L_B, is determined by the half average spacing between two neighboring clefts, 5 μm, along the cross-sectional perimeter of the capillary. For frog mesentery, approximately six clefts are evenly distributed on the cross-section of the capillary wall. Region B describes the mixing in the wake from an individual junction strand orifice immediately surrounding the cleft exit in the tissue space. Figs. 3.6 and 3.7 in the results section show that the protein concentration profiles in the tissue have a steep concentration gradient that extends roughly 2 μm from the cleft exit. Therefore, the radius of region B, L_B=5 μm, is sufficient for the mixing of the individual exit jet to form a uniform flow at the entrance to region C. The jet from each individual cleft merges with those from the adjacent clefts in region C. The continuity of protein concentration and flux are satisfied at the interface between region B and region C. Since the steepest gradients occur in the immediate vicinity of the cleft exit, the effect of the curvature of the vessel wall is very small.

The protein concentration at the far end of region C, where the mesothelium is damaged for back loading of the tissue, is prescribed. After 45 minutes of loading the albumin concentration at the edge of region C has the same protein concentration as the superfusate, C_i=C_c. If there is no tissue loading, the protein concentration at the far end of region C will approach the ratio of the two fluxes, C_i=J_s/J_v, when the steady state is

achieved as demonstrated by Michel and Phillips (1987). Here, J_s is the total protein flux entering into the tissue space and J_v is the total fluid flux into the tissue space. If protein-free solution continuously washes the outside of the tissue where the mesothelium is damaged, the boundary condition at the far edge of region C becomes C_i=0.

2. Mathematical formulation

The model consists of an ordered matrix at the endothelial surface which forms the primary molecular filter to macromolecules, in series with pathways for water and solute through infrequent breaks in the junctional strand. The geometry of these breaks in frog mesenteric microvessels has been quantified using serial section electron microscopy (Adamson and Michel, 1993). Thus the model is an extension of the fiber matrix model of Curry and Michel (1980), which is modified to take into account the three-dimensional geometry of the cleft between adjacent endothelial cells and the breaks in strand and a more rigorous description of the hydraulic resistance due to the surface matrix layer. The development and evaluation of the three-dimensional model using permeability data from frog mesenteric microvessels (including permeability coefficients for small and intermediate sized solutes) has been described in a series of papers over the past decade from our laboratories and has been reviewed in detail recently (Michel and Curry, 1999) and Weinbaum (1998).

In its present form, the surface matrix-junction break model uses rigorous hydrodynamic theory, for (i) the resistance to water flows through an ordered array of surface fibers; (ii) the additional resistance due to the walls of the cleft and (iii) flows through orifice-type openings in the junction strand. A comparison of the original fiber matrix theory as described by Curry and Michel (1980) and the revised theory is given in

Michel and Curry (1999). The new model combines the properties of a sieving matrix and the important role of series barriers in the cleft introduced by Perl *et al.* (1971).

The detailed description of the basic theoretical model that was used to describe the concentration profiles and analyze the experimental results is provided in Hu and Weinbaum (1999). Here, we summarize only its most important features. The present model and that in Hu and Weinbaum (1999) differ from all previous studies in that a new form of the Starling equation is proposed in place of equation (1.1). Both the hydrostatic and oncotic pressures are evaluated locally across the surface matrix layer. The new equation is

$$J_v / A = L_p[P_c - P(0,y) - \sigma_f(\pi_c - \pi(0,y))]. \qquad (3.1)$$

Here, P(0,y) and $\pi(0,y)$ are the local hydraulic pressure and osmotic pressure just behind the fiber matrix at x=0, respectively, see Fig. 2.2. Equation (3.1) differs fundamentally from equation (1.1) in that it is applied just across the sieving matrix, rather than in a global sense across the capillary wall, and that it is spatially heterogeneous at the cellular level. Both P(0,y) and $\pi(0,y)$ vary along the length of the cleft due to the orifice openings in the junction strand.

A locally, one-dimensional convection-diffusion equation across the surface matrix was solved to obtain the velocity and concentration distribution across the surface matrix. The local coupling equation at the interface between the backside of the surface matrix and the cleft requires that the combined convective and diffusive flux of solute entering the cleft be equal to the total flux of solute leaving at the backside of the matrix. However, in this coupling condition the concentration, velocity and pressure at the backside of the matrix are all unknown and these parameters are non-linearly related to

each other. This non-linear coupling requires that all regions be treated simultaneously using iterative convergence techniques.

Within the cleft itself, region A, the height of the cleft is small compared to both the average distance between the pores and the depth of the cleft, so that the water flow in the wide part of the cleft can be approximated by Hele-Shaw flow, as first proposed in Tsay and Weinbaum (1989). The local velocity profile is parabolic and satisfies Laplace's equation for the pressure. Similarly, the concentration field satisfies a two-dimensional convection-diffusion equation, which is averaged across the cleft height. The treatment of regions B and C, the cleft exit region and larger tissue space, was simplified in Hu and Weinbaum (1999) to provide for closed form analytic solutions. The same simplifications are applied herein except that the concentration at the edge of region C is required to equal the concentration in the superfusate where the mesothelium is damaged.

3. Parameters

The geometry of the junction strand and surface matrix is shown in Figs. 2.2a,b. We shall also present results for other junction strand geometry to show the effect of orifice spacing, orifice width and junction strand location on the filtration flow and effective oncotic pressure. Small solutes have only a minor influence on the oncotic force across the surface matrix because the fiber matrix only a minor resistance to the small solutes. In our previous study (Fu *et al.*, 1994), we showed the primary resistance for small solutes was determined by the two-dimensional diffusion through the breaks in the junction strand of endothelial cleft. The selection of the diffusion coefficient, D_f, for albumin in the surface glycocalyx is determined by the requirement that our current model provides an optimum fit to the measured steady state filtration profile in the absence of tissue

loading. The model predicts a dense matrix whose effective value for D_f for albumin is 3 orders of magnitude smaller than its value in solution. This is discussed at length in Hu and Weinbaum (1999). The value of reflection coefficient for albumin in the surface matrix, σ_f, is determined by our experimental measurements of the effective oncotic pressure in the high filtration limit ($\sigma_f^2\pi_c$) in Tables 3.1 and 3.2. The values of σ_f fall in the range of 0.8 to 0.94.

3.3 Results

3.3.1 Experimental results

Figure 3.2 shows an example of an experiment from the first series of experiments on a single venular microvessel where multiple measurements of the transcapillary water flows, J_v/A, were made first with albumin solution (50 mg/ml) in the perfusate and no albumin in the superfusate, then with albumin (50 mg/ml) in both the perfusate and the superfusate. When the pressure was quickly dropped to 10 cm H_2O there was significant reabsorption. In fact, the effective oncotic pressure exerted across the filtration barrier in the vessel wall was 17 cm H_2O. After albumin was allowed to distribute throughout the tissue the striking result was that the transcapillary fluid fluxes at pressures of 35 and 10 cm H_2O were the same as when albumin was absent from the tissue. In particular, reabsorption was still measured at a pressure of 10 cm H_2O, showing that the presence of albumin in the superfusate at the same concentration as in the perfusate did not reduce the effective oncotic pressure to close to zero as expected if diffusion of albumin in the tissue raised the concentration of albumin on the tissue side of the filtration barrier. The results from four experiments in the first series of experiments with a mean L_p of $3.8\pm1.5\times10^{-7}$ cm/(cmH_2O·s) showed no significant difference between filtration rates and effective oncotic pressures exerted by albumin measured before albumin was added to the superfusate and those measured after albumin was added to the superfusate as summarized in Table 3.1. The mean oncotic pressure with no albumin in the tissue was 18.2±1.7(SEM) cm H_2O and with albumin in the tissue was 18.2±3.1 cm H_2O. Thus after filtration at high capillary pressures the oncotic difference was established across the

primary oncotic barrier within the capillary wall even though there was no effective concentration difference between lumen and tissue.

To further test our hypothesis, we extended this approach to set up initial steady states not only at 35 cm H_2O, but also at lower capillary pressures as outlined in the methods for the second series of experiments. Figure 3.3 compares the transient reabsorption rates measured at 10 cm H_2O with additional filtration measurements made after setting up steady state filtration at a pressure of 10 cm H_2O. Albumin was in the superfusate throughout the experiment. If albumin was able to diffuse into the water pathway at lower filtration rates, then we expected that the effective oncotic pressure difference would be close to zero, and the filtration rate would be determined mainly by the difference in capillary pressure across the wall, in this case 10 cm H_2O. The dotted line is the expected filtration rate if there were no effective oncotic difference. The line has the same slope as the initial transient experiments (dash-dot line; $L_p = 2.44\times10^{-7}$ cm/(cm H_2O·s)). The results of the experiment show that, after establishing steady state filtration at 10 cm H_2O, the filtration rate was 0.0054×10^{-4} cm/sec which is 20% of the filtration rate expected in this microvessel if no oncotic force was opposed to the applied pressure of 10 cm H_2O. This result indicates that there was a significant oncotic pressure due to an albumin concentration difference even under low filtration rate conditions. The results suggest that some mechanism protects a region on the downstream side of the filtration barrier from back diffusion. The same result was obtained in four microvessels. Three additional experiments were carried out in which steady state filtration was set up at pressures of 10, 20 and 35 cm H_2O. The results of all four experiments are shown in Figs. 3.4a-d, where each experiment has been specifically modeled using the approach

explained below. The transient measurements for these four experiments are not plotted in Figs. 3.4a-d in order to simplify the figures. The values of the L_p's and the oncotic pressure intercepts ($\Delta\pi$) for these four experiments are shown in Table 3.2. The mechanisms leading to the maintenance of the concentration difference of albumin across the endothelial glycocalyx under our experimental conditions are illustrated using the following theoretical results which model the experimental conditions described above.

3.3.2 Theoretical results

1. Detailed concentration distribution

The key predictions of the theoretical model corresponding to the experimental results shown in Fig. 3.2 are presented in Figs. 3.5-7 where the concentration profiles for albumin from the lumen to the tissue are plotted at three positions within the cleft: along the centerline (y=0) of the orifice break in the junctional strand, along the edge of the orifice (y=75 nm) and at y=2160 nm, corresponding to y=D, the half spacing of the neighboring orifices. The junction strand lies at the midpoint of the cleft depth, x=200 nm, and the other parameters are shown in Fig. 3.4, which are the typical values based on the microstructural measurements of frog mesentery capillaries (Adamson and Michel, 1993). Thus, the hydraulic permeability of the wall is evaluated to be 2.43×10^{-7} cm/(cmH_2O·s), which is similar to mean value of L_p in Tables 3.1 and 3.2. The effect of junction strand geometry and location will be examined later. The concentration profiles in the surface glycocalyx, the cleft and tissue space when the albumin is in the perfusate alone are shown in Fig. 3.5 for the high filtration flow, P_c=35 cm H_2O. The protein concentration just behind the surface glycocalyx at y=0 and within the break is 0.066 for σ_f=0.94. The values approach the high filtration limit, $(1-\sigma_f)C_c$, as expected when the

concentration leaving the tissue is determined by the steady state flux of albumin and water through the vessel wall. The tissue concentration is set at zero at a distance of 100 μm from the vessel wall because the resistance of the mesothelium was deliberately reduced by placing a glass rod on the tissue to damage the mesothelial barrier. As a result the albumin concentration falls towards zero in the tissue side of the cleft and in the tissue. It is important to note that, because of the wide spread of the water flow in the tissue space, the Peclet number Pe in the tissue, region C in the model, is << 1 and this region is diffusion dominated. Thus, the concentration decreases almost linearly with distance in the tissue as shown in the inset of Fig. 3.5.

The concentration profiles in the surface glycocalyx, the cleft and tissue space with the superfusate containing albumin 50 mg/ml are shown in Fig. 3.6. The concentration in the cleft and tissue space is non-uniform, although the interstitial fluid concentration is clamped at the same value as the plasma at a distance of 100 μm where the mesothelium is damaged. Steady state filtration was established at a pressure of 35 cm H_2O. High filtration flow washes away the protein in the region between the rear of the surface glycocalyx and the junction strand, and the albumin concentration directly behind the junctional strand is 0.13 to 0.15C_c. These values indicate the difference in albumin concentration across the glycocalyx has been reduced from 0.94 C_c to 0.87 C_c; less than 10% in spite of a large concentration gradient for albumin on the tissue side of the cleft. As shown in Fig. 3.6, the tissue concentration gradients in the pericapillary space extend into the cleft on the tissue side of the junction strand, but have only a minor effect on the concentration distribution in the protected region, 0<x<200 nm, between the back of the surface matrix layer and the junction strand. The presence of the junction strand reduces

the back diffusion, so there is only a small change in the concentration behind the surface glycocalyx. The remarkable result is that even though the oncotic pressure due to albumin in the tissue has been increased from zero in the control state to 27.2 cm H_2O, the same as the plasma, the fluid flux does not change significantly as shown in the experimental results. As noted above, the albumin gradients in the tissue are almost linear; the gradient is determined by arbitrarily setting the albumin concentration equal to the superfusate concentration 100 μm from the vessel. We show later that the position of the damage site does not modify the conclusion that the main oncotic pressure difference lies across the surface glycocalyx though it does affect the tissue gradients in regions B and C.

The transient reabsorption at pressures below the plasma oncotic pressure (Fig. 3.2) can not be sustained. The protein would accumulate at the backside of the surface glycocalyx and back diffusion from the tissue would elevate the concentration between the surface glycocalyx and junction strand after sufficient time. Thus, the absorptive force across the surface glycocalyx would decrease gradually, and eventually a new steady state with a small net filtration would be achieved where one expects that the concentration difference of albumin across the glycocalyx would be close to zero because the back diffusion would dominate over the washout of the protein at low filtration rates. Fig. 3.7 illustrates the new steady-state concentration distribution for the low filtration flow, P_c=10 cm H_2O, in the cleft and tissue space. The striking result is that even for the low filtration flow, the concentration distribution in the cleft and tissue space is non-uniform. The concentration behind the surface glycocalyx is raised, but is still washed down to a value lower than the tissue space and is protected somewhat from back diffusion by the junction strand.

2. Filtration-pressure curves

The comparison of the experimental results with the predictions of the theoretical model are shown in Figs. 3.4a-d for four microvessels with hydraulic conductivity L_p ranging from 0.67 to 3.0 cm/(cmH_2O·s). Also shown are the theoretical predictions of the classical Starling theory with tissue loading and the steady state predictions of the present model without tissue loading. Because Adamson and Michel (1993) found that the length of the breaks in the junction strand in frog vessel was relatively constant, L_p was varied by changing break frequency. The filled circles are our experimental measurements for tissue loading. The value of the reflection coefficient σ_f in our experiment ranged from 0.8 to 0.94. To show the effect of the variation of σ_f we show results for the two extreme values, σ_f=0.8 and σ_f=0.94. The dotted and dash-triple-dot curves in these figures show the steady state relation between the fluid filtration and capillary pressure without tissue loading, where the tissue concentration reaches the equilibrium value $C_i=J_s/J_v$ predicted by Michel and Phillips (1987). The dotted curve is for σ_f=0.94 and the dash-triple-dot curve is for σ_f=0.8. The solid curve is the steady state relation predicted when the tissue has been loaded to the same protein concentration as the plasma and σ_f=0.94 and the long-dashed curve is for σ_f=0.8. The dash-dot line is the result calculated using the classical Starling equation, where P and π are evaluated using the global values for the concentration in the lumen and tissue. When the tissue concentration is the same as the plasma, $C_i=C_c$, equation (1.1) reduces to $J_v/A=L_p(P_i-P_c)$.

Our present model provides reasonable agreement with the experimental data, whereas the classical application of the Starling equation predicts filtration rates that are far larger than observed. According to the classical application of Starling equation, the

actual Starling force is zero when the tissue has the same protein concentration as the lumen. However, the measured fluid filtration is also higher than the steady state when albumin is not in the tissue (dotted line), especially for the low filtration condition. This indicates that back diffusion from the tissue penetrates the junction strand orifice and raises the protein concentration behind the surface glycocalyx at lower flow rates. The result is a decrease in the effective Starling force across the surface glycocalyx and an increase in the fluid filtration across the endothelium. This elevation in the fluid filtration, however, is not significant at high capillary pressure. For the high filtration condition, the high convective flow washes away the protein at the junction strand orifice and inhibits the back diffusion from the tissue side. The degree of the back diffusion depends on the Peclet number at the junction strand orifice as will be analyzed in the discussion.

3. Effect of junction strand structure and location

We also investigated the effect of changes in the length and frequency of the breaks in the junction strand by determining combinations of length and frequency which give the same L_p as measured. For example, for L_p=4.6×10^{-7} cm/(cmH_2O·s), we can either maintain a 2d of 150 nm but decrease the spacing of the junction strand orifices to 2D=1478 nm or double the break length to 2d=300 nm and have a 2D=2010 nm. Although break length has been doubled from 150 nm to 300 nm, the change in the fluid filtration curve is negligible, as shown in Fig. 3.8. Similar results are presented for L_p=0.67×10^{-7} cm/(cmH_2O·s), a low filtration rate that approaches mammalian muscle capillaries, where results are shown for 2d=40 and 150 nm and 2D=6696 and 10,160 nm, respectively. For both high and low L_p one observes that the detailed structure of the strand has only a minimal effect on the curves for the steady state water flux.

The location of the junction strand, however, does have a small but significant effect on the effective Starling force, as shown in Fig. 10. The solid line is for a junction strand at the midpoint, L_1=200 nm, of the cleft depth and the dotted line is for a junction strand close to the cleft entrance, L_1=25 nm. Both have the same L_p=2.43×10^{-7} cm/(cmH_2O·s) and the same junction orifice length 2d=150 nm. To achieve the same L_p, the spacing of the junction strand 2D was reduced to 2940 nm for the junction strand close to the matrix. The filtration-pressure curve for the junction strand at L_1=200 nm lies beneath the curve for the junction strand close to the entrance. The velocity and concentration profiles (not shown), show that as the junction strand moves closer to the entrance, the velocity profile behind the surface glycocalyx is a more highly convergent flow with a higher maximum velocity on the centerline y=0. In the region removed from the junction orifice, the velocity is close to zero and the concentration field diffusion dominated. Thus, the concentration in the region removed from the junction orifice is increased due to diffusion from the lumen. The Starling force is therefore reduced and the fluid filtration increased.

4. Diffusion distance in tissue

The length of region C is determined by the location where the mesothelium is damaged to facilitate diffusion from the superfusate to the tissue. The location of damage is difficult to control and, thus, we have explored different values of L_C. For a short distance, L_C=15 μm, the boundary condition C_i=C_c is applied much closer to the microvessel at a distance that is the sum of L_B and L_C, 20 μm, using our present model. The results shown in Fig. 3.10 indicate that even if the albumin concentration near the cleft exit is increased by reducing the diffusion distance in the tissue, the increased

tendency for back diffusion remains small and would account for at most a 15 percent increase in filtration above that predicted for a diffusion distance of 100 μm.

3.4 Discussion

Both the current experiments with loading of albumin in the tissue and their theoretical interpretation conform to the hypothesis that for the continuous capillaries of frog mesentery the oncotic and hydrostatic pressures which determine transcapillary fluid flux apply across the endothelial cell glycocalyx. Further, the results demonstrate that the local protein concentration and pressure behind the surface matrix layer can differ greatly from the tissue concentration and pressure with the result that the Starling forces across the surface matrix layer will depart significantly from the global Starling forces across the entire endothelial layer, as shown in Figs. 3.2, 2.3, 3.6 and 3.7. The novel aspect of our experimental design and calculations is the focus on the gradients in the cleft and tissue, and the precise link between gradients of albumin in the tissue and the albumin concentrations and hydrostatic pressures in the cleft. In the following discussion we first review the ultrastructural basis for the model in frog mesenteric capillaries and evaluate new aspects of our experimental design, and then consider the application of this conclusion to mammalian microvessels. We note in particular that Levick (1994) demonstrated that high velocity water flows downstream from localized fenestrae resulted in a larger oncotic pressure difference across the fenestral diaphragm than expected from the blood to tissue concentration difference after loading the tissue with elevated albumin concentrations.

3.4.1 Mechanism of the junction strand shielding

The crucial insight into the detailed mechanism as to when the junction strand will serve to create a protected region on the lumen side of the junction strand that prevents

back diffusion through the junction strand pores is obtained by examining the Peclet number Pe at the orifice openings in the strand. The Peclet number represents the ratio of convection to diffusion and when Pe>1.0 at the orifice break, solutes on the tissue side of the cleft will have difficulty diffusing upstream against the convective flux of solutes that is being funneled through the orifice openings by the filtration flow. In this sense the junction strand pores act much like a sonic throat in a Laval nozzle where pressure disturbances can not travel upstream when the Mach number is >1.0. The calculated values of Pe at the breaks in the junction strand in Figs. 3.5-3.7 are 2.34, 2.51 and 0.32, respectively. These values of Pe explain why the oncotic pressure on the backside of the surface glycocalyx is nearly the same in Figs. 3.5 and 3.6, where Pe>1, even though the tissue concentration of albumin is equal to that in the perfusate in Fig. 3.5. It also explains why there is significant back diffusion in Fig. 3.7 where the steady state filtration is low and Pe=0.32.

The concentration behind the surface glycocalyx is raised due to the back diffusion when Pe at the junction orifice is less than one, but is still washed down to a value lower than the tissue space as shown in Fig. 3.7. In fact the value of the albumin concentration at the back of the glycocalyx (0.75 C_s) predicts that the oncotic pressure difference across the glycocalyx is 8.6 cm H_2O. This value is comparable to the predicted value of 9.9 cm H_2O from the steady state formula of Michel and Phillips (1987) which does not take into account back diffusion. Note that, under the same conditions, the concentration of albumin at the cleft exit approaches 90% of the concentration in the tissue, and the maximum oncotic pressure across the entire capillary wall is less than 2 cm H_2O. These results clearly demonstrate that oncotic gradients across the entire capillary wall are not

the determinants of the fluid balance. Rather the fluid balance is determined by the albumin concentration differences across the surface glycocalyx maintained by a protected region between the downstream side of the surface glycocalyx and the break in the junctional strand. The principal mechanism acting to prevent albumin accumulation on the tissue side of the glycocalyx is the throat effect of the break in the strand which increases the local fluid velocity sufficiently to reduce the tendency of albumin to back diffuse from the tissue and thereby abolish the concentration difference across the glycocalyx.

3.4.2 The pathways for water and solutes

The basic hypothesis in our mathematical model is that the surface glycocalyx provides both the primary molecular sieve and diffusive barrier for plasma proteins crossing via porous pathways and that this sieving matrix does not fill the entire interendothelial cleft. If the sieving matrix were to fill the entire endothelial cleft, the shielding effect of the junction structure were to be lost and the model would reduce to the single layer model first presented in Michel and Phillips (1987). In this limit, the throat effect of the orifice will be lost and the difference in the concentration between the cleft exit and tissue would be greatly reduced. The pores in the junction strand would behave similar manner to the fenestra pores studied by Levick (1994). In this case, the convective effect of the flow in washing away the protein in the vicinity of the pores in the junction strand would be greatly reduced.

At present the evidence for the structure of glycocalyx is only indirect since the matrix under most conditions is difficult to stain and preserve intact for electron microscopy. The most convincing evidence that the sieving structure is confined to a

surface layer is the detailed calculations for L_p for frog mesentery in Fu *et al.* (1994), the measurements of the surface matrix layer thickness for frog mesenteric microvessels, Adamson and Clough (1992), and the recent theory and experiments for the labeling of the cleft using high molecular weight tracers (1997). Furthermore, the serial section electronmicrographs in (Adamson and Michel, 1993) clearly reveal that the gap height of the breaks in the junction strand, 20 nm, is essentially the same as the wide part of the cleft. Thus, the junction strand itself is unlikely to provide the molecular sieve for plasma proteins. This combined evidence has led Michel (1997), Weinbaum (1998) and Hu and Weinbaum (1999) to hypothesize that the surface glycocalyx is the molecular filter, at least for frog mesenteric capillaries.

Detailed evaluation of the model parameters and the methods to solve the coupled nonlinear equations to describe the flows of water and albumin through the matrix, cleft, and tissue spaces has been described (Hu and Weinbaum, 1999). The new variations of the model described in the present work include a modification of size and frequency of the breaks in the junctional strand to describe the actual range of experimental L_p's measured in our test vessels (Figs. 3.4a-d) and to demonstrate that such variation in the junction geometry does not significantly modify the predictions of the model (Fig. 3.8). There is a tendency for the experimental data to fall slightly higher than the predicted values. One source of this discrepancy may be experimental, reflecting the difficulty of maintaining a uniform pressure in the vessel during partial occlusion, while steady state filtration was set up at a pressure of 10 cm H_2O. For example, if the capillary pressure were close to 7 cm H_2O during partial occlusion instead of 10 cm H_2O, the increase in pressure after occluding the vessel to measure filtration, combined with a smaller

transcapillary albumin concentration difference, would impose a small transient filtration on the steady state flux. This small transient would cause an overestimate of steady state water flux, but the extent of the error is about 20%.

The other model parameter which we evaluated both experimentally and theoretically was the diffusion distance from the vessel wall to the region where the mesothelium was disrupted. In control experiments we found that placing a glass rod at 4-5 positions along the length of a vessel at a distance of about 100 μm from the vessel disrupted the mesothelium sufficiently to allow albumin to diffuse into the tissue, but did not damage the microvessel wall as demonstrated by a constant microvessel L_p before and after the procedure. The glass rod had a diameter of at least 15 μm, and disrupted mesothelial cells with a mean diameter of at least 30 μm. Thus albumin was likely to cross the barrier at distances closer than 100 μm from the vessel. Our calculation shows that there is no significant change in the fluid filtration for a low hydraulic permeability and degree of increase in fluid filtration depends on the frequency of the junction orifice.

3.4.3 Mammalian Microvessels

One of the key results obtained in the previous section is that the junction strand structure has only a minor effect on the Starling force if L_p is unchanged. This is important in extending our theoretical model to continuous mammalian vessels. The structure of the interendothelial cleft and the organization of the junction strand observed in rat heart capillaries by Bundgaard (1984) is qualitatively similar to frog mesenteric capillaries except that the length of the breaks is much shorter, typically the width of a single transmission section, 40-50 nm. However, there was insufficient data to accurately

determine break frequency. At present there are no ultrastructural studies for mammalian capillaries equivalent to Adamson and Michel (1993) for frog mesentery. In the latter study, measurements of L_p were performed on the same vessels for which serial reconstructions were obtained for both the junction structure and the cleft depth. Figure 3.8 demonstrates that we could account for the measured filtration rates in one vessel with an L_p of 0.67×10^{-7} cm/(cm H_2O·s) by reducing the break length from 150 to 40 nm (with a corresponding change in break frequency). The L_p of this vessel overlaps the upper range of values in mammalian muscle microvessels. Thus, the same basic mechanisms whereby high water velocities at the breaks in the strand reduce the diffusion of tissue proteins in the cleft between endothelial cells are expected to apply in mammalian microvessels. Mammalian microvessels with smaller L_p's or with only a fraction of the total water flow through a junctional pathway could be described if the frequency of breaks in the strand was much smaller than in frog mesenteric vessels, or if the pathways for flow were more tortuous than described above. As suggested by Michel (1997), it is likely that most of these proteins enter the tissue by parallel pathways formed by large pores or vesicles. The extension of present theory to predict the effective Starling force for mammalian capillaries with continuous endothelium if the surface glycocalyx is the primary sieving layer for proteins warrants further investigation.

There is still some controversy as to whether the surface glycocalyx or small pores in the junction strand provide the molecular filter for proteins. Bundgaard (1984) also observed narrow gaps with 4-6 nm width and 10-20 nm height between adjacent membranes using ultrathin 10-15 nm EM sections and suggested that these gaps might serve as a molecular sieve. While such small pores could serve as molecular filter for

albumin they do not account for the fact that most of the water and solute would pass through the non-selective large breaks (40-50 nm) in the junction strand whose height is the same as the wide part of the cleft. Vink and Duling (1996) have used fluorescent tracers to measure the thickness of a glycocalyx layer in hamster cremaster muscle capillary *in vivo*. They found that the thickness of the layer which excludes FITC-dextran is 0.4 to 0.5 μm. It is not known whether all or a fraction of this layer would serve as a molecular sieve for plasma proteins or what the displacement of the cationized ferritin layer would be if an experiment equivalent to Adamson and Clough (1992) could be performed on hamster cremaster microvessels. Experiments are needed to investigate the surface glycocalyx and the size and frequency of junctional strand breaks in mammalian microvessels.

The role of highly localized water flows on the downstream side of fenestrae has been examined both experimentally and theoretically by Levick and coworkers with reference to fluid exchange in the synovium. In experiments in which the tissue concentration of albumin was increased, these investigators also showed that the effects of extravascular albumin on fluid exchange were much less that intravascular albumin. The explanation in the fenestrated vessel is that the high water velocity exiting the fenestra decreases the albumin concentration downstream of the fenestra in a region that extends a few microns into the tissue. Our calculations show that such tissue gradients also form at the cleft exit in continuous capillaries although the water velocities are much lower than in fenestrated microvessels. However, for continuous capillaries, the primary interaction of high water velocities and tissue protein occurs within the cleft at the highly localized breaks in the junctional strand. Nevertheless, the elegant studies of Levick and

his colleagues in synovium also conform to the hypothesis tested in the present experiments that the Starling forces which determined transcapillary fluid exchange are not the global difference in hydrostatic and oncotic pressure between blood and tissue, but the hydrostatic and oncotic pressure across a selective matrix across the glycocalyx or fenestral diaphragm.

Lastly, we emphasize that for either frog or mammalian microvessels it is very difficult, if not impossible, to measure the concentration distribution of the oncotic protein within the cleft itself under experimental conditions. A detailed theoretical model is thus essential to fill in the gaps and provide essential insights as to what is occurring at the cellular microstructural level. The power of the theoretical model is that it has the flexibility to explore in detail the effect of detailed junctional ultrastructure on measured macroscopic behavior.

Table 3.1 **Summary of the effective osmotic pressures with albumin in the superfusate and no albumin in the superfusate for different vessels.**

	L_p $\times 10^7$ cm/($cmH_2O \cdot s$)	$\Delta\pi$ (cm H_2O) (no albumin in the superfusate)	$\Delta\pi$ (cmH_2O) (50 mg/ml albumin in the superfusate)
Vessel 1	2.6	15.4	14.3
Vessel 2	3.1	23.0	27.5
Vessel 3	4.6	17.0	15.5
Vessel 4	3.3	17.5	15.5
Average	3.8±1.5	18.2±1.65	18.2±3.1

Table 3.2 **Summary of the L_p's and effective oncotic pressures with albumin in the superfusate (shown as *) and with no albumin in the perfusate for 4 vessels in which both transient and steady state measurement of filtration were made.**

Vessel	L_p $\times 10^7$ cm/(cmH_2O·s)	$\Delta\pi$ (cm H_2O)
# 1 (8a)	0.76	19
# 2 (8b)	1.2	15.5, 18*
# 3 (8c)	3.0	25
# 4 (8d)	2.4	21*
Average	1.8±0.45	20.1±1.4

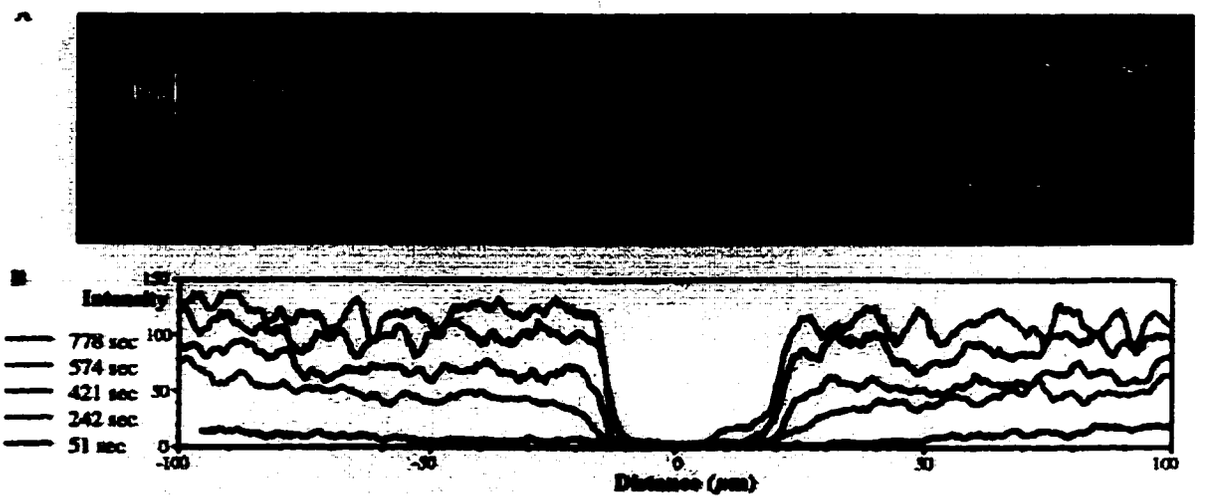

Figure 3.1 Concentration gradients of FITC-Albumin in the tissue of the frog mesentery obtained using a fluorescence confocal microscope to form images of the mesentery transverse to the longitudinal axis of a venular capillary. Prior to the experiment the mesothelium, approximately 100 μm on either side of the capillary, was gently stroked with a fine glass rod to disrupt the mesothelial barrier to facilitate albumin diffusion into the tissue. After 12 minutes the albumin tracer concentration was close to 130 units, and after 20 mins equals to that in the superfusate (160 units).

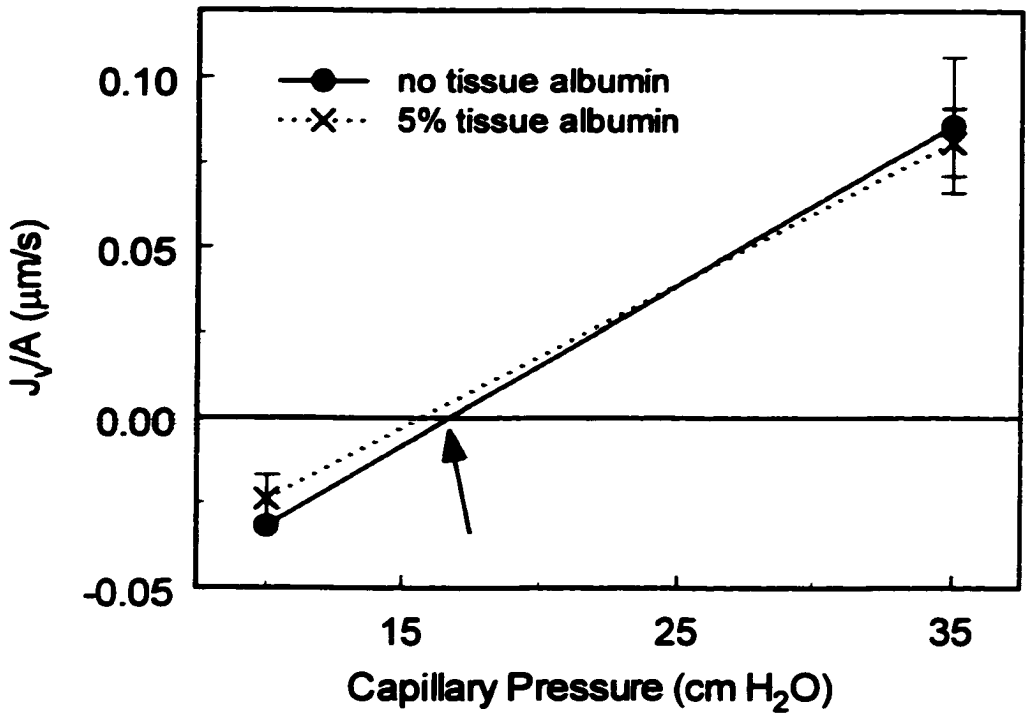

Figure 3.2 Experimental results from an experiment in which steady state filtration was set up at 35 cm H_2O, and fluid flux, J_v/A, measured at capillary pressures of 35 cm H_2O and 10 cm H_2O immediately after occluding the vessel (transient measurements). 3-4 measurements of J_v/A were made at each pressure. Filtration was measured by transiently occluding the microvessel for 5-7 seconds, with up to 1-2 minutes between occlusions. The solid line is the control measurements with albumin perfusate concentration set at 50 mg/ml and no albumin in the superfusate, and the dotted line is the measurements with the high protein concentration (50 mg/ml, same as perfusate concentration) in the superfusate. The arrow points to the effective oncotic pressure. It shows the effective oncotic pressure with tissue loading is nearly indistinguishable from the control. $L_p=4.6\times10^{-7}$ cm/(cmH_2O·s).

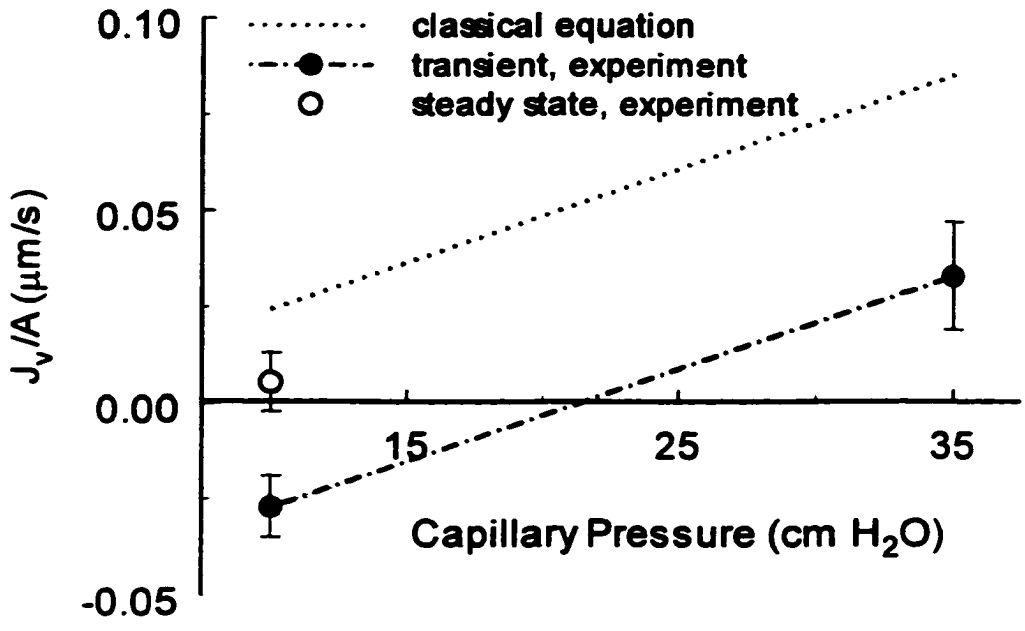

Figure 3.3 The results of an experiment in which the transient filtration (at 35 cm H_2O) and reabsorption (at 10 cm H_2O) were first measured with albumin in the perfusate after steady state filtration at 35 cm H_2O (as in Fig. 3.2). 3-4 measurements of J_v/A were made at each pressure. L_p was 2.44×10^{-7} cm/(cm H_2O·s) and the effective oncotic pressure of albumin was close to 21 cm H_2O (dash-dot line). After albumin was loaded into the tissue, there was no change in the measured filtration rate at 35 cm H_2O as in Fig. 3.2. Instead of rapidly dropping pressure to 10 cm H_2O as in Fig. 3.2, we set the capillary pressure at 10 cm H_2O for 2 min then measured the filtration rate resulting from this new low pressure steady state. The filtration rate was only 20 percent of that expected if the oncotic pressure difference due to albumin had been abolished under these low filtration rate conditions (dotted line). The results of this experiment together with three additional experiments with steady state filtration measured at 10, 20 and 35 cm H_2O are shown in Fig. 3.4 where they are compared with the model predictions.

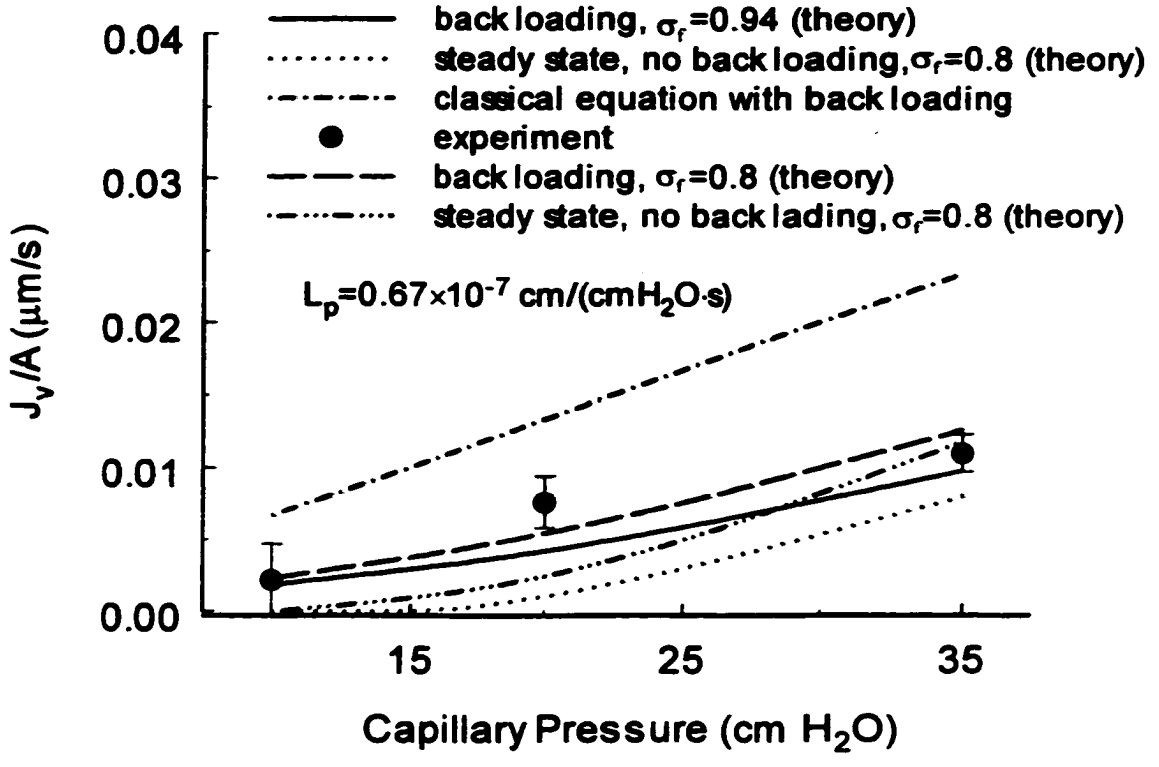

a

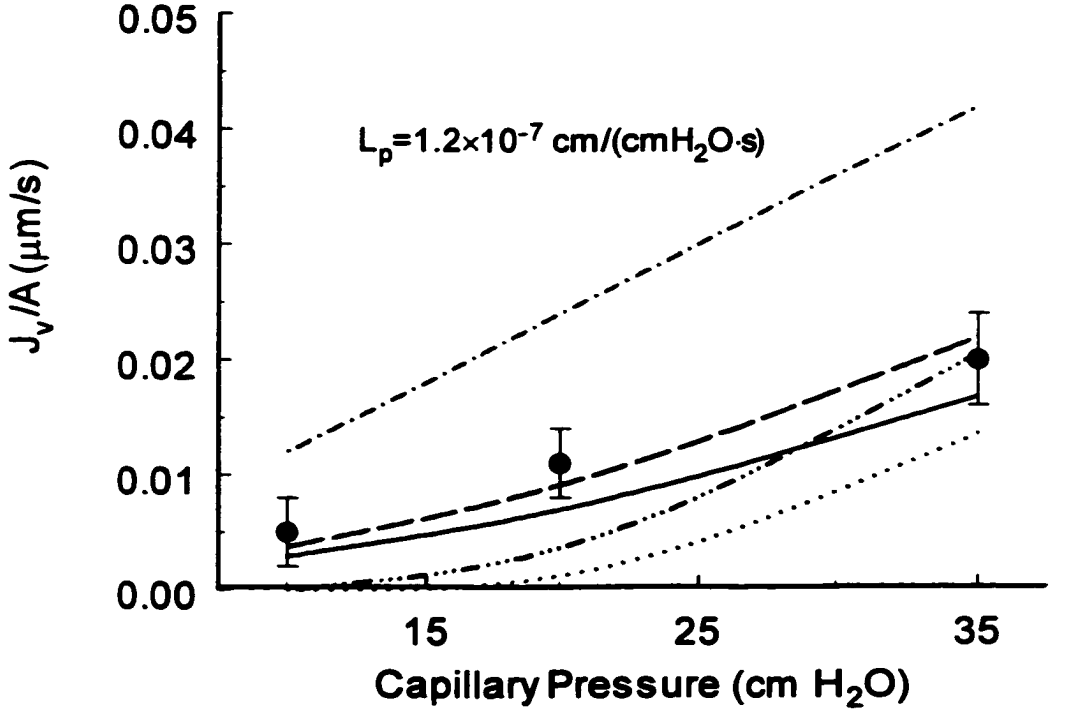

b

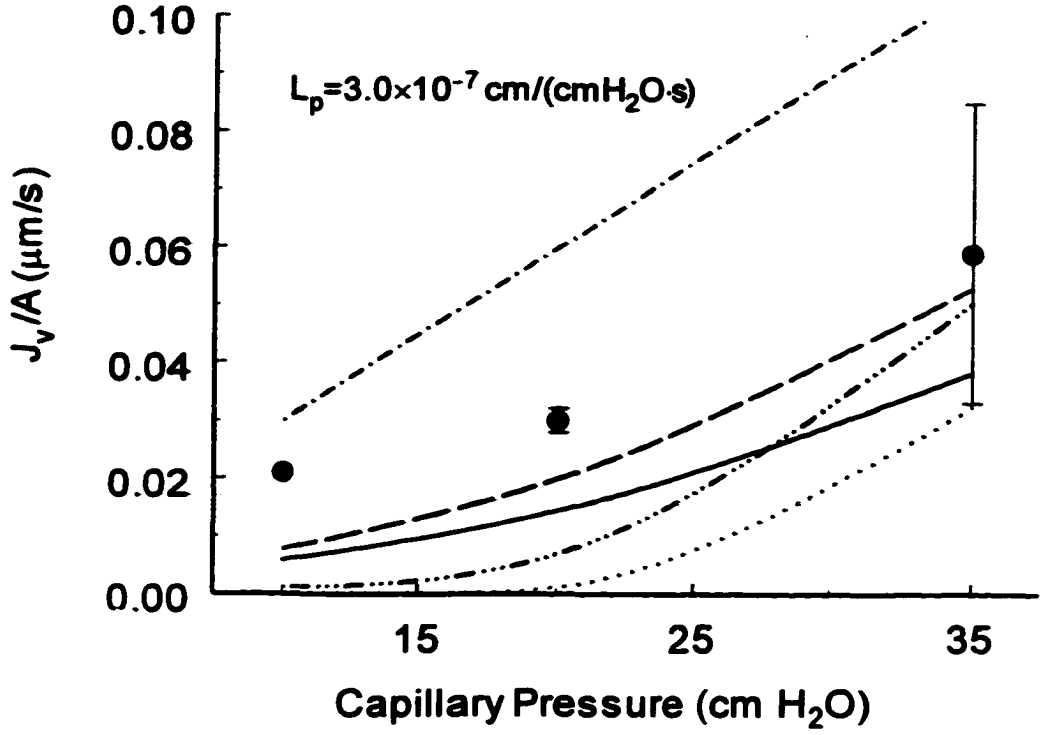

c

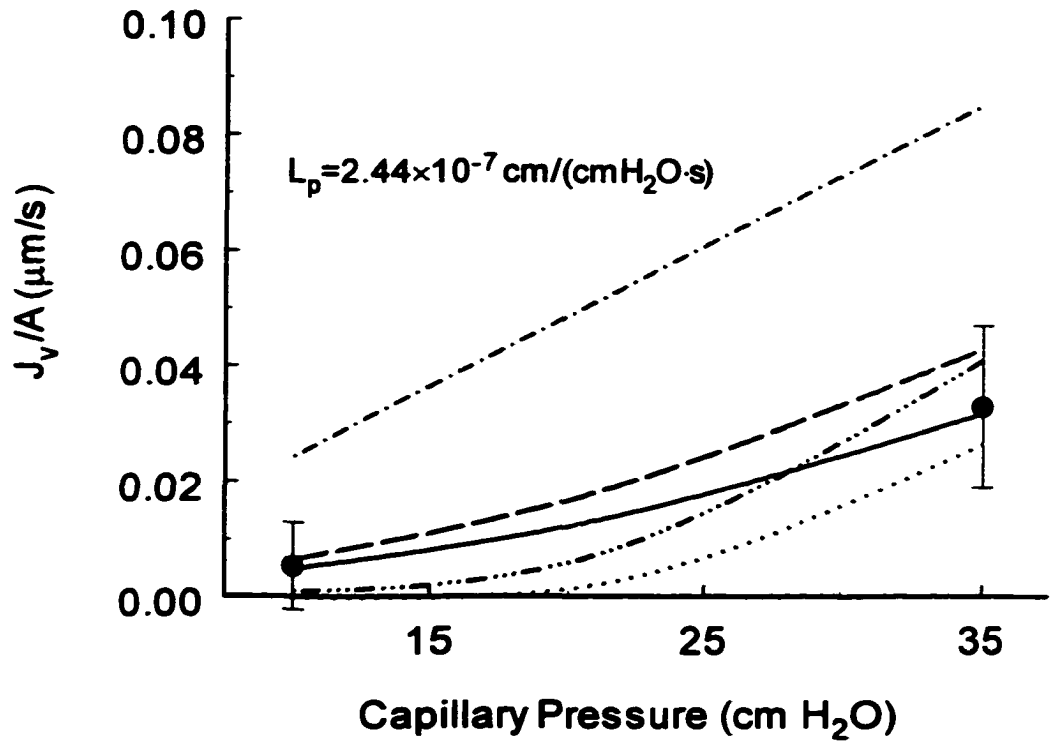

d

Figure 3.4 The comparison of the filtration flux, J_v/A, predicted by the present model for the steady state with the experimental value from four experiments (including Fig. 3.3). The filled circles are measured experimental data. The dotted line is the steady state without tissue loading, $C_i=J_s/J_v$, and $\sigma_f=0.94$ and the dash-three-dot curve is for $\sigma_f=0.8$. The solid line is the steady state curve in the presence of tissue loading, $C_i=C_c$, and $\sigma_f=0.94$ and the long-dashed curve is for $\sigma_f=0.8$. This range of reflection coefficients corresponds to a net effective oncotic force in the high filtration limit of 17-23 cmH_2O (calculated as $\sigma_f^2\pi_c$) in Tables 3.1 and 3.2 in the absence of tissue albumin. The dash-dot line is based on classical theory, where P_i and π_i are evaluated in the tissue space. It indicates that the classical theory overestimates the fluid filtration and the present model can predict the experimental fluid filtration results very well except Fig. 3.4c. Fig. 3.4a, $L_p=0.67\times10^{-7}$ cm/(cmH_2O·s) and 2D=10160 nm. Fig. 3.4b, $L_p=1.2\times10^{-7}$ cm/(cmH_2O·s) and 2D=5666 nm. Fig. 3.4c, $L_p=3.0\times10^{-7}$ cm/(cmH_2O·s) and 2D=2266 nm. Fig. 3.4d (Data from Fig. 3.3), $L_p=2.44\times10^{-7}$ cm/(cmH_2O·s) and 2D=2786 nm. In all figures 2d=150 nm, $L_C=95$ μm, $L_l=25$ nm.

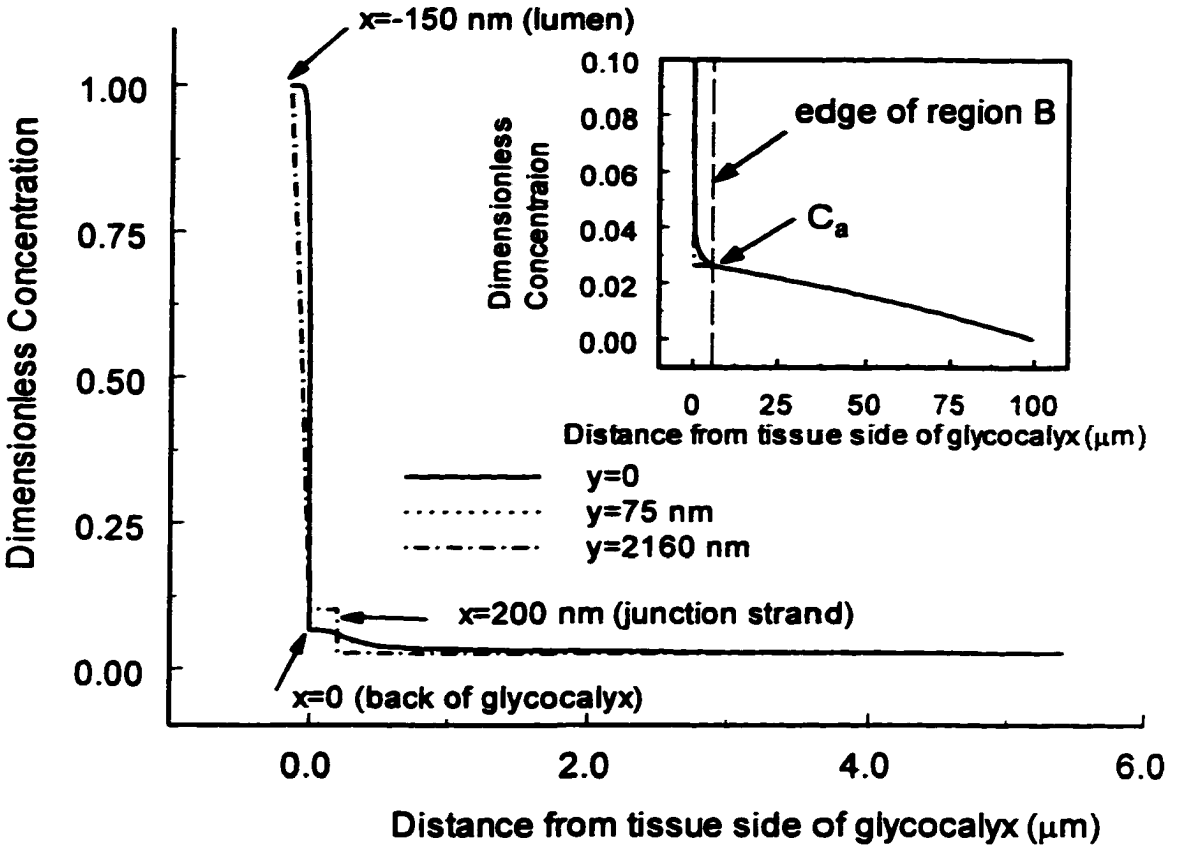

Figure 3.5 Predictions of the theoretical model without tissue loading for dimensionless concentration profiles in the cleft and tissue space at different y locations for the high filtration steady state, P_c=35 cm H_2O. Protein concentration at x=0, just behind the surface glycocalyx, approaches the convection limit, $(1-\sigma_f)C_c$. Curves y=0 and y=75 nm nearly overlap. The inset shows that the concentration in region C decreases nearly linearly with distance to x=100 μm where tissue concentration is assumed to be the same as in the superfusate. Plasma albumin concentration C_c=50 mg/ml and the corresponding osmotic pressure π_c=27.2 cm H_2O. The superfusate albumin concentration C_i=0, reflection coefficient of the surface glycocalyx σ_f=0.94 and diffusion coefficient of the matrix $D_f=0.001D_\infty$.

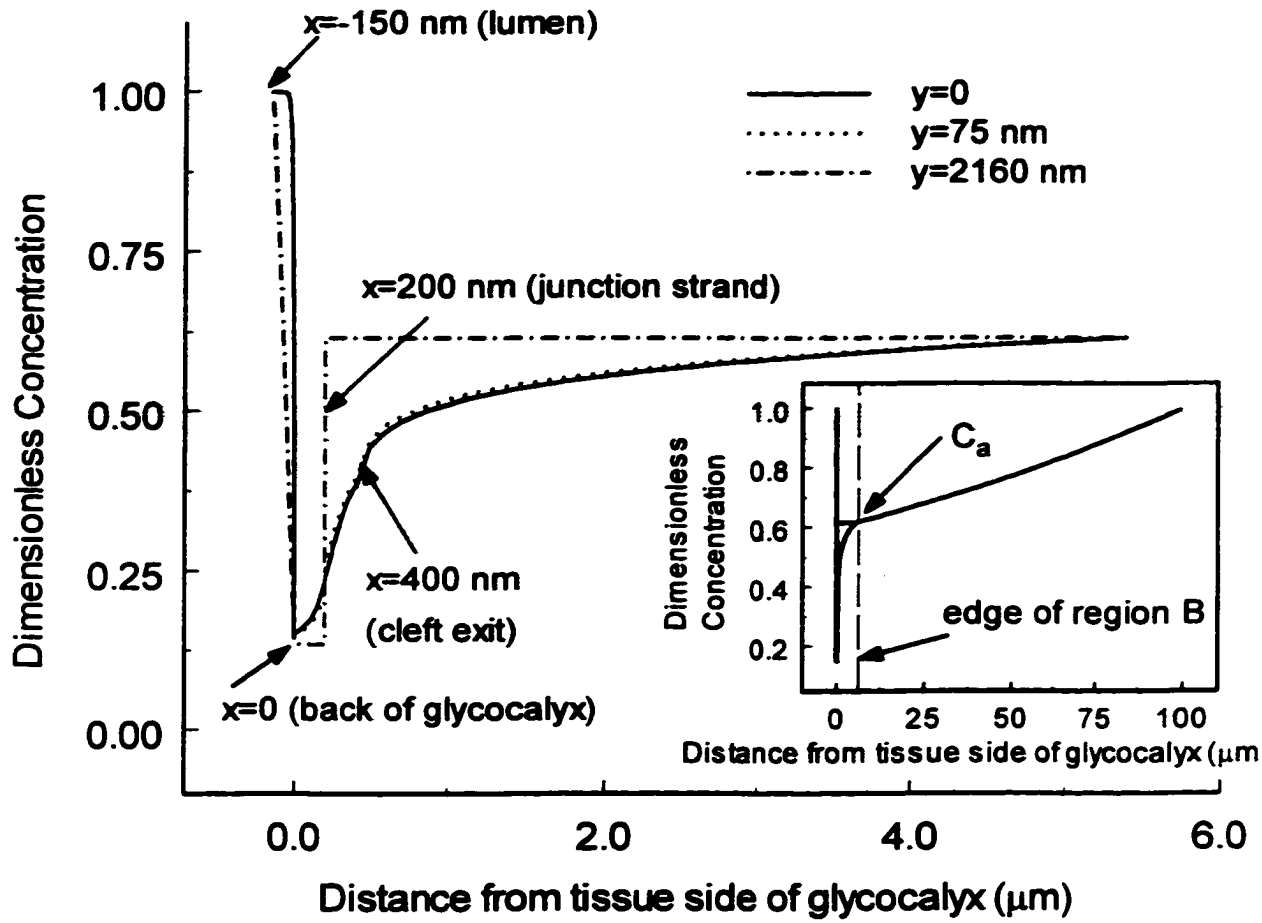

Figure 3.6 Predictions of the theoretical model with tissue loading for dimensionless concentration profiles in the cleft and tissue space at different y locations for the high filtration steady state, P_c=35 cm H_2O. Protein concentration at x=0, just behind the surface glycocalyx, approaches the convection limit, $(1-\sigma_f)C_c$. The inset shows that the concentration in region C increases linearly with distance to tissue loading site at x=100 μm. Plasma albumin concentration C_c=50 mg/ml is the same as the superfusate concentration and the corresponding osmotic pressure π_c=27.2 cm H_2O. All other parameters same as in Fig. 3.5.

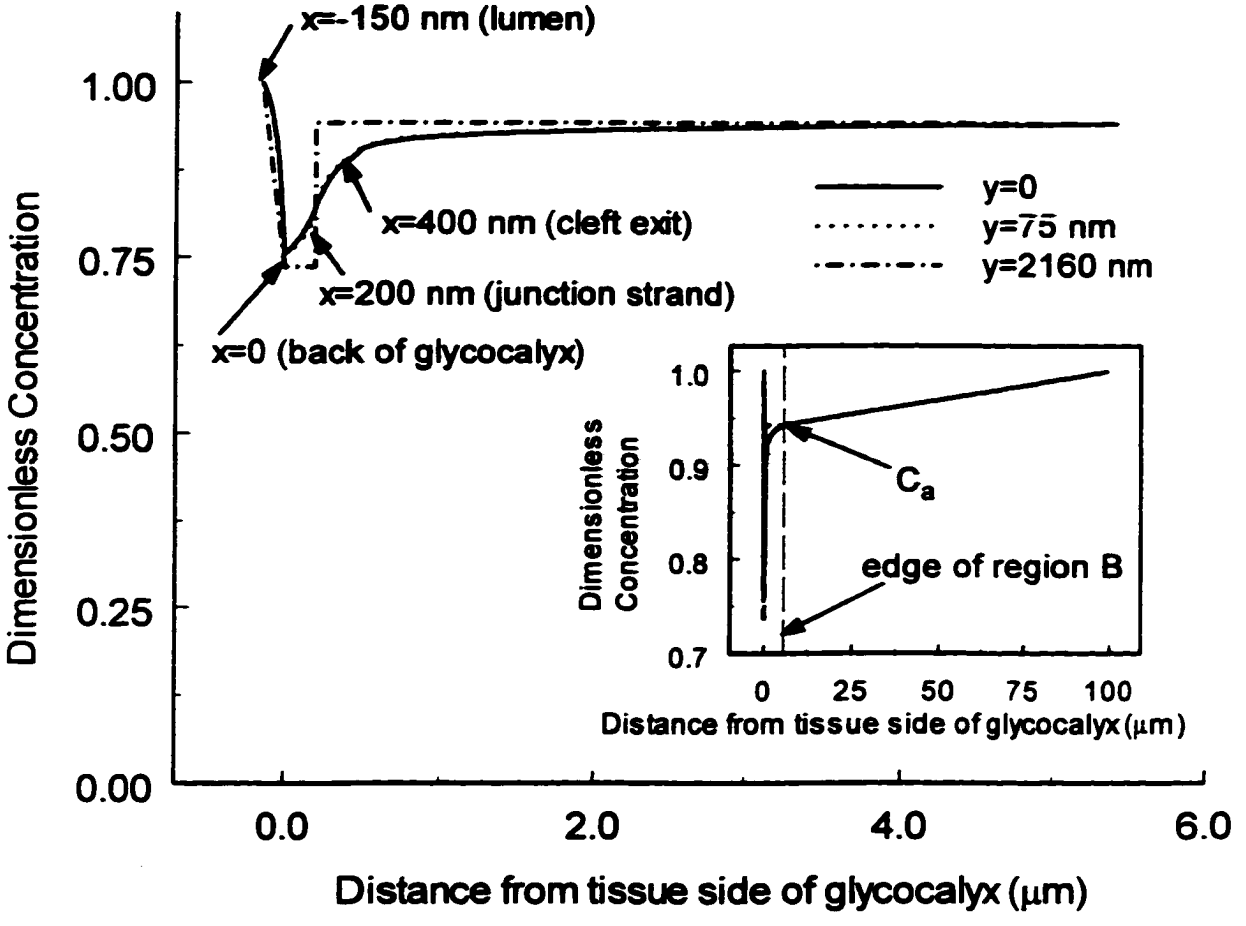

Figure 3.7 Predictions of the theoretical model with tissue loading for dimensionless concentration profiles in the cleft and tissue space at different y locations for the low filtration steady state, P_c=10 cm H_2O. Protein concentration at x=0, just behind the surface glycocalyx, is now raised because of diffusion through the surface matrix and back diffusion from the tissue since the Peclet number at the junction strand pore is less than unity. The inset shows that the concentration in region C increases linearly with distance. Plasma albumin concentration C_c=50 mg/ml is the same as superfusate concentration and the corresponding osmotic pressure π_c=27.2 cm H_2O. All other parameters same as Fig. 3.5.

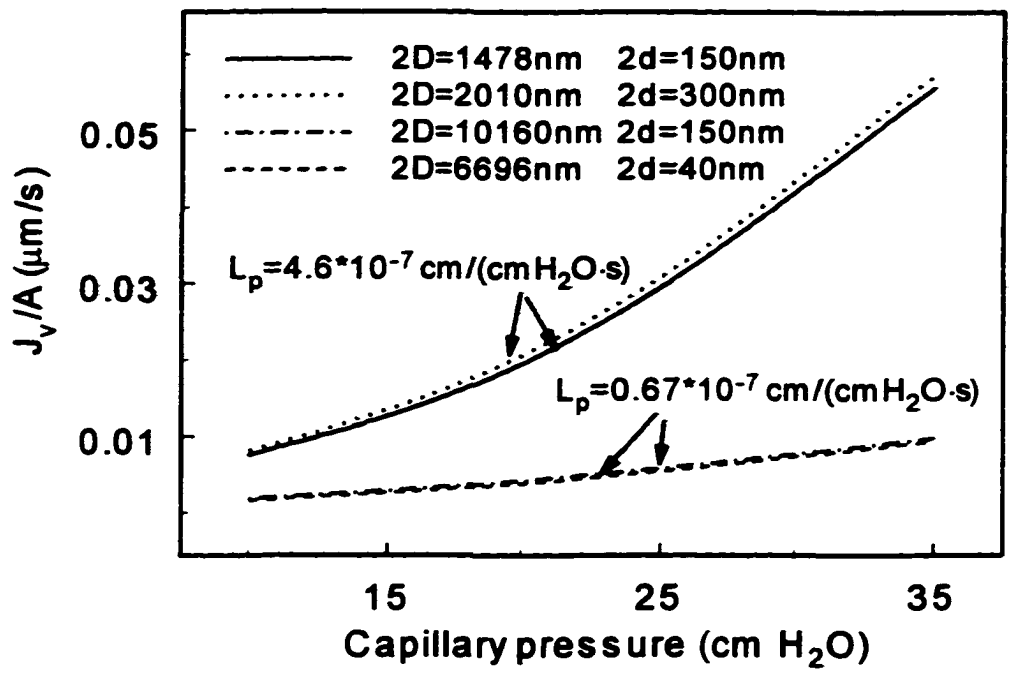

Figure 3.8 Effect of spacing of the junction strand and junction orifice on the Starling force. It shows that there is only a minor change in the fluid filtration for the different spacings of the junction strand and junction orifice if L_p is unchanged. L_C=95 μm and C_c=C_i=50 mg/ml. 2D and 2d are shown on the figure. All other parameters are the same in Fig. 3.5.

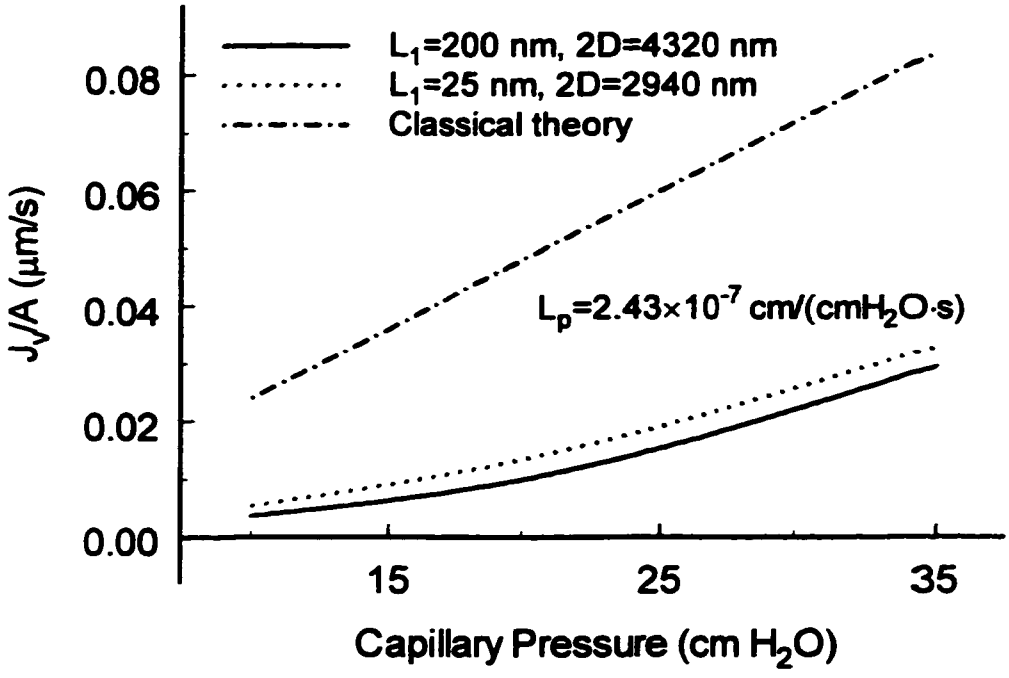

Figure 3.9 Effect of the junction strand location on the Starling force. The solid curve is for a junction strand at L_1= 200 nm, midway across cleft, and the dotted curve is for a junction strand close to the cleft entrance, L_1=25 nm. There is a small increase in back diffusion when the junction strand moved toward to the cleft entrance.

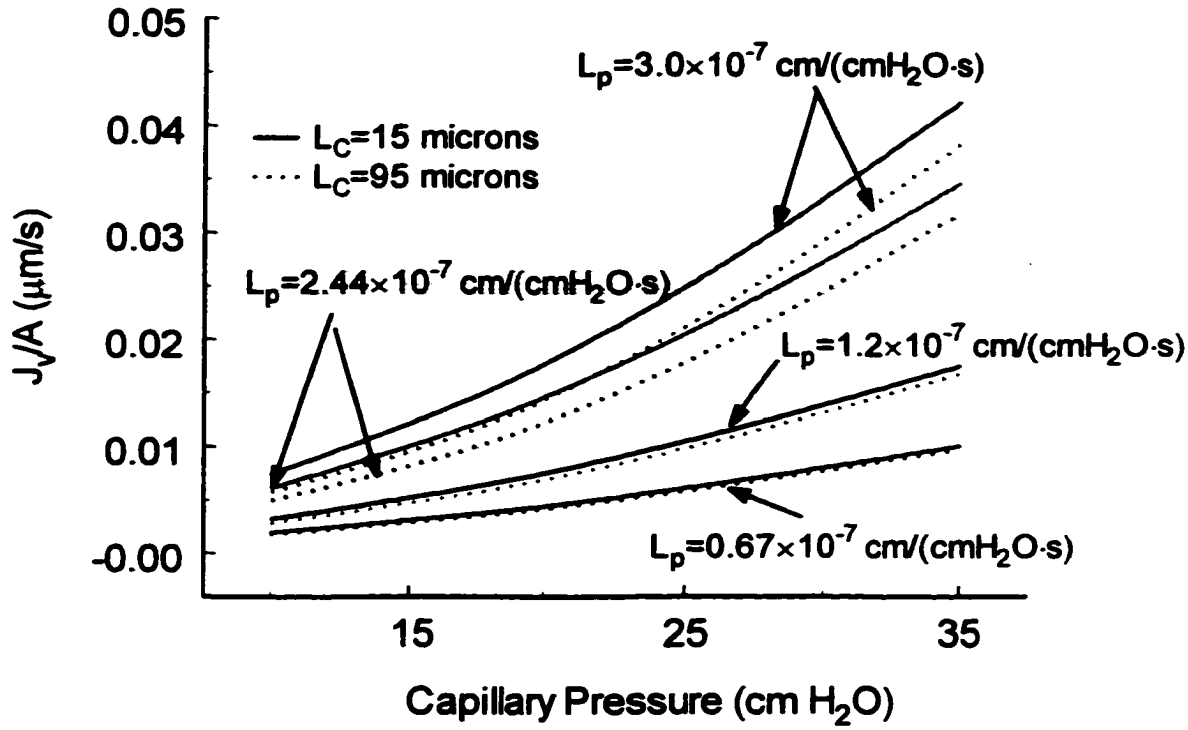

Figure 3.10 Effect of the diffusion distance in the tissue on the fluid filtration. The solid curve is for L_C=15 μm, close to the cleft exit. The dotted curve is for L_C=95 μm, far from the cleft exit. The other parameters are the same as Fig. 3.5.

Chapter 4 Effect of non-convective pathways on fluid filtration through endothelium

4.1 Introduction

Several investigators (Guyton and Lindsey, 1959, Perl *et al.*, 1975, Michel and Phillips, 1987, Weinbaum, 1998 and Hu and Weinbaum, 1999) have demonstrated that fluid is filtered out of the continuous capillaries from the plasma into the tissue in most organs except the intestinal mucosa and renal peritubule. The latter three studies have shown that there is no sustained absorption at the venous end of the capillaries. If there is no venous reabsorption under steady state conditions, the fluid filtrate across the capillary should be consistent with the amount of the low lymphatic flow. Levick (1991) pointed out that the average difference between hydraulic and osmotic pressure, which determines the fluid filtration across the capillary wall, should only amount to 1-2 mmHg if one is to satisfy this low lymphatic flow. However, the value estimated from experimental measurements in most tissues (Levick, 1991) is much higher than this desired value. Michel (1997) first proposed the hypothesis to explain this discrepancy and suggested that there are two different pathways for the transport of water and protein across the capillary, as shown in Fig. 4.1. The principal pathway for water transport is small pores, which are the interstices of the surface glycocalyx covering the entire endothelium. Most water and small hydraulic solutes cross the surface glycocalyx and follow a tortuous pathway through the junctional complex in the interendothelial clefts. Protein transport across the capillary is via large pores, which may present either very occasional breaks in

the glycocalyx or pathways through the endothelial cells, such as vesicles and transcytosis (Michel, 1996). The protein-poor filtrate emerging from the intercellular clefts mixes with the protein-rich solution released by vesicles at the abluminal side of the endothelium in the tissue to become a relatively higher protein concentration in the tissue than the fluid filtrate in the clefts. However, the effective osmotic force, which opposes the fluid filtration, is determined by the local concentration difference across the surface glycocalyx, if the surface glycocalyx is the sieving layer for proteins. Michel (1997) hypothesized that this local difference in oncotic pressure across the surface glycocalyx could differ greatly from the global difference between the plasma and the interstitium because the high protein-poor fluid flow through the cleft washes away the protein in the vicinity of the cleft exit and inhibits the back diffusion from the tissue upstream into the cleft. He also estimated the value of the Pe number for protein transport inside the intercellular clefts using the parameters for frog mesenteric capillary and concluded that the convection in the clefts should dominate over the diffusion if the driving force for convection is only 1 cmH_2O. Thus, the back diffusion due to a relatively high protein concentration in the tissue could be greatly impeded and the local protein concentration behind the surface glycocalyx would be much lower than the global concentration in the tissue, as demonstrated in the previous chapter when the tissue is back loaded.

However, mammalian muscle capillary has a fivefold lower permeability due to the smaller width (40-50 nm) of its junction strand orifice and its long tortuous intercellular pathway (Bundgarrd, 1984). The mean velocity of the fluid flow in the intercellular cleft is greatly reduced, which leads to a significant decrease in Pe number in

the cleft. Thus, diffusion may dominate over convection in the cleft. The answer to the question as to whether the back diffusion from the tissue, due to the elevated protein concentration in the tissue space emerging from the non-convective pathway, raises the local concentration behind the surface glycocalyx is, therefore, uncertain. In this chapter, we will quantitatively investigate the effect of non-convective transport on the effective Starling force and fluid filtration across the capillary. We will clarify the factors that effect the degree of back diffusion due to the presence of non-convective pathway. We shall extend our methods to examine mammalian capillaries to resolve the basic question whether the back diffusion is significant for a capillary with very low permeability, assuming that the surface glycocalyx remains the primary sieving layer for the protein.

The specialized pathway for macromolecular transport across the vessel wall has been vigorously debated over the years since Grotte (1956) observed that macromolecular clearance in the tissue drops rapidly when the molecular diameter is over 2 nm, but decreases slowly as the molecular diameter exceeds 7.2 nm. He proposed a two-pore theory in which there are two sets of pores in microvascular walls, small pores available to small and intermediate-sized molecules and large pores responsible for macromolecular permeability.

The most convincing evidence supporting the hypothesis that macromolecular transport is due to convection through intercellular clefts is the study by Rippe (1979). Rippe designed experiments to demonstrate that albumin clearance increases linearly with the filtration rate and is insensitive to the cooling on isolated rat hindquarters indicating that vesicular transport was not likely involved. He concluded that large pores in the intercellular clefts only accounted for the transport of molecules whose dimensions were

larger than albumin. Rippe and Haraldsson (1994) comprehensively reviewed two-pore theory for macromolecular transport in various vascular beds. However, ultrastructural serial section of the endothelium shows the morphological existence of vesicles (Palade, 1953 and 1960). Wagner and Chen (1991) have taken continuous thin serial sections of continuous capillaries in eels in which patches of terbium are trapped between pericytes. These sections revealed that the terbium deposits are bounded and limited to regions of the capillary wall devoid of interendothelial associations. Schnitzer's group (1994 and 1995) found that albumin transport in the rat lung could be inhibited by ablation of endothelial cavolae with filipin and by blocking the fusion of vesicles with N-ethylmaleimide (NEM), which supplies strong evidence to support the hypothesis that albumin is also transported by vesicles.

Heretofore, there has been no adequate theory or experiment to quantify the amount of albumin transport that occurs through non-convective pathways across the endothelium. In this chapter, we will vary the ratio of the albumin flux emerging from the non-convective pathways to that from the intercellular clefts to investigate the effect of non-convective transport on the fluid filtration. The three-dimensional ultrastructural model for frog mesenteric capillary is similar to that introduced by Hu and Weinbaum (1999), which is based on the microstructural measurements of frog mesenteric capillaries (Adamson and Michel, 1993). The presence of vesicles in frog mesenteric capillaries has also been observed by Clough and Michel (1979 and 1981). These investigators found that the rate of labeling of endothelial vesicles with ferritin on isolated frog mesenteric capillary was consistent with rates of macromolecular transport between the blood and tissue. The structure of the interendothelial cleft and the organization of the junction

strand for mammalian capillaries observed by Bundgaard (1984) is qualitatively similar to frog mesenteric capillaries except that the length of the breaks is much shorter, typically the width of a single transmission section, 40-50 nm. For hamster cremaster muscle, Vink and Duling (1996) have observed a thick endothelial surface glycocalyx in front of the cleft entrance, whose thickness is 400 nm. We will modify the current model using these measured parameters for mammalian capillaries so as to extend our theory to apply mammalian vessels.

In Hu and Weinbaum (1999) and Hu *et al.* (2000), we asked the question whether the effective Starling force, which opposes the fluid filtration, is the local difference across the surface glycocalyx or the global difference across the entire endothelium between the plasma and the tissue. In these studies the protein concentration in the tissue space was purposely raised to a higher value than the convective limit, $(1-\sigma)C_c$, at a distance 100 μm far from the cleft exit. Here, C_c is protein concentration in plasma and σ is the reflection coefficient of the capillary wall for albumin. In contrast, in this chapter, the protein concentration in the tissue space is elevated close to the cleft exit due to the release of protein-rich solution by vesicles at the abluminal side of the endothelium. We will modify our theoretical model to examine the mixing of the protein-rich fluid from the vesicular pathway with the protein-poor fluid entering the tissue from the intercellular cleft pathway as shown in Fig. 4.1. We shall also compare the concentration profiles in the cleft and the tissue with the solution in Hu *et al.* (2000) for tissue back loading.

4. 2 Mathematical model

Our mathematical model for the microstructure of frog mesenteric capillary is similar to one introduced by Hu and Weinbaum (1999). The essential physics contains four regions, as shown in Fig. 4.2. The innermost region is the endothelial surface glycocalyx. This 150 nm thick layer covers the entire endothelium and is assumed to be the primary sieving layer for macromolecule transport across the vessel wall. The second region is region A, the intercellular cleft. The junction strand is idealized as a barrier with periodically distributed junction orifices located in the midway across the cleft depth. Most of the water that filters through the capillary endothelium passes through these junction orifices and enters the interstitium (Fu and Weinbaum, 1994 and Michel and Curry, 1999). There are three different mechanisms for macromolecular transport across the endothelium: diffusion, convection and transcellular non-convective transport. Diffusive and convective transport follows a tortuous intercellular pathway through the junction orifice. The dimensions of the junction orifice for frog mesentery are 150*20 nm, which is too wide for the orifices to serve as a molecular filter for albumin (7 nm diameter). The surface glycocalyx is, therefore, the sieving layer for albumin and the oncotic force is only felt across this matrix layer. The local fluid filtration across the capillary wall is determined by the local difference in hydraulic and oncotic pressure across the surface glycocalyx.

The pericapillary region is divided into two regions, region B immediately surrounding the cleft exit, and region C far from the cleft exit, as shown in Fig. 4.2b. The width of region B, 2S=10 μm, is the distance between two neighboring clefts along the perimeter of the capillary wall. For frog mesentery, approximately six clefts are evenly

distributed on the cross section of the capillary wall. The model in Hu *et al.* (2000) predicts that the protein concentration profiles in the tissue have a steep concentration gradient that extends roughly 2 μm from the cleft exits. Therefore, the length of region B, L_B=5 μm, is sufficient for the protein-poor fluid from the cleft exit to mix with the protein-rich fluid from the transcellular vesicular pathways. This mixing results in a uniform flow at the entrance to region C. This uniform jet from each periodic unit merges with that from the adjacent periodic units in region C. The dimensions of each periodic unit are 4320 nm (length)× 10 μm (width), as shown in Fig. 4.2a, b.

The governing equations and boundary conditions for the pressure and concentration at the surface glycocalyx, regions A and C are the same as those described in Hu and Weinbaum (1999). The principle difference between the present model and the model in Hu and Weinbaum (1999) is the boundary condition at the abluminal side of the endothelium, the entrance to region B, where the protein-rich solution carried by the vesicles is released to the interstitium. In our current model, there are two sources of solute flux entering region B, as shown in Fig. 4.2b. One, J_{sc}, is by convective and diffusive transport through the interendothelial cleft, which spreads radially from the cleft exit. The other, J_{sv}, is by vesicular transport, which crosses everywhere along the vessel wall. Region B can no longer be described by just the mixing of a line source of variable strength along the length of the cleft exit as in our previous model (Hu and Weinbaum, 1999). Instead, a fully three-dimensional convection-diffusion model is required to describe the mixing of the two fluxes, J_{sc} and J_{sv}, in region B.

The local protein flux j_{sv} from non-convective pathways is directly proportional to the protein concentration difference across the vessel wall. Thus, the protein flux by vesicular transport is given by

$$j_{sv} = K[C_c - C(L,y,z)] \tag{4.1}$$

Here j_{sv} is the solute flux per unit area of the vessel wall through non-convective pathways, C_c is the plasma protein concentration, and C(L,y,z) is the protein concentration just behind the endothelium on the tissue side. K is a coefficient, which depends on the vesicular volume that passes from the plasma to the interstitium per unit time and the partition of solute molecules in the vesicular plasma (Renkin, 1992). Currently, there is no adequate theory or experimental data to predict K. Thus, several different values of this coefficient are chosen to provide a reasonable range of values for the ratio of the two solute fluxes, namely, the protein flux entering the tissue by the non-convective pathway, J_{sv}, over the flux through the intercellular cleft, J_{sc}. We choose this ratio to vary from zero to five, in the high filtration limit, P_c=35 cmH_2O. When J_{sv}/J_{sc} is zero, all the protein transport is through the intercellular cleft and there is no vesicular transport. When J_{sv}/J_{sc} equals five, the protein flux due to non-convective transport is five times that through the interendothelial cleft and the tissue concentration after mixing is approximately 0.4 C_c, an average value for many tissues summarized in Levick (1991).

The hydraulic resistance in the tissue can be neglected, compared with the resistance in the cleft due to the junction strand. Thus, the velocity in the intermediate region B, V(x,y,z), decays as 1/r where $r=\sqrt{(x-L)^2+z^2}$ is the distance to the cleft exit in the x-z plane, L is the cleft depth and x is the distance from the backside of the surface glycocalyx. Although V(x,y,z) is a function y, the transport of momentum in the y

direction is neglected in the tissue. This is a reasonable approximation if V(x,y,z) is slowly varying along the length of the cleft exit. Thus, from simple continuity arguments,

$$2h \times u_{exit}(y) = \pi r |V(x,y,z)|. \tag{4.2}$$

Here h is the cleft half height and $u_{exit}(y)$ is the locally varying average velocity at the cleft exit. Rearranging equation (4.2), one obtains

$$|V(x,y,z)| = \frac{2h \times u_{exit}(y)}{\pi r}. \tag{4.3}$$

The velocity components in the x and z directions can be expressed as

$$u_x(x,y,z) = \frac{x-L}{r}|V(x,y,z)|, \tag{4.4a}$$

$$u_z(x,y,z) = \frac{z}{r}|V(x,y,z)|. \tag{4.4b}$$

Since protein gradients in the y direction near the cleft exit are smaller than x-z gradients (Fu *et al.* 1994), convective and diffusive terms in the y direction are neglected. Thus, the governing equation for the concentration in region B becomes

$$D_t\left(\frac{\partial^2 C(x,y,z)}{\partial x^2} + \frac{\partial^2 C(x,y,z)}{\partial z^2}\right) = \chi_t\left[u_x(x,y,z)\frac{\partial C(x,y,z)}{\partial x} + u_z(x,y,z)\frac{\partial C(x,y,z)}{\partial z}\right]. \tag{4.5}$$

Here D_t and χ_t are the protein diffusion and retardation coefficients in the tissue space.

The boundary and matching conditions for equation (4.5) are

$$x = L,\ |z| \le h \qquad C(L,y,z) = C_{exit}(y) \tag{4.6a}$$

$$-D_t \left.\frac{\partial C(x,y,z)}{\partial x}\right|_{x=L} + \chi_t u_x(L,y,z)C(L,y,z) = q_{exit}(y) \tag{4.6b}$$

$$x = L,\ |z| \geq h \qquad -D_t \left.\frac{\partial C(x,y,z)}{\partial x}\right|_{x=L} = j_{sv}(y,z) \tag{4.6c}$$

$$x = L + L_B \qquad C(L + L_B, y, z) = C_a(y,z) \tag{4.6d}$$

$$-D_t \left.\frac{\partial C(x,y,z)}{\partial x}\right|_{x=L+L_B} + \chi_t u_x (L + L_B, y, z) C(L + L_B, y, z) = q_c(y,z) \tag{4.6e}$$

$$z = \pm S \qquad -D_t \left.\frac{\partial C(x,y,z)}{\partial z}\right|_{z=\pm S} = 0 \tag{4.6f}$$

Here L_B is the length of region B and S is its half width, the average half spacing between adjacent clefts. $C_{exit}(y)$ and $q_{exit}(y)$ are the local protein concentration and protein flux at the cleft exit, obtained from region A. $j_{sv}(y,z)$ is the protein flux by vesicular transport through a unit area of capillary wall, given by equation (4.1). $C_a(y,z)$ and $q_c(y,z)$ are the protein concentration and the total protein flux at the entrance to region C. Boundary conditions (4.6a-e) require that the continuous protein concentration be continuous and that there be a continuity of solute flux at the cleft exit and the edge of region B, respectively. Equation (4.6f) is periodic distribution of the intercellular cleft along the capillary wall. The boundary condition problem defined by equations (4.5) and (4.6) is solved using the same numerical method described by Hu and Weinbaum (1999). Regions A and B are calculated simultaneously because these two regions are coupled at the cleft exit.

One needs to define the boundary condition at the edge of region C. It is reasonable to assume at this large distance that tissue can be treated as a well-mixed reservoir. Therefore, the protein concentration is the ratio of the two fluxes, the total solute flux including diffusive, convective and transcellular non-convective transport divided by the total fluid flux entering the tissue (Michel and Phillips, 1987).

4.3 Results

4.3.1 Concentration profiles in the absence or presence of non-convective pathways

The protein concentration at the tissue space would be significantly raised if the protein transport through non-convective pathway contributes greatly to the total protein flux across the vessel wall. Fig. 4.3a shows the protein concentration profiles from the lumen to the tissue along the mid-plane z=0 for different protein transport rates through non-convective pathways. There are two sets of curves in this figure. The upper set of the curves shows the concentration profiles for P_c=15 cmH_2O and the lower set shows the profiles for P_c=35 cmH_2O. These pressures are typical of the venous and arterial side of capillaries. Currently, there is no sufficient experiment or theory to predict the value of K that appears in equation (4.1) for the vesicular transport. K is the coefficient describing the magnitude of the flux through non-convective pathways. In the absence of data for K, we will choose this value such that albumin flux transported by non-convective pathways is zero, one, two and five times that through the intercellular cleft in the high convective limit, P_c=35 cmH_2O. These values of flux ratio will be satisfied when K=0, 1.097, 2.402 and 8.237 nm/s, respectively. Fig. 4.3a shows the protein concentration profiles along the centerline y=0 proceeding from the lumen to the edge of region B. The protein concentration is uniform far from the cleft exit and, thus, the profiles in region C are omitted in Fig. 4.3a. Fig. 4.3a also shows the concentration profile along the edge of the cleft, y=2160 nm, the half distance between two neighboring orifices for K=8.237 nm/s.

When K=8.237 nm/s, this profile is the typical of profiles for all values of K. Therefore, the profiles for other values of K are not plotted, so not clutter the figure.

One observes that most of the albumin concentration drop occurs across the surface glycocalyx, the sieving layer for albumin, if all the albumin transport passes through the intercellular cleft (the solid line). The albumin concentration in the cleft and tissue is almost uniform for both values of P_c. At P_c=35 cmH_2O, the concentration approaches the convective limiting value, $(1-\sigma)C_c$. For non-zero values of K, the protein-rich solution emerging from non-convective pathways mixes with the protein-poor filtrate through the intercellular cleft in region B. The protein concentration in the tissue far from the cleft exit is elevated to two, three and six times that for K=0 at P_c=35 cmH_2O. The concentration is also greatly increased for P_c=15 cmH_2O. There is a large concentration gradient in the vicinity of the cleft exit and also in the cleft on the tissue side of the junction strand. The striking result is that even though the protein concentration in the tissue is greatly increased, the protein concentration at the backside of the surface glycocalyx is raised insignificantly above that for K=0. The local protein concentration at the backside of the surface glycocalyx, y=0, differs greatly from the protein concentration in the tissue as Michel (1997) hypothesized.

Fig. 4.3a also shows that there is a discontinuity of the concentration profile across the junction strand at y=2160 nm for K=8.237 nm/s (the long-dash line). A smaller discontinuity barrier should be observed for smaller values of K. This indicates that the junction strand in the cleft blocks the back diffusion to the region in front of the junction strand. Only location where any back diffusion can occur is the orifice opening, which occupies less than 6% of the cleft length.

Michel (1997), Weinbaum (1998) and Hu and Weinbaum (1999) proposed that the effective Starling force opposing the fluid filtration is the local concentration difference across the surface glycocalyx, rather than the global difference between the plasma and tissue if the surface glycocalyx is assumed to be the sieving layer for proteins. Therefore, we have special interest in examining the concentration at the backside of the surface glycocalyx. These concentration profiles are shown in Fig. 4.3b for the same representative values of K and P_c. One observes, at both P_c=15 cmH_2O and P_c=35 cmH_2O, there is only a small increase in the concentration behind the surface glycocalyx. The increase in the concentration behind the surface glycocalyx in general is much lower than in the tissue, as shown in Fig. 4.3a. One also observes that the protein concentration at the backside of the surface glycocalyx is almost uniform. Therefore, it is reasonable to use the average concentration representing the protein concentration at the backside of the surface glycocalyx.

4.3.2 Average protein concentration behind the surface glycocalyx

Figure 4.4 shows the average protein concentration $\overline{C}(0)$ behind the surface glycocalyx and the concentration C_a at the edge of region B as a function of pressure in the presence or absence of the non-convective pathways. The solid curve shows the relationship between the protein concentration in the tissue, C_a, and the capillary pressure, P_c, for steady state conditions when K=0. The tissue protein concentration is determined by the ratio of two fluxes, the total solute flux entering the tissue space divided by the total fluid flux into the tissue. One observes that when P_c exceeds π_c (27.2 cmH_2O), the protein concentration approaches the convective limit $(1-\sigma)C_c$ for K=0. The curve starts

to bend and there is a sharp inflection of the curve at $P_c=\sigma^2\pi_c$, the maximum effective oncotic pressure (24 cmH_2O) for σ=0.94. When $P_c<\sigma^2\pi_c$, there is a linear increase in the interstitial protein concentration, which eventually approaches one when P_c=0 (note the origin is P_c=10 cmH_2O). The interstitial protein concentration is significantly raised for K=8.237 nm/s and decreased almost linearly with increase in P_c. This is shown by the dotted curve in Fig. 4.4.

One observes in Fig. 4.4 that there is indistinguishable difference in the concentration profiles between the backside of the surface glycocalyx (dash-dot line) and the tissue (solid line) when K=0. In contrast, the protein concentration behind the surface glycocalyx (dashed line) differs greatly from that in the tissue (dotted line) where K=8.237 nm/s. For the low value of K, we observed in Fig. 4.3a that the concentration is nearly uniform everywhere behind the surface glycocalyx. Whereas, for the high value of K, the presence of the junction strand prevents the back diffusion to the lumen side of the cleft. The average protein concentration behind the surface glycocalyx does increase due to the back diffusion from the tissue. However, the increase in the average protein concentration $\overline{C}(0)$ as K increases far exceeds the increase in the interstitial protein concentration C_a. One also observes that the difference in $\overline{C}(0)$ curves for K=0 and K=8.237 nm/s becomes vanishingly small for a large values of P_c and also tends towards zero as P_c approaches zero. This suggests that there may be a maximum difference in the intermediate range in the vicinity of $\sigma^2\pi_c$. We will examine this behavior in the next section.

4.3.3 Increase in average protein concentration behind the surface glycocalyx due to the back diffusion

In Fig. 4.5, we have plotted the increase in the average protein concentration $\overline{C}(0)$ behind the surface glycocalyx as a function of P_c for representative values of K. These curves clearly illustrate the existence of the maximum concentration difference mentioned above. One observes that the maximum difference for all values K occurs at $P_c=\sigma^2\pi_c$. The magnitude of the maximum difference increases as K increases. Intuitively, one might anticipate that, as the capillary pressure increases, the high fluid flow washes away the protein and prevents the back diffusion through the junction orifices. Therefore, the increase in the average concentration at the backside of the surface glycocalyx is decreased and, eventually, approaches to zero. This conventional view is only consistent with the curve for $P_c>\sigma^2\pi_c$. This puzzle, why the concentration difference decreases as $P_c<\sigma^2\pi_c$, motivates us to more carefully examine what determines the back diffusion from the tissue when the interstitial protein concentration is elevated.

4.3.4 Factors that effect the back diffusion

The most important determinant for the back diffusion is Peclet number Pe at the junction orifice, which is shown in Fig. 4.6 for several different values of K. Pe is defined by $\chi_c uL/D_c$, where u is the average velocity at the orifice opening, L is the cleft depth and χ_c and D_c are the retardation and diffusion coefficients of albumin in the cleft, respectively. The value of Pe number increases at given P_c as K increases. The reason for this is that the protein concentration behind the surface glycocalyx increases due to non-

convective transport. This leads to reduction in the oncotic pressure difference across the surface glycocalyx and increase in the fluid filtration.

One notices that the maximum back diffusion in Fig. 4.5 occurs at P_c=24 cmH_2O where the Pe number is less than a unit, rather than the lowest Pe number. This suggests that there are two competing mechanisms. When Pe>1, convection dominates over diffusion and the fluid filtration washes away the protein in the vicinity of the junction orifice. Therefore, the back diffusion from the tissue decreases sharply and the high protein concentration in the tissue has little effect on the concentration behind the surface glycocalyx. In contrast, when Pe<1, diffusion dominates over convection and the concentration gradient in the cleft becomes the primary force effecting the back diffusion from the tissue. Let us now reexamine Fig. 4.4 to find when the maximum protein concentration difference occurs between the backside of the surface glycocalyx and the tissue. The dash-dot curve in this figure represents the protein concentration at the backside of the surface glycocalyx as a function of the capillary pressure. As we mentioned earlier, the sharp inflection of the curve is centered around the effective osmotic pressure $\sigma^2\pi_c$. When $P_c>\sigma^2\pi_c$, the concentration approaches the convective limit $(1-\sigma)C_c$. If $P_c<\sigma^2\pi_c$, the concentration increases rapidly and approaches the plasma protein concentration when P_c equals zero. However, the relationship between the protein concentration and capillary pressure is almost linear when K>1, shown as the dotted line in Fig. 4.4. The maximum concentration difference between the tissue and the backside of the surface glycocalyx occurs at the inflection point where $P_c=\sigma^2\pi_c$.

4.3.5 Comparison of the concentration profile due to non-convective pathway and tissue loading

In our previous models (Hu and Weinbaum, 1999 and Hu *et al.*, 2000), the protein concentration in the tissue far from the cleft exit was back loaded to a high prescribed value to test whether the effective Starling force is the local oncotic pressure difference across the surface glycocalyx or the global difference between the blood and tissue. In this chapter, the protein concentration in the tissue is raised due to the parallel transcellular non-convective pathways rather than the back loading. Fig. 4.7 shows the concentration profiles along the centerline y=0 and the mid-plane z=0 for these two cases. In this calculation, one assumes the protein concentration at the edge of region B is loaded to the same concentration as that would be achieved by non-convective pathways. One observes that the difference in the concentration profiles is nearly indistinguishable.

4.3.6 Mammalian Capillary

The previous figures are based on the microstructural model of frog mesenteric capillaries. We now wish to extend our methods to explore mammalian muscle capillaries that the hydraulic permeability L_p is roughly a factor of five smaller than frog mesentery. This reduction in L_p is achieved by increasing the average spacing to 11.2 μm, decreasing the junction opening to 50 nm and increasing the thickness of the surface glycocalyx to 400 nm. The 50 nm width of the junction orifice is consistent with the observation by Bundgaard (1984) and the 400 nm thickness of the surface glycocalyx has been observed by Vink and During (1996). The calculated permeability is $0.5*10^{-7}$ cm/(cmH_2O·s) if one assumes the other parameters are the same as Fig. 4.2 for frog mesentery.

The concentration profiles along the centerline y=0 and the mid-plane z=0 are shown in Fig. 4.8 for various values of K. These profiles have the same qualitative behavior as the frog mesentery profiles in Fig. 4.3a except the interstitial protein concentration is significantly high. The concentration behind the surface glycocalyx differs greatly from that in the tissue. Even though the interstitial protein concentration is raised due to the parallel pathway and there is a large concentration gradient around the cleft exit, the protein concentration behind the surface glycocalyx varies relatively little.

The increase in the average protein concentration behind the surface glycocalyx due to the non-convective transport for mammalian capillaries is shown in Fig. 4.9 for the different three values of K. The maximum concentration difference between K=0 and K≠0 again occurs at $P_c=\sigma^2\pi_c$. When the capillary pressure is higher or lower than this value, the average concentration difference at the backside of the surface glycocalyx between K=0 and K≠0 is decreased. The reason is the same as for frog mesentery discussed earlier.

Figure 4.10 shows the Peclet number as a function of pressure for the same values of K as shown in Fig. 4.6. The surprising result is that even though L_p for the mammalian capillary is only one fifth of the frog mesenteric capillary, the Peclet number for mammalian capillary at the junction orifice is even higher than that for frog mesenteric capillary.

4.4 Discussion

4.4.1 Effect of non-convective pathways on the fluid filtration

The protein concentration in the tissue is significantly raised if the protein transport across the capillary walls by non-convective pathways contributes greatly to the total transcapillary protein flux. However, the results in Figs. 4.3a, 4.4 and 4.8a show that the local concentration behind the surface glycocalyx can differ greatly from the tissue because the presence of the junction strand in the endothelial cleft greatly impedes the back diffusion from the tissue through the junction orifice to the lumen side of the junction strand. Therefore, the non-convective transport, which would significantly raise the interstitial protein concentration, has little effect on the protein concentration at the backside of the surface glycocalyx, as observed in Figs. 4.3a and 4.8a. The fluid filtration across the capillary is determined by the local difference in the hydraulic and oncotic pressure across the surface glycocalyx, rather than the global difference between the blood and tissue. Thus, there is a minor increase in the transcapillary fluid filtration with the non-convective transport. If one uses the global values of hydraulic and oncotic pressure difference between the blood and tissue, one would greatly overestimate the transcapillary fluid filtration. This hypothesis conforms to Michel's hypothesis (1997) that protein-rich flux through the vesicular pathway would not have significant influence on the oncotic force felt across the surface glycocalyx. It also explains Levick's paradox (1991) that one can have a low lymph flow in most tissues without venous absorption.

The crucial insight into the detailed mechanism as to when the junction strand will serve to create a protected region on the lumen side of the junction strand that prevents

back diffusion through the junction orifice can be obtained by examining the Peclet number Pe at the junction orifice and the concentration gradients established across the cleft. In contrast to the conventional view that the back diffusion only depends on the Peclet number at the junction orifice, the maximum back diffusion occurs when the capillary pressure equals the maximum effective oncotic pressure, $\sigma^2\pi_c$. When Pe>1, the high filtration flow washes away the protein in the vicinity of the junction orifice and prevents the back diffusion upstream through the junction orifice from the tissue. The degree of the back diffusion from the tissue decreases with the increase in Pe and the protein concentration at the backside of the surface glycocalyx approaches the convective limit, $(1-\sigma)C_c$. When Pe<1, the diffusive transport, which is the product of the local diffusion coefficient and concentration gradient, dominates. The concentration gradients established across the cleft become the main driving force for the back diffusion. We observe from Fig. 4.4 that the maximum concentration gradient occurs at the inflection point of the $\bar{C}(0)$-P_c curve where $P_c=\sigma^2\pi_c$. Thus, the back diffusion achieves the maximum effect when $P_c=\sigma^2\pi_c$.

In this chapter, we also extend our methods to examine the mammalian capillary, which has a fivefold lower hydraulic permeability due to smaller width and greater spacing of the junction orifice and a thicker surface glycocalyx than frog mesentery. However, similar behaviors are obtained for the mammalian capillary. The frequency of the pores does not effect the local velocity at the junction orifice when the interaction between adjacent pores can be neglected. This flow depends on the location of the junction strand, the size of the pore, the cleft depth and the resistance of the surface glycocalyx. The convergence of the flow to the smaller pores actually increases the

velocity and raises the Peclet number at the same capillary pressure. For this reason, even though the overall fluid filtration per unit area of capillary wall is greatly reduced for mammalian capillaries, the back diffusion from the tissue actually diminishes.

In our previous paper (Hu *et al.*, 2000), we have investigated the effect of the location and structure of the junction strand on the effective Starling force and fluid filtration across the capillary. The structure and location of the junction strand has only a minor effect on the effective Starling force and the fluid filtration across the capillary. One would anticipate that it would also be true for the mammalian capillary.

4.4.2 Assumptions of the mathematical model

The model makes several simplifying assumptions. We will discuss the two major assumptions here. The first is we assume most transendothelial water flow passes through orifices in the junction strand following a tortuous pathway through the junctional complex in interendothelial clefts. Michel and Curry (1999) have quantitatively estimated fluid exchange through other pathways across endothelial cell membranes and suggested that these contribute little to the total fluid flow for the continuous microvessel at normal conditions. Curry *et al.* (1976) estimated that water exchange between the plasma and tissue through the exclusive water pathway alone has an L_p value of $1.1*10^{-8}$ cm/(s·cmH_2O) which was less than 10% of the overall L_p for frog mesenteric microvessels. This exclusive water pathway may come from water channels of cell membranes, aquaporins, which were identified in continuous microvascular endothelia (Pallone *et al.*, 1997). The water exchange through the water channels will slightly dilute the protein concentration in the vicinity of these channels at the tissue side of the endothelium, but won't change the results we predicted in this chapter.

The second major assumption we made is that the rate of the protein transport through the non-convective pathway is proportional to the concentration difference between the lumen and ablumen side of the vessel. We also assumed that the vesicular flux is distributed uniformly everywhere across the endothelium, *i.e.*, K in equation (4.1) is constant. We are unable to precisely describe the detailed process of the vesicle movement across the endothelium and localization of the vesicle distribution due to insufficient data from experiment. One of the key results obtained in Fig. 4.7 is that the protein concentration profiles across the surface glycocalyx, cleft and tissue are insensitive to the manner which we raise the tissue protein concentration. Despite the two very different methods, vesicular transport and back loading, one obtains virtually the same concentration in regions B and C. Thus, the effective Starling force and transcapillary fluid filtration are nearly identical. The detailed distribution of the vesicular transport is unimportant.

Currently, there are no experiments to predict the effect of capillary pressure on the vesicular transport. Here, we assume the coefficient K in equation (4.1) is independent on the capillary pressure. Recent experiments indicate that capillary pressure can have some influence on the vesicular transport (Michel and Curry, 1999). Previous investigators (Clough and Michel, 1982) have observed the effect of the temperature on the vesicles. The number of vesicles decreases dramatically as the temperature is decreased. However, the effect of temperature on the effective macromolecular transport is still unknown (Michel, 1996).

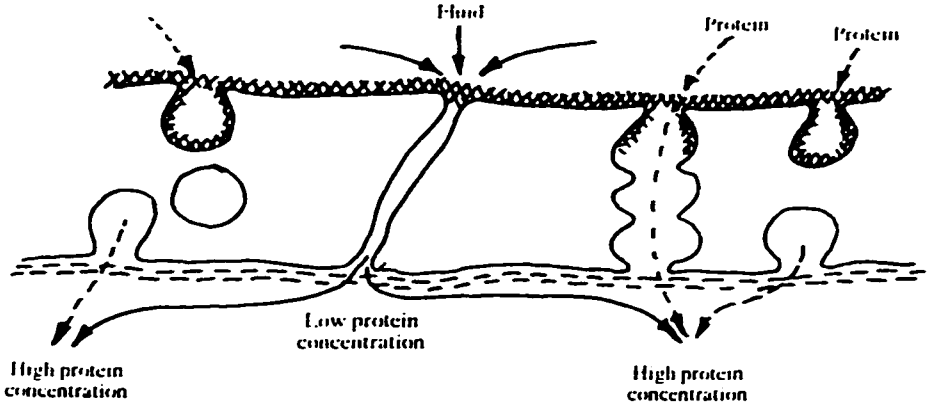

Figure 4.1 Schematic of the microvascular endothelium showing separate pathways for fluid (through the intercellular cleft) and protein (through the parallel non-convective pathway). [From Michel (1997), with permission].

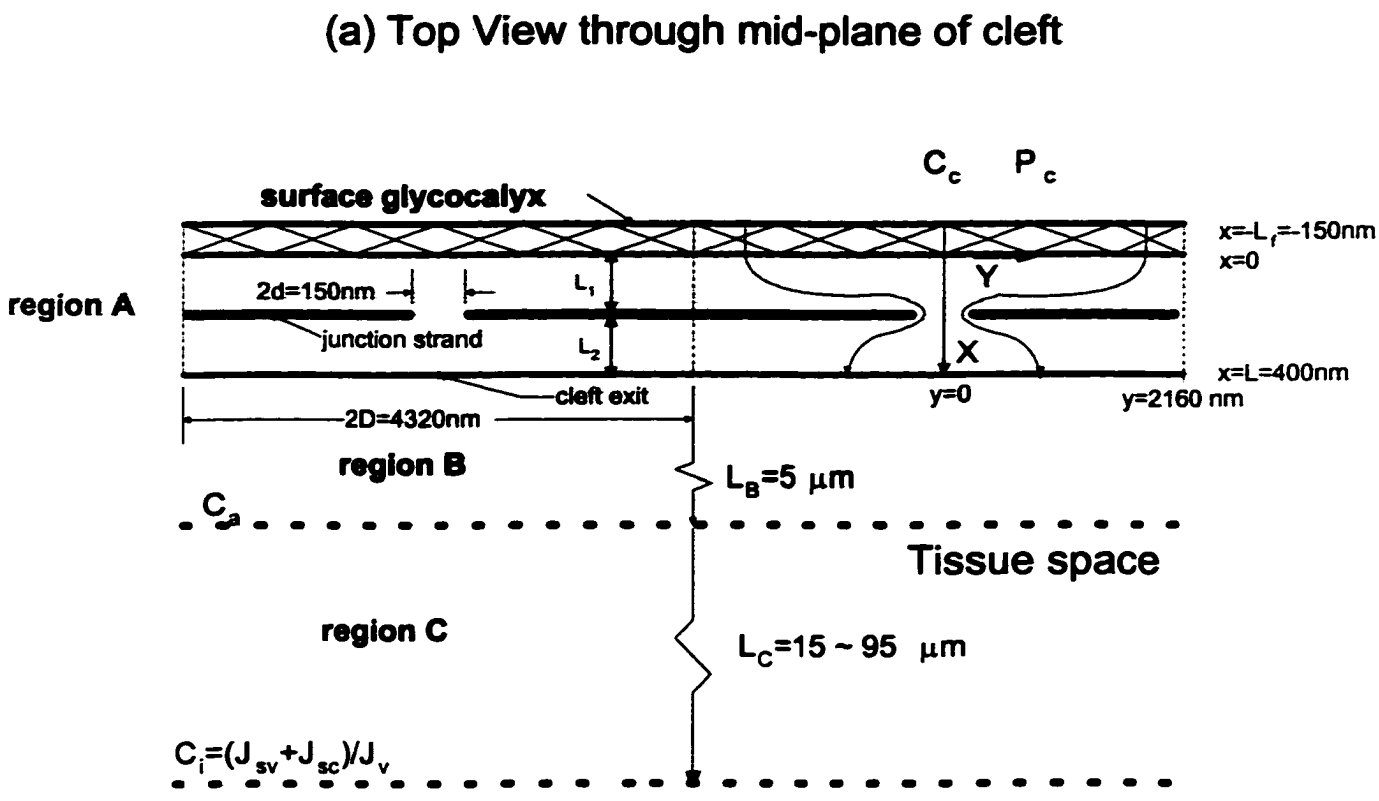

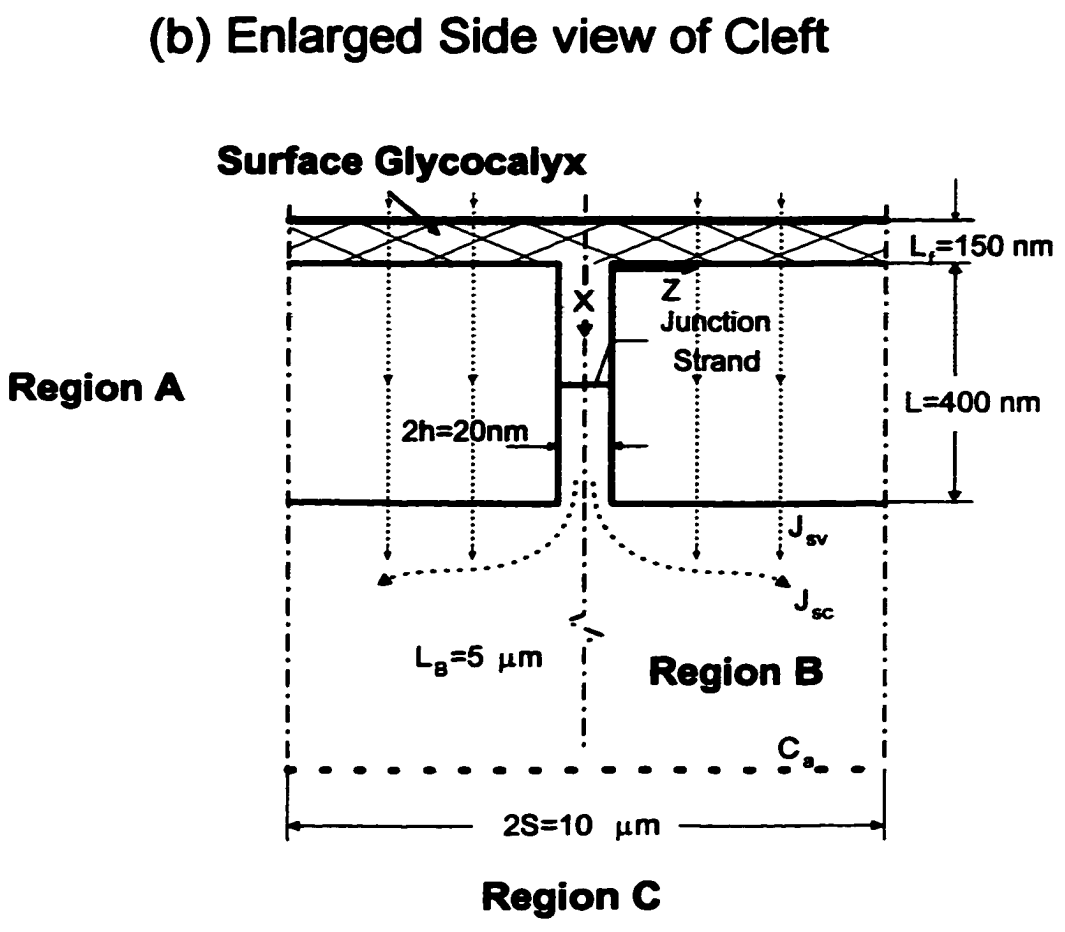

Figure 4.2 (a) Schematic of the idealized mathematical model showing the surface matrix layer, cleft region A with junction strand and tissue regions B and C describing mixing at the cleft exit. Dimensions shown are typical for frog mesentery capillary. (b) Side view of the cleft showing cleft height and the width of region B.

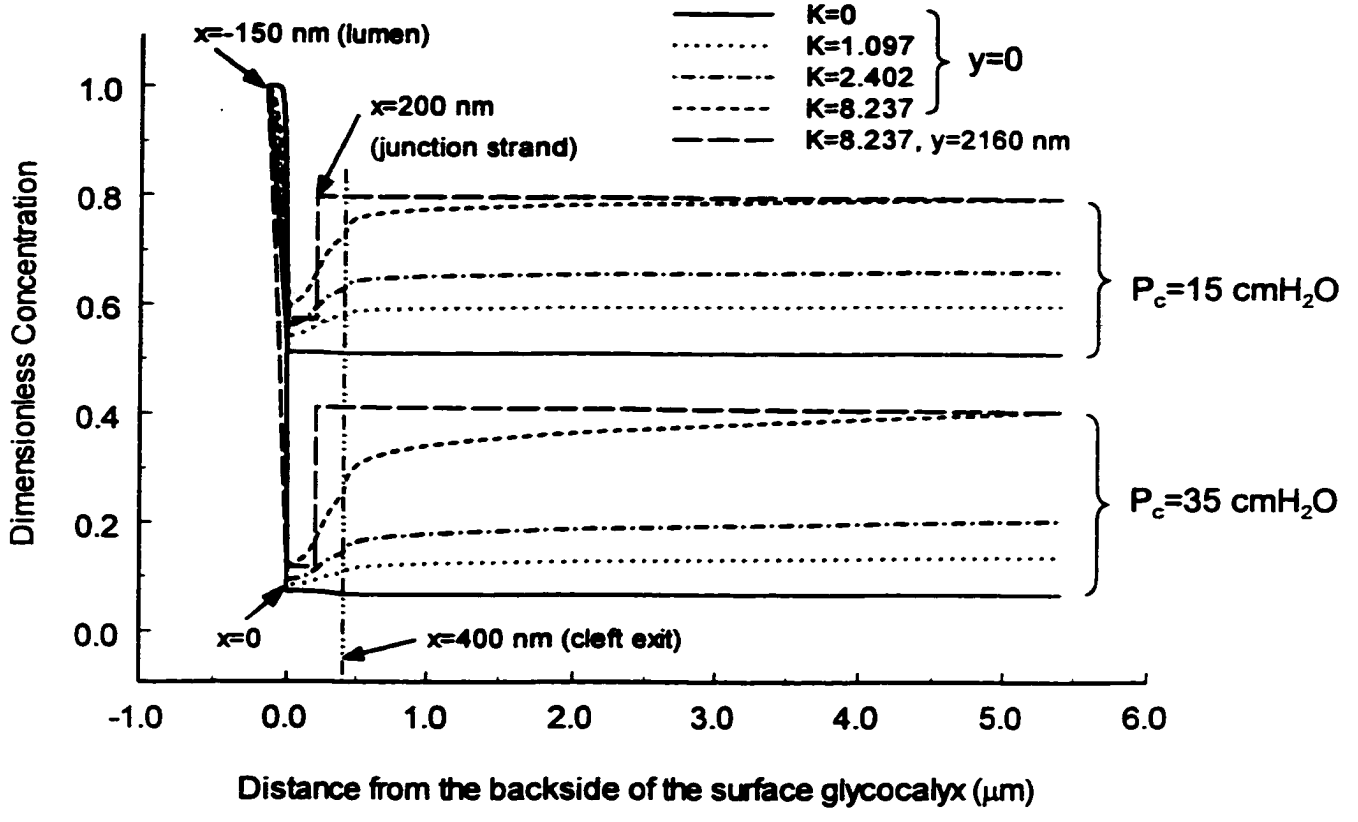

a

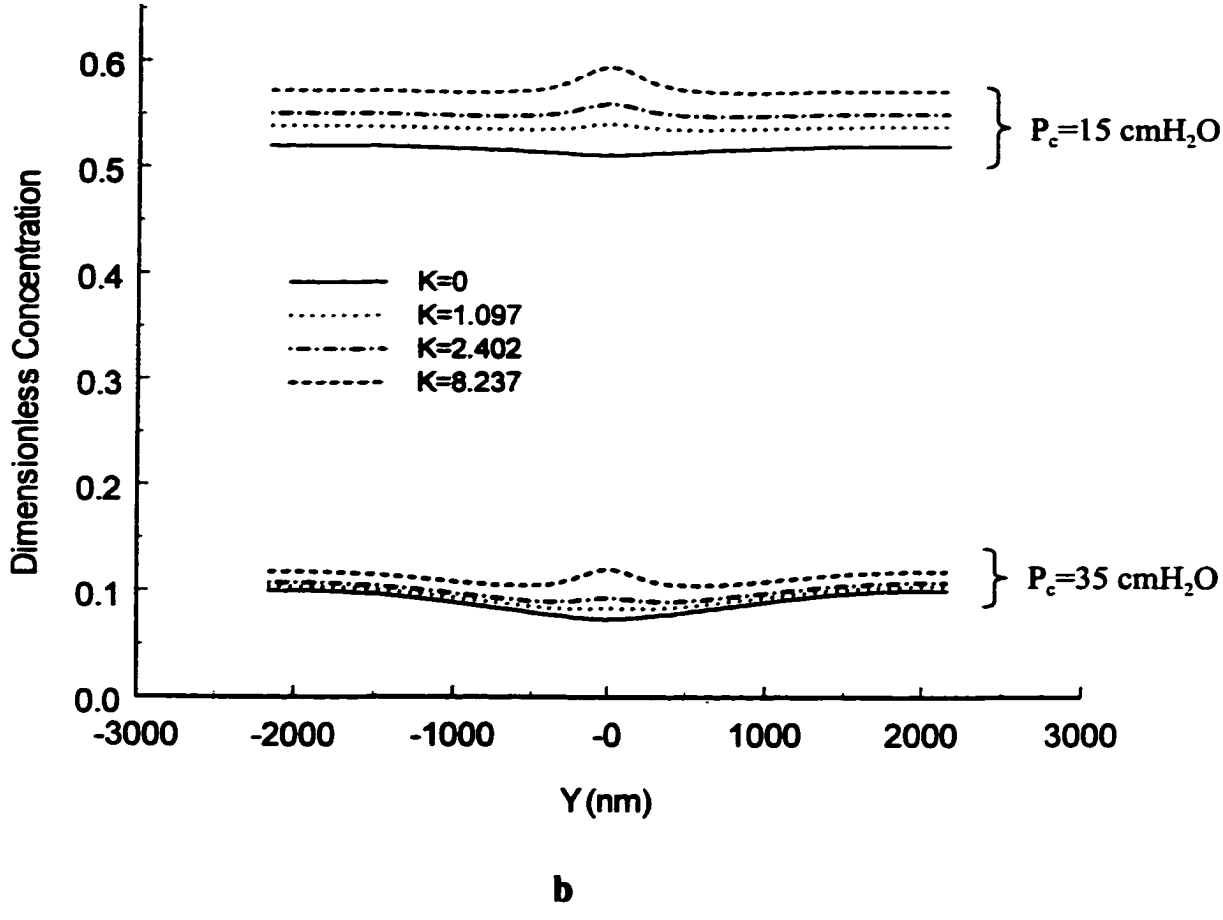

Figure 4.3 Concentration profiles at P_c=15 cm H_2O and P_c=35 cmH_2O for different protein transport rates by non-convective pathways for frog mesentery capillaries. (a) The concentration profiles along the centerline of the cleft y=0 and the edge of the cleft y=2160 nm at the mid-plane z=0 proceeding from the lumen to region B. (b) The concentration distribution at the backside of the surface glycocalyx. The unit of K is nm/s. The plasma oncotic pressure is 27.2 cmH_2O and σ=0.94.

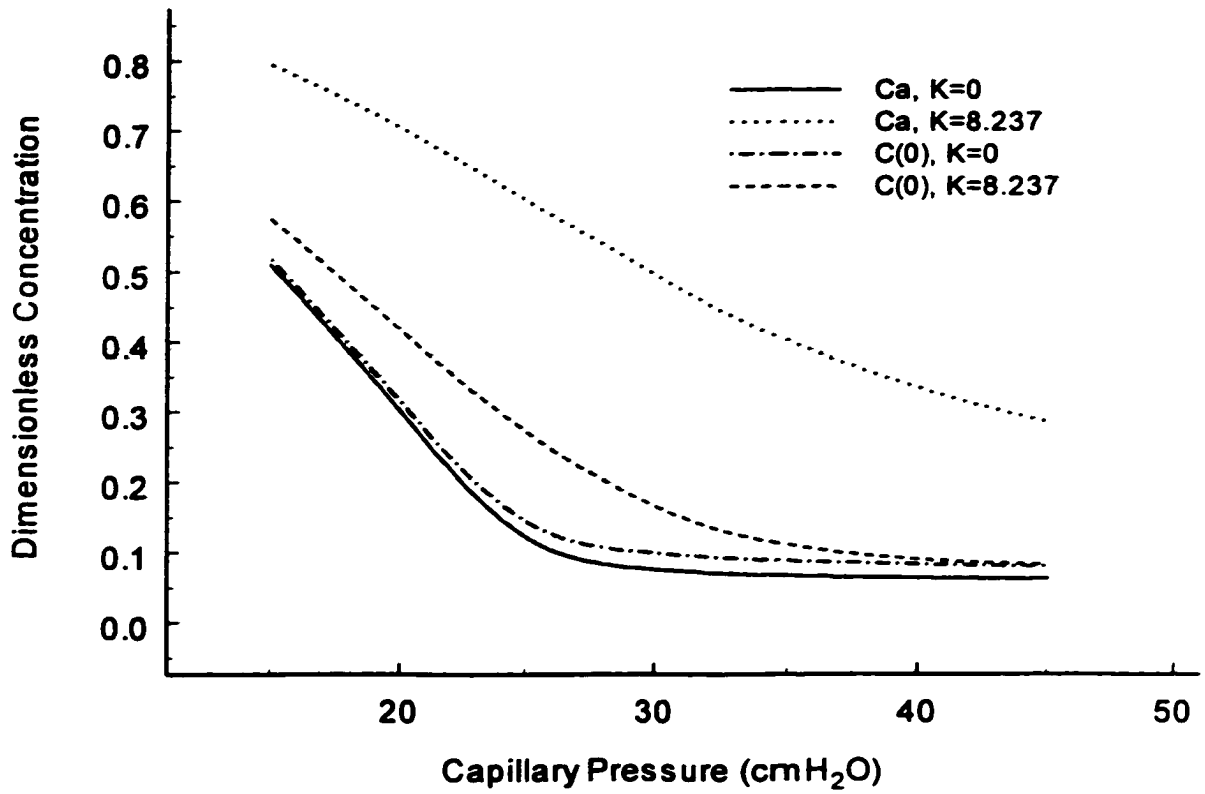

Figure 4.4 The average protein concentration behind the surface glycocalyx, $\overline{C}(0)$, and the interstitial protein concentration, C_a, for different values of K for frog mesentery capillaries. The interstitial protein concentration is greatly increased due to the non-convective transport and there is a slight increase in $\overline{C}(0)$. The concentration behind the surface glycocalyx differs greatly from the interstitial protein concentration. The unit of K is nm/s. The other parameters are the same as Fig. 4.3.

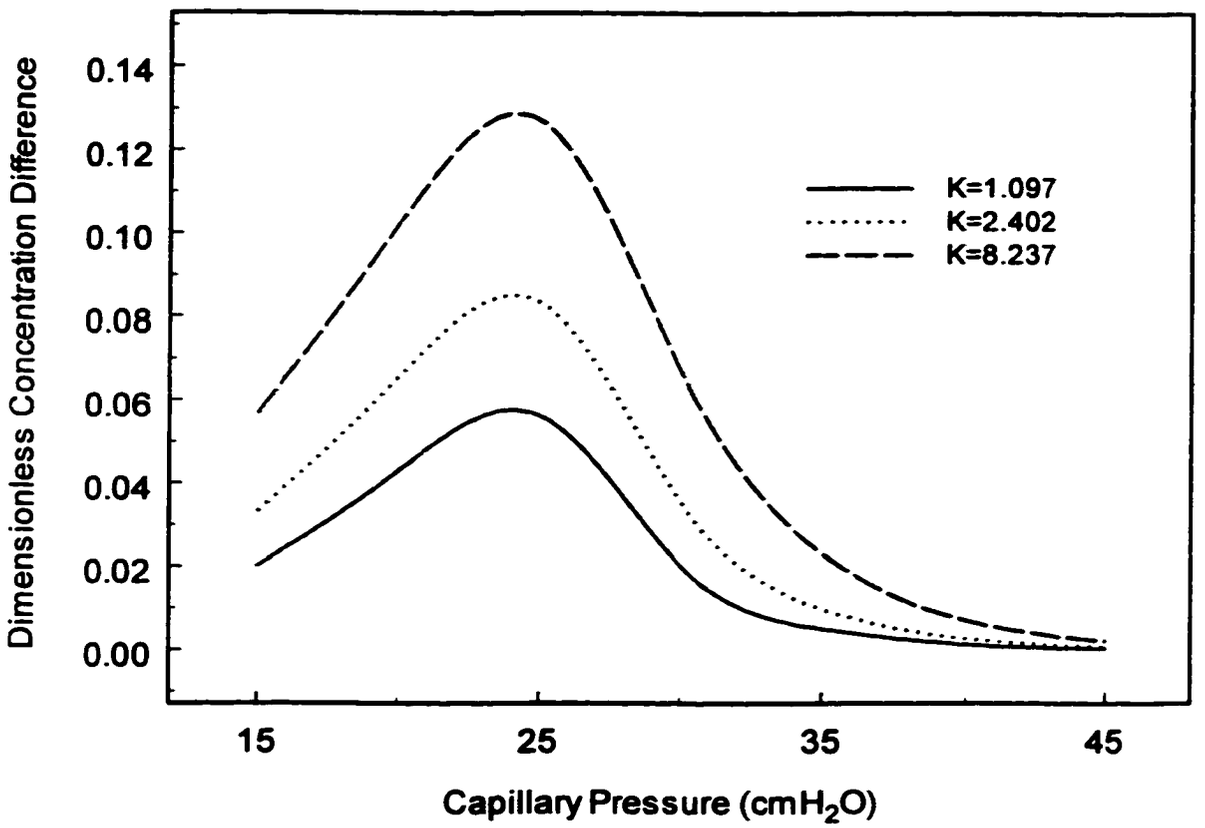

Figure 4.5 The increase in the average protein concentration behind the surface glycocalyx due to the back diffusion from the tissue for different values of K for frog mesentery capillaries. One observes that there is maximum value at P_c=24 cmH_2O for all values of K. The unit of K is nm/s. The other parameters are the same as Fig. 4.3.

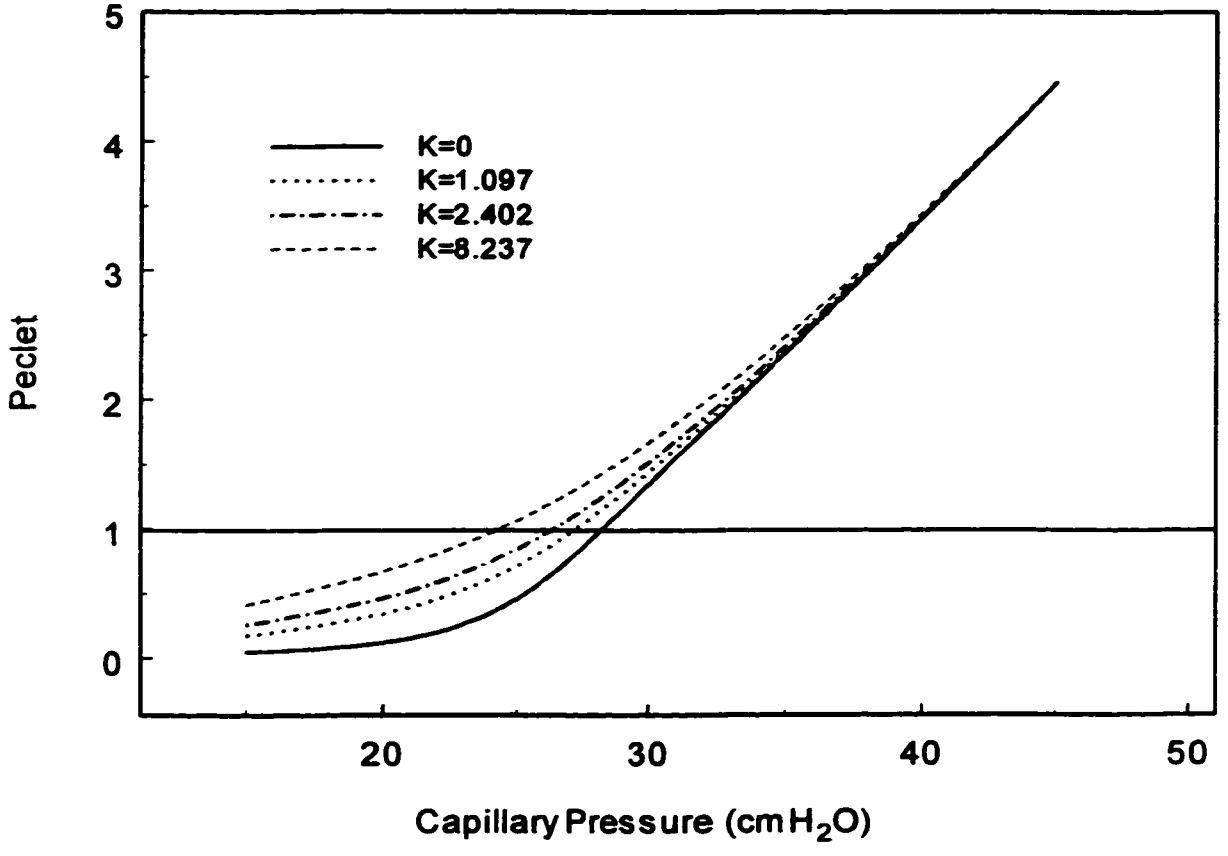

Figure 4.6 The relationship between Peclet number Pe and the capillary pressure for different values of K for frog mesentery capillary. The value of Pe increases at a given pressure as K increases. The unit of K is nm/s. The other parameters are the same as Fig. 4.3.

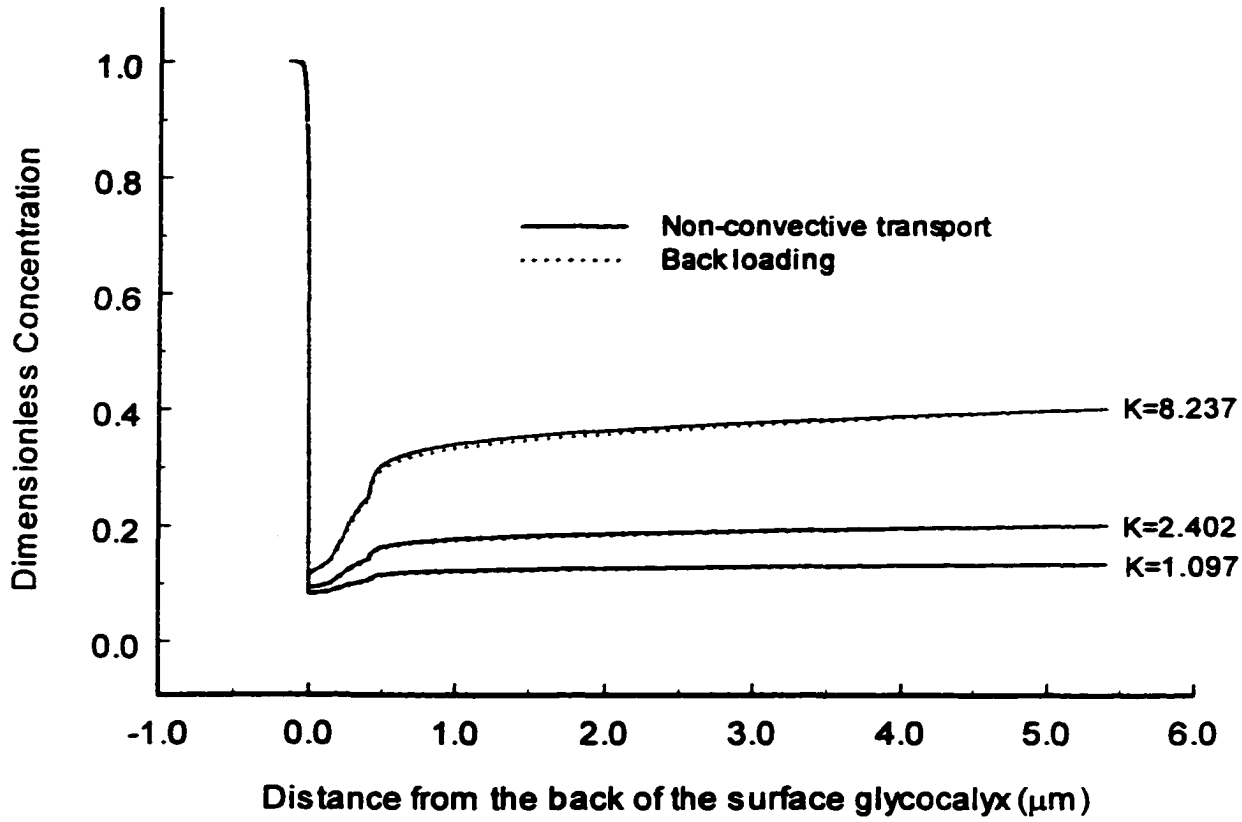

Figure 4.7 The protein concentration profiles along the centerline y=0 at the mid-plane z=0 for the tissue back loading and non-convective transport for frog mesentery capillaries. It is assumed that the tissue is loaded to have the same concentration at the edge of region B as that would be achieved by the non-convective transport. There is no significant difference of the protein concentration profiles for these two cases. The unit of K is nm/s. The other parameters are the same as Fig. 4.3.

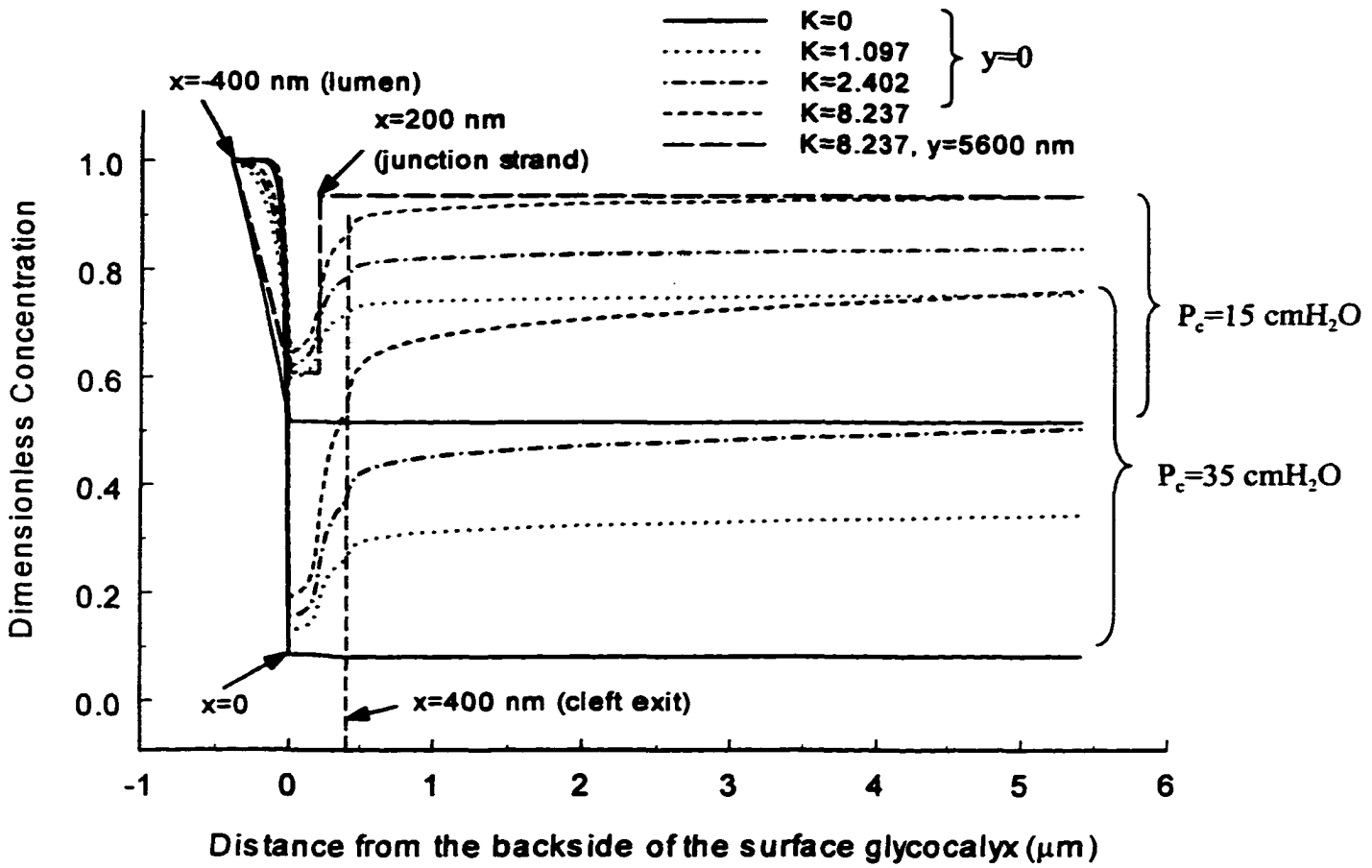

Figure 4.8 The protein concentration profiles along the centerline y=0 and the edge of the cleft y=5600 nm at the mid-plane z=0 at P_c=15 cmH$_2$O and P_c=35 cmH$_2$O for different values of K for mammalian capillaries. The spacing of the junction orifice 2D=11.2 μm, the width of the junction orifice 2d=50 nm and the thickness of the surface glycocalyx L_f=400 nm. The other parameters are the same as Fig. 4.2 for frog mesentery. The calculated permeability L_p=0.5×10^{-7} cm/(cmH$_2$O·s).

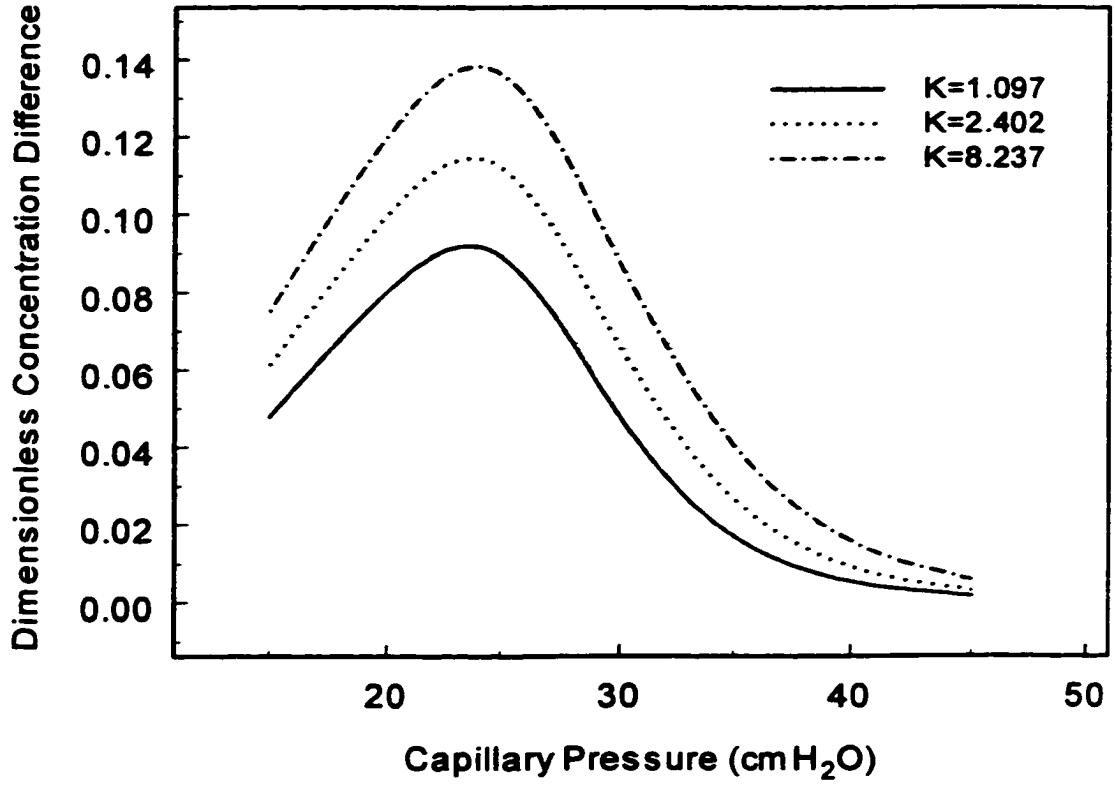

Figure 4.9 The increase in the average protein concentration behind the surface glycocalyx due to the back diffusion from the tissue for different values of K for mammalian capillaries. There is a maximum value at P_c=24 cmH_2O. The parameters are the same as Fig. 4.8.

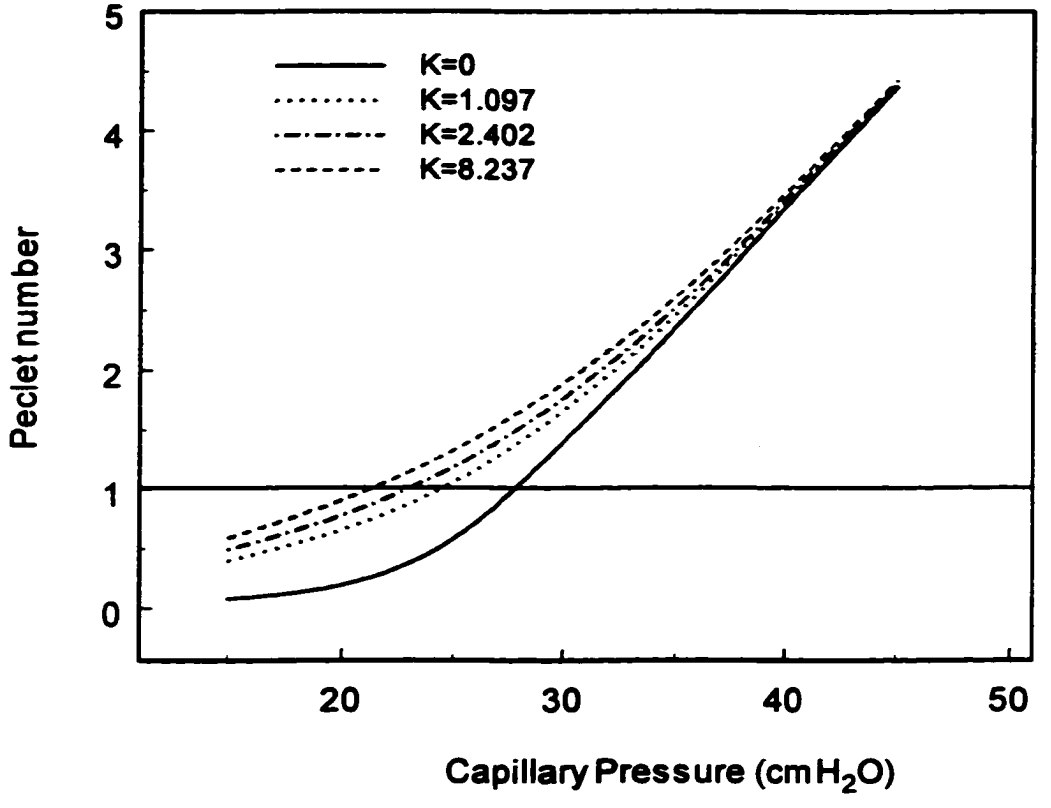

Figure 4.10 The relations between Peclet number and the capillary pressure for different values of K for mammalian capillaries. The Peclet number in the presence of the non-convective transport is higher than that when all albumin transport passes through the intercellular cleft. The parameters are the same as Fig. 4.8.

Chapter 5 Concluding Remarks

In this dissertation we quantitatively investigate the hypothesis proposed in Michel (1997) and Weinbaum (1998) that the Starling forces are determined by the local difference in the hydrostatic and colloid osmotic pressure across the endothelial surface glycocalyx, which we propose is the primary molecular sieve for plasma proteins, rather than the global difference in the hydrostatic and oncotic pressure across the capillary wall between the plasma and tissue, as has been universally assumed until now. In Chapter 2, we develop a spatially heterogeneous microstructural model to explain at the cellular level why there is oncotic absorption at low capillary pressures in the short lived transient experiments of Michel and Phillips (1987) on frog mesenteric capillary, but a small positive filtration once a steady state is achieved. The new model also predicts that the local protein concentration behind the surface glycocalyx can differ greatly from the tissue protein concentration, since the convective flux of proteins through the orifice like pores in the junction strand will greatly impede the back diffusion of the proteins into the lumen side of the cleft when the local Peclet number at the orifice is >1. The net result is that the filtration in the capillaries is far less than, heretofore, realized and there may be no need for venous reabsorption.

In chapter 3, we further test this hypothesis by applying our model to two new series of experiments performed by our collaborators at University of California at Davis in which the tissue is backloaded to establish known global osmotic gradients across the microvessel wall. The effective osmotic pressure exerted across the microvessel wall is measured in isolated microvessels of frog mesentery superfused with solutions containing 50 mg/ml albumin, which is not significantly different from that measured when the

perfusate alone contained albumin at 50 mg/ml. Measurements are made during transient filtration and reabsorption, and steady state filtration at capillary pressures between 10 and 35 cmH_2O. A cellular level model of coupled water and solute flows in the interendothelial cleft shows that the water flux through small breaks in the junction strand limits the back diffusion of albumin into the protected space on the tissue side of the glycocalyx. Thus osmotic forces opposing filtration are larger than those estimated from blood to tissue protein concentration differences, and transcapillary fluid flux is significantly smaller than estimated from global differences in osmotic and hydrostatic pressures.

In chapter 4, we investigate the effect of parallel transcellular non-convective pathways on the fluid filtration across the capillary wall. The three-dimensional model for frog mesenteric capillary is developed to describe the mixing of the protein-rich flux from the non-convective pathways with the protein-poor flux from the cleft exit. Even though the interstitial protein concentration is significantly raised due to the non-convective transport, the protein concentration at the backside of the surface glycocalyx differs greatly from the tissue protein concentration, as previously observed in chapters 2 and 3. The back diffusion from the tissue is significantly reduced due to the presence of the junction strand in the cleft. A fundamental new insight is revealed, namely, that back diffusion is maximized when the capillary pressure equals the effective oncotic pressure across the surface glycocalyx at the high filtration limit, $\sigma^2\pi_c$. We carefully examined the two competing mechanisms, Pe number at the orifice opening and concentration gradient in the cleft. Back diffusion from the tissue is a maximum when concentration gradient at the orifice is greatest. In this chapter, the three-dimensional mathematical model is

modified for mammalian capillaries to provide the first predictions of the new microstructural model for mammalian muscle tissue. Even though the hydraulic permeability for the mammalian muscle capillary is only one fifth of the frog mesenteric capillary, the Peclet number at the junction orifice is even larger than that for the frog mesenteric capillary.

Appendix

In this appendix the expression for the steady-state protein concentration in the tissue far from the cleft exit is derived for the case where the entire solute flux passes through the cleft. The protein concentration in the steady-state is equal to ratio of the total solute flux, J_s, to the total fluid flux, J_v. From continuity, these two fluxes are identical at every cross-section for steady state conditions. For convenience, we evaluate J_s and J_v at x=0, the cleft entrance. The local fluxes j_s and j_v can be written as

$$j_s(y) = \frac{D_f}{L_f}[C_c - C(0,y)]\frac{Pe}{e^{Pe}-1} + \frac{2}{3}C_c(1-\sigma_f)u_0(0,y) \tag{A1}$$

$$j_v(y) = \frac{2}{3}u_0(0,y) \tag{A2}$$

where

$$Pe = \frac{j_v(1-\sigma_f)L_f}{D_f}.$$

The total solute and fluid fluxes across each cross-section are given by

$$J_s = 2B \times \int_D^D j_s(y)dy \tag{A3}$$

$$J_v = 2B \times \int_D^D j_v(y)dy. \tag{A4}$$

Thus, the expression for C_i is given by

$$C_i = \frac{\int_D^D \left[\frac{D_f}{L_f}(C_c - C(0,y))\frac{Pe}{e^{Pe}-1} + \frac{2}{3}C_c(1-\sigma_f)u_0(0,y)\right]dy}{\frac{2}{3}\int_D^D u_0(0,y)dy}. \tag{A5}$$

Bibliography

1. Adamson, R. H. and G. Clough. Plasma proteins modify the endothelial cell glycocalyx of frog mesenteric microvessels. *J. Physiol.* 445: 473-486, 1992.

2. Adamson, R. H. and C. C. Michel. Pathways through the intercellular clefts of frog mesenteric capillaries. *J. Physiol.* 466: 303-327, 1993.

3. Adamson, R. H., J. F. Lenz, and F. E. Curry. Quantitative laser scanning confocal microscopy on single capillaries permeability measurement. *Microcirculation* 1: 251-265, 1995.

4. Adamson, R. H., B. Liu, G. Nilson-Fry, L. L. Rubin and F. E. Curry. Microvascular permeability and number of tight junctions are modulated by cAMP. *Am J Physiol.* in press, 1998.

5. Anderson, J. M. and C. M. Van Itallie. Tight junctions and the molecular basis for regulation of paracellular permeability. *Am J Physiol.* 269: G467-475, 1995.

6. Aukland, K. Interstitial fluid balance in experimental animals and man. *Interstitial lymphatic liquid and solute movement.* 110-123. 1987.

7. Baxter, L. T. and R. K. Jain. Transport of fluid and macromolecules in tumors. I. Role of interstitial pressure and convection. *Microvascular Res.* 37: 77-104, 1989.

8. Bundgaard, M. The three-dimensional organization of tight junctions in a capillary endothelium revealed by serial-section electron microscopy. *J. Ultrastruct. Res.* 88: 1-17, 1984.

9. Clough G and C. C. Michel. The sequence of labelling of endothelial cell vesicles with ferritin in the frog. *J Physiol* (Lond) 292:61P-62, 1979.

10. Clough G. and C. C. Michel. The role of vesicles in the transport of ferritin through frog endothelium. *J Physiol* 315:127-142, 1981.

11. Clough G. and C. C. Michel. The effects of temperature on ferritin transport by endothelial cell vesicles in capillaries of the frog mesentery. *Int J Microcirc* 1:29-39, 1982.

12. Crone, C. and D. G. Levitt. Capillary permeability to small solutes. In: *Handbook of Physiology. Cardiovascular System. Microcirculation.* Bethesda, MD: Am. Physiol. Sect. 2, Vol. IV, Chapter 10, p. 411-466, 1984.

13. Curry, F. E., V. H. Huxley and I. H. Sarelius. Techniques in the microcirculation: measurement of permeability, pressure and flow. In Cardiovascular Physiology, Techniques in the Life Sciences. New York, Elsevier, p1-34, 1983.

14. Curry, FE, J. C. Mason and C. C. Michel. Osmotic reflection coefficients of capillary walls to low molecular weight hydrophilic solutes measured in single perfused capillaries of the frog mesentery. *J Physiol* (Lond) 261:319-336, 1976.

15. Curry, F. E. and C. C. Michel. A fiber matrix theory of capillary permeability. *Microvasc. Res.* 20: 96-99, 1980.

16. Curry, F. E. Determinants of capillary permeability: A review of mechanisms based on single capillary studies in the frog. *Circ. Res.* 59: 367-380, 1986.

17. Curry, F. E. Regulation of water and solute exchange in microvessel endothelium: Studies in single perfused capillaries. *Microcirculation* 1: 11-26, 1994.

18. Duffer, M. E., B. Hainau, S. Ho and C. J. Bentzel. Regulation of epithelial tight junction permeability by cyclic AMP. *Nature* 294(5840): 451-453, 1981.

19. Fadnes, H. O., R. K. Reed, and K. Aukland. Interstitial fluid pressure in rats measured with a modified wick technique. *Microvasc. Res.* 14: 27-36. 1977.

20. Fu, B. M., R. Tsay, F. E. Curry and S. Weinbaum. A junction-orifice-entrance layer model for capillary permeability: Application to frog mesenteric capillaries. *ASME J. Biomech. Eng.* 116: 502-513, 1994.

21. Fu, B. M., F. E. Curry and S. Weinbaum. A diffusion wake model for tracer ultrastructure-permeability studies on microvessels. *Am. J. Physiol.* 269: H2124-H2140, 1995.

22. Fu, B. M., F. E. Curry, R. H. Adamson and S. Weinbaum. A model for interpreting the tracer labeling of interendothelial clefts. *Annals of Biomedical Eng.*, 25: 375-397, 1997.

23. Ganatos, P., S. Weinbaum, J. Fischbarg and L. Lieboyitch. A hydrodynamic theory for determining the membrane coefficients for the passage of spherical molecules through an intercellular cleft. *Adv. Bioeng.* 3: 193-196, 1981.

24. Grotte, G. Passage of dextran molecules across the blood-lymph barriers. *Acta Chirurg Scand* Suppl 211:1-84, 1956.

25. Guyton, A. C. A concept of negative interstitial pressure based on pressures in implanted perforated capsules. *Circulation Research*. 12: 399-414, 1963.

26. Guyton, A. C. and A. W. Lindsey. Effect of elevated left atrial pressure and decreased plasma protein concentration on the development of pulmonary edema. *Circ. Res.* 7, 649-657, 1959.

27. Hu, X, R. H. Adamson, B. Liu, F. E. Curry and S. Weinbaum. The Starling forces that oppose filtration after tissue oncotic pressure is increased. Submitted. 2000.

28. Hu, X and S. Weinbaum. The new view of Starling's Hypothesis at the microstructural level. *Microvasc Res* 58: 281-304, 1999.

29. Huxley, V. H., F. E. Curry, M. R. Powers and B. Thipakorn. Differential action of plasma and albumin on transcapillary exchange of anionic solute. *Am. J. Physiol.* 264: H1428-H1437, 1993.

30. Kim, D., P. M. Armenante and W. N. Duran. Mathematical modeling of mass transfer in microvascular wall and interstitial space. *Microvascular Res.* 40: 358-378, 1990.

31. Landis, E. M. Micro-injection studies of capillary blood pressure in human skin. *Heart.* 15: 209-228, 1930a.

32. Landis, E. M. The capillary blood pressure in mammalian mesentery as determined by the micro-injection methods. *Am. J. Physiol.* 93: 353-362, 1930b.

33. Landis, E. M. and J. R. Pappenheimer. Exchange of substances through the capillary walls. In: Handbook of Physiology. Circulation, edited by W. F. Hamilton and P. Dow. Washington, DC: *Am. Physiol. Soc.*, 1963, sect. 2, vol. II, chapt. 29, p.961-1034.

34. Langeler, E. G. and V. W. Van Hinsbergh. Norepinephrine and iloprost improve barrier function of human endothelial cell monolayers: role of cAMP. *Am J Physiol* 260: C1052-1059, 1991.

35. Levick, J. R. Capillary filtration-absorption balance reconsidered in light of dynamic extravascular factors. *Experimental Physiology.* 76: 825-857, 1991.

36. Levick, J. R. An analysis of the interaction between interstitial plasma protein, interstitial flow, and fenestral filtration and its application to synovium, *Microvascular Res.* 47: 90-125, 1994.

37. Levick, J. R. *An Introduction to Cardiovacular Physiology.* Butterworth-Heinemann Ltd., Oxford. 1995, Chapter 10. pp. 158-187.

38. McDonald, J. N. and J. R. Levick. Effect of extravascular plasma protein on pressure-flow relations across synovium in anaesthetized rabbits. *J. Physiol.* 465: 539-559, 1993.

39. Michel, C. C. and M. E. Phillips. Steady-state fluid filtration at different capillary pressures in perfused frog mesenteric capillaries. *J. Physiol.* 388: 421-435, 1987.

40. Michel, C. C. Capillary permeability and how it may change. *J. Physiol.* 404: 1-29, 1988.

41. Michel, C. C. Microvascular permeability, venous stasis and edema. *International Angiology.* 8: 9-13, 1989.

42. Michel C. C. Transport of macromolecules through microvascular walls. *Cardiovasc Res* 32: 644-653, 1996.

43. Michel, C. C. Starling: The formulation of his hypothesis of microvascular fluid exchange and its significance after 100 years. *Experimental Physiol.* 82: 1-30, 1997.

44. Michel, C. C. and F. E. Curry. Microvascular permeability. *Physiol Rev* 79:703-761, 1999.

45. Michel, C. C. and S. Kendall. Differing effects of histamine and serotonin on microvascular permeability in anaesthetized rats. *J. Physiol.* 501: 657-662, 1997.

46. Palade G. E. Fine structure of blood capillaries. *J Appl Physics* 241:1423, 1953.

47. Palade G. E. Transport in quanta across the endothelium of blood capillaries. *Anat Rec* 136:254, 1960.

48. Pallone, T. L., B. K. Kishore, S. Nielsen, P. Agre and M. A. Knepper. Evidence that aquaporin-1 mediates NaCl-induced water flux across descending vasa recta. *Am J Physiol* 272: F587-F596, 1997.

49. Pappernheimer, J. R. and A. Soto-Rivera. Effective osmotic pressure of the plasma proteins and other quantities associated with the capillary circulation in the hindlimbs of cats and dogs. *Am. J. Physiol.* 152: 471-491, 1948.

50. Perl, W. Modified-permeability model of transcapillary transport-a solution to the Pappenheimer pore puzzle? *Microvasc. Res.* 3:233-251, 1971.

51. Perl, W., P. Chowdhury and F. P. Chinard. Reflection coefficients of dog lung endothelium to small hydrophilic solutes. *Am. J. Physiol.* 228(3), 797-809, 1975.

52. Renkin E. M. Cellular and intercellular transport pathways in exchange vessels. *Am Rev Respir Dis* 146(5 pt 2): S28-31, 1992.

53. Renkin E. M., M. Gustafson-sgro and L. Sibley. Coupling of albumin flux to volume flow in skin and muscles of anaesthetized rats. *Am J Physiol* 255: H458-H466, 1988.

54. Rippe B and B. Haraldsson. Transport of macromolecules across microvascular walls: the two-pore theory. *Physiol Rev* 74(1): 163-219, 1994.

55. Rippe B, A. Kamiya and B. Folkow. Transcapillary passage of albumin, effects of tissue cooling and of increases in filtration and plasma colloid osmotic pressure. *Acta Physiol Scand* 105:171-187, 1979.

56. Sakakibara, A., M. Furuse, M. Saitou, Y. Ando-Akatsuka and S. Tsukita. Possible involvement of phosphorylation of occludin in tight junction formation. *J Cell Biol* 137: 1393-1401, 1997.

57. Schneeberger, E. E. and M. Hamelin. Interactions of serum proteins with lung endothelial glycocalyx: Its effect on capillary permeability. *Am. J. Physiol.* 247: H206-H217, 1984.

58. Schnitzer, J. E., P. Oh, E. Pinney and J. Allard. Filipin sensitive caveolae-mediated transport in endothelium: reduced transcytosis, scavenger endocytosis and capillary permeability of select macromolecules. *J Cell Biol* 127: 1217-1232, 1994.

59. Schnitzer, J. E., P. Oh and J. Allard. NEM inhibits transcytosis, endocytosis and capillary permeability: implication of caveolae fusion in endothelia. *Am J Physiol* 268: H48-H55, 1995.

60. Schulze, C. and J. A. Firth. The interendothelial junction in myocardial capillaries: evidence for the existence of regularly spaced, cleft spanning structures. *J. Cell Science.* 101: 647-655, 1992.

61. Starling, E. H. On the absorption of fluids from the convective tissue spaces. *J. Physiol.* 19: 312-326, 1896.

62. Taylor, A. E. and D. N. Granger. Exchange of macromolecules across the microcirculation. IN: E. M. Renkin and C. C. Michel, eds. American Handbook of Physiology Sect 2, Vol IV. American Physiology Society, Bethesda, Maryland. pp467-520, 1984.

63. Taylor, A. E. and M. I. Townsley. Evaluation of the Starling fluid flux equation. *News Physiol. Sci.* 2: 48-52, 1987.

64. Tray, R. and S. Weinbaum. Viscous flow in a channel with periodic cross-bridging fibers of arbitrary aspect ratio and spacing. *J. Fluid Mech.* 226: 125-148, 1991.

65. Tsay, R., S. Weinbaum and R. Pfeffer. A new model for capillary filtration based on recent electron microscopic studies of endothelial junctions. *Chem. Eng. Commun.* 82: 67-102, 1989.

66. Tschugguel, W., Z. Zhegu, L. Gajdzik, M. Maier, B. R. Binder and J. Graf. High precision measurement of electrical resistance across endothelial cell monolayers. *Pflugers Arch* 430: 145-147, 1995.

67. Vink, H. and B. R. Duling. Identification of distinct luminal domains for macromolecules, erythrocytes, and leukocytes within mammalian capillaries. *Circulation Res.* 79: 581-589, 1996.

68. Wagner, R. and S. C. Chen. Transcapillary transport of solute by the endothelial vesicular system: evidence from thin serial section analysis. *Microvasc Res* 42:139-150, 1991.

69. Weinbaum, S. 1997 Whitaker distinguished lecture: models to solve mysteries in biomechanics at the cellular level; a new view of fiber matrix layers. *Ann. Biomedical Eng.* 26: 1-17, 1998.

70. Weinbaum, S., R. Tray and F. E. Curry. A three-dimensional junction-pore-matrix model for capillary permeability. *Microvasc. Res.* 44: 85-111, 1992.

71. Weinbaum, S. and F. E. Curry. Modeling the structural pathways for transcapillary exchange. *The Society for Experimental Biology 1995.* 323-345, 1995.